Study on stratospheric–tropospheric ozone and its exchange, including total column- and surface-ozone variations using ground–based and satellite observations in South African sites

By

Thumeka Mkololo

211550431

A thesis submitted in fulfillment of the academic requirements for the degree of Doctor of Philosophy

College of Agriculture, Engineering and Science

School of Chemistry and Physics

Discipline of Chemistry

University of KwaZulu-Natal Durban

Supervisor: Prof. Venkataraman Sivakumar

May 2021

DECLARATION

PREFACE

I declare that this dissertation is my own work to fulfill the requirements of a Doctor of Philosophy degree (Atmospheric Chemistry) at the University of KwaZulu-Natal under the supervision of Prof. Venkataraman Sivakumar. All people's opinions and work has been referenced and acknowledged.

This work has not been submitted for any degree or examination at any other University.

This work include manuscripts that have been previously submitted to scientific journals (MDPI Atmosphere and Clean Air Journal). In addition, some of the work was presented and published in South African Society for Atmospheric Sciences (SASAS) conference peer reviewed proceedings.

…… …….

(Thumeka Mkololo, student)

……16……..day of…May…….2021

…….

(Prof. Venkataraman Sivakumar, supervisor)

……16……..day of……May…….2021

DECLARATION: PLAGIARISM

I, Thumeka Mkololo declare that:

- This is my original work and has never been submitted in any University for the fulfillment of any degree.
- Text used in this document has been re-written and previous authors are referenced accordingly.
- This work do not include information that has been copied from the internet or other documents. Where applicable, websites used for the information quoted are referenced on the text and graphs.
- Photos and graphs used in this study are my original work. In cases where photos and graphs are from other peoples work, references to the original work is provided.
- All people and institutions who played a role in this study have been acknowledged.
- Data used in this study is the original data from ground-based and satellite observations. Acknowledgement is provided to data originators.

…… …….

(Thumeka Mkololo, student)

……16……..day of……May…….2021

DECLARATION: MANUSCRIPTS AND PUBLICATIONS

I, Thumeka Mkololo declare that the current study include work that has been submitted in the following Journals:

- **Day-time and Night-time Ozone increase at Cape Point GAW Station as observed by ground based instruments**
  T. Mkololo, N. Mbatha, V. Sivakumar, C. Labuschagne, W. Jourbet, E.T. Mbambalala, and L. Martin.
  Proc. of the 35th Annual conference of South African Society for Atmospheric Sciences (SASAS), River Sun, Vanderbijl Park, Gauteng, ISBN : 978-0-6398442-0-6, *Pg84-87, 8-9 October, 2019.*

- Stratosphere–troposphere exchange and O_3 variability in the lower stratosphere and upper troposphere over the Irene SHADOZ site, South Africa
  Thumeka Mkololo, Nkanyiso Mbatha, Venkataraman Sivakumar, Nelson Bègue, Gerrie Coetzee and Casper Labuschagne. Atmosphere **2020**, 11(6), 586. doi.10.3390.atmos/1060586

- Analysis of day-time and night-time Cape Point surface ozone mole fractions using linear regression and no-parametric tests techniques.
  Thumeka Mkololo, Nkanyiso Mbatha, Venkataraman Sivakumar, Casper Labuschagne, Warren R. Joubert, Ernest Mbambalala, Lynwill Martin and Danie van der Spuy, *Clean Air Journal*, https://www.cleanairjournal.org.za/authorDashboard/submission/8025.4 *March, 2020.*

- Validation of Stellenbosch Dobson Total Column Ozone observations with satellite observations.
  T. Mkololo, V. Sivakumar, N. Mbatha, H. Bencherif, G. Coetzee, E. Mbambalala and D. vanderSpuy, that is prepared for submission in *South African Journal of Science*.

ACKNOWLEDGEMENTS

I would like to thank the following people and institutions for their role in the accomplishment of this study:

- My extended gratitude to national research foundation (NRF) Protea France–South Africa programme and South African Weather Service for funding the research.
- Gratitude to South African Weather Service for allowing me to use their data (meteorology, total column ozone, balloon ozonesondes and surface ozone data) and ECMWF for access to the dataset.
- My gratitude acknowledgements to my supervisor Prof. Venkataraman Sivakumar for his guidance, critical comments and recommendations.
- Many thanks to Dr. Nkanyiso Mbatha for co-supervision, critical comments, guidance and motivation.
- I would like to acknowledge Dr. Nelson Bègue for providing potential vorticity data.
- My acknowledgements to my colleagues (Gerrie Coetzee, Warren Joubert, Danie van der Spuy, Ernest Mbambalala, Casper Labuschagne and Lynwill Martin) for their continuous motivation.
- My extended gratitude to Mr. Ernst Brunke for his motivation and being a good mentor in my early career days.
- My sincere gratitude to all the co-authors of the manuscripts for their critical comments.
- To my family (Nozie Mkololo, Mncedisi Mkololo, Simbongile Mvinjelwa, Duma Mkololo, Yonela Mkololo, Bukho and Buhle Mvinjelwa), I appreciate their permanent motivation, endure love and continuous support.
- I dedicate this work to my grandfather (Mpayipheli Mkololo) for his motivation and words of intelligence.

Abstract

South Africa is one of the countries that adhere to the Vienna Convention and its Montreal Protocol to protect the ozone (O_3) layer. Hence, the country conducts O_3 vertical profiles, Total Column Ozone (TCO) and surface O_3 measurements. Atmospheric O_3 can be either beneficial or harmful to the environment and human health depending on its abundance in the atmosphere. Therefore, continuous monitoring of atmospheric O_3 is essential to protect the environment and human health. Even though most of the O_3 is found in the stratosphere, O_3 can propagate from the stratosphere to the troposphere through a process called stratospheric–tropospheric exchange (STE).

This study investigates the STE over Irene by using 2000–2007 and 2012–2015 O_3 vertical profiles. The monthly 90^{th} and 95^{th} percentile composites were calculated and used as threshold to identify high O_3 events. In addition, the potential vorticity (PV) of 2PVU was used as a tracer of stratospheric air masses. Days exceeding the monthly 90^{th}, 95^{th} percentile composites and 2PVU were classified as high O_3 events that originates from the stratosphere. Furthermore, the medians, 5^{th} and 95^{th} percentiles were used to investigate the annual and seasonal O_3 changes at different altitudes.

The study also validates 2017 and 2018 Stellenbosch Dobson spectrophotometer TCO with Ozone Monitoring Instrument (OMI) and Atmospheric Infrared Sounder (AIRS) satellite TCO observations. The OMI satellite data was obtained from OMI–Total Mapping Spectrometer (OMI-TOMS) and OMI–Differential Optical Absorption Spectroscopy (OMI-DOAS). In addition to satellite validations, Stellenbosch Dobson TCO data was compared with Modern-Era Retrospective Analysis for Research and Applications (MERRA-2) observations by calculating percentage difference, percentage error and correlation coefficient.

The study also investigates variability and trends of surface O_3 by using 2000 to 2018 Cape Point data (all–data, day and night–time). The annual, seasonal and weekday-weekend trends were investigated by using linear regression and Theil-Sen slope methods. In addition, 2000 to 2007 Cape Point wind and radon data was used to investigate the effect of winds in O_3 mole fractions. The study extends to identify extreme maximum and minimum O_3 values observed and a case study has been explored for initial bench mark. However, a more detailed study may be required for any conclusive remarks.

TABLE OF CONTENTS

LIST OF FIGURES

LIST OF TABLES

Acronyms and Abbreviations

Acronyms/Abbreviations	Abbreviated term
AIRS	Atmosphere Infrared Sounder
AMSU	Advanced Microwave Sounding Unit
Br	Bromine
BrO	Bromine Oxide
CAAA70	Clean Air Act Amendments of 1970
CF_2Cl_2 (CFC-12)	Dichlorofluoromethane
CFCl3 (CFC-11)	Trichlorofluoromethane
CFCs	Chloroflouro carbons
CH_3Cl	Methyl chloride
CH_4	Methane
Cl	Chlorine
ClO	Chlorine Oxide
CO	Carbon monoxide
CO	Carbon monoxide
CO_2	Carbon dioxide
CSIR	Council of Scientific and Industrial Research
DS	Direct Sun
HNO_3	Nitric acid
EDGAR	Emission Database for Global Atmospheric Research
ENSO	El Nino-Southern Oscillation
EOS-Aura	Earth Observing System-Aura
GAW	Global Atmosphere Watch
GEOS	Goddard Earth Observing System
GMAO	Global Modeling and Assimilation Office
GOME	Global Ozone Monitoring Experiment
H_2O	Water
HCFCs	Hydro chlorofluorocarbons
HNO_3	Nitric acid
HO_2	Hydroperoxyl radical
IASI	Infrared Atmospheric Sounding Interferometer

IPCC	Intergovernmental Panel on Climate Change
MERRA	Modern Retrospective Analysis Research and Applications
METOP-A	Meteorological Operational Satellite-A
MIMOSA	Modélisation Isentrope du transport Méso–échelle de l'Ozone Stratosphérique par Advection
MLS	Microwave Limb Sounder
N_2	Nitrogen
N_2O	Nitrous Oxide
N_2O_5	Dinitrogen Pentoxide
NASA	National Aeronautics and Space Administration
NASA	National Aeronautics Space Administration
NO	Nitrogen Oxide
NO_2	Nitrogen dioxide
NO_3	Nitrate
NO_x	Nitrogen Oxides
NRC	National Research Council
O	Oxygen atom
O_2	Oxygen molecule
O_3	Ozone
ODS	Ozone Depletion Substances
OH	Hydroxyl radical
OMI	Ozone Monitoring Instrument
OMI-DOAS	OMI-Differential Optical Absorption Spectroscopy
OMI-TOMS	OMI-Total Mapping Spectrometer
ppb	Parts per billion
PSC	Polar Stratospheric Clouds
PV	Potential Vorticity
SAFARI	Southern African Fire Atmospheric Research Initiative
SANParks	South Africa National Parks
SASAS	South African Society for Atmospheric Sciences
SH	Southern Hemisphere
SHADOZ	Southern Hemisphere Additional Ozonesondes
SI	Stratosphere Intrusion

SO_2	Sulphur dioxide
STE	Stratosphere Troposphere Exchange
TCO	Total Column Ozone
TES	Technology Experiment Satellite
UV	Ultra Violet
VOCs	Volatile Organic Compounds
WCC-EMPA	World Calibration Centre- EMPA
WMO	World Meteorological Organization
ZB	Zenith Blue
ZC	Zenith Cloud

CHAPTER 1: INTRODUCTION

1.1 Background on Ozone

South Africa air quality is affected by pollution that originate from mines, glass industries, fuel refining, vehicle traffic, airport operations, aircrafts (operation and maintenance) and fuel storage sites (Walton, 2005). The polluters release hydrocarbons, carbon monoxide (CO), nitrogen oxides (NO_x), sulfur dioxide (SO_2) and particulates (Walton, 2005). Most of these pollutants listed above are the surface ozone (O_3) precursors that form O_3 in the presence of sunlight.

O_3 is an important greenhouse gas that contributes to the global climate warming or green-house effect. In the absence of greenhouse gases, temperatures on earth will drop below zero every night (Kinney et al., 1996). Unlike other trace gases such as CO_2, methane and CO which maximize in the troposphere, O_3 accumulates in the stratosphere to form a layer called the O_3 layer. This layer occurs approximately 20 to 30 km from the Earth's surface (Liou, 2002; Schott, 2007). The O_3 layer plays an important role in protecting the environment and human health from dangerous ultraviolet (UV) radiation (www.epa.gov). If substantially decreased, 'O_3 hole' is formed and more UV penetrate to the troposphere. The term 'O_3 hole' is used when a hole is formed in the O_3 layer and O_3 mole fractions are less than 220 DU (Nazir and Zaman, 2016). The first documented paper on 'O_3 hole' was published in 1985. Farman et al. (1985) reported a decrease in total column O_3 over Halley Bay station in Antarctica. While other studies (e.g. Proffitt et al., 1990 and Anderson et al., 1991) reported a relationship between O_3 depletion and polar vortex. Hassler et al. (2011) reported similar relationship of total O_3 and polar vortex over Antarctica. Polar vortex is important in O_3 depletion and 'O_3 hole' formation (Solomon, 1999). In addition, polar vortex plays an important role in distributing O_3 and other trace traces (Waugh and Polvani, 2010). The polar vortex is formed in autumn, maximize in winter and breaks in late winter and spring (Waugh and Polvani, 2010). According to Angell and Korshover (2005), the observed 'O_3 hole' was related to the increasing chlorofluorocarbons (CFCs) in the atmosphere. Halogens are emitted at earth surfaces all over the stratosphere. Most of these gases have no natural removal processes in the lower atmosphere. Halogens enter the stratosphere through the tropical tropopause and transported in the stratosphere and Polar Regions by atmospheric motions

(Solomon, 1999). Several studies reported negative impacts of high UV radiation in the troposphere. These studies reported that high UV radiation affect eyes (Wargent et al., 2013), causes skin cancer (Andersen et al., 2005; Tian et al., 2009), affect DNA (Shindell et al., 1998), asthma (Wargent et al., 2013), affect the aquatic system and agricultural productivity (Anwar et al., 2016). While the Intergovernmental Panel on Climate Change (IPCC, 2013), reported a global average radiative forcing of 0.40 ±0.20 W/m^2 due to tropospheric O_3. Due to these negative impacts of O_3 in the troposphere, more than twenty nations signed the Montreal protocol in 1987 to protect the O_3 layer from anthropogenic activities that releases O_3 Depletion Substances (ODS) such as chlorine and bromine containing compounds (Andersen et al., 2002). After the successful implementation of the Montreal protocol, stations monitoring ODS reported a decreasing trend of ODS in the atmosphere (Figure 1.1). However, the lifespan of these gases is long and may take several years to deplete in the atmosphere (Molina and Rowland, 1974). It is evident from the above-mentioned studies that high O_3 mole fractions play a positive role in the stratosphere by protecting human and the environment. However, the abundance of O_3 in the troposphere have negative affects to human health and the environment at large.

Due to the important role of O_3 in the stratosphere, and its negative effects in abundance in the troposphere, South Africa is one of the countries that took essential steps to terminate ODS and developed a number of O_3 monitoring stations. These stations include Dobson TCO observations, O_3 vertical profiles and surface O_3 monitoring stations. The TCO observations are conducted at Irene, Springbok and Stellenbosch. These observations are part of the Global Atmosphere Watch (GAW under the world meteorological organization) regional activities of South African Weather Service. While O_3 vertical profiles are monitored over Irene. There are many stations monitoring surface O_3 in the country. These stations are under the management of government, local municipalities and industries. In addition, surface O_3 measurements are conducted by North West University at the Welgegund air quality research station. Of all the surface O_3 stations operating in the country, Cape Point GAW station has the longest record of thirty-seven years of surface O_3 data and serves as the background station.

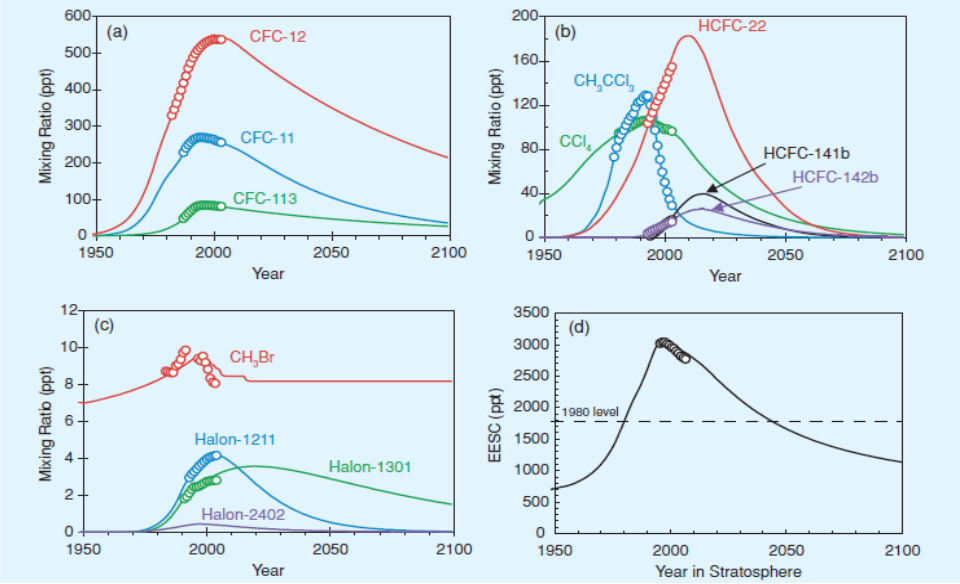

Figure 1.1: Global atmosphere mixing ratios (ppt) of most abundant CFCs, HCFCs, choridesolvents and brominated gases (obtained from WMO, 2003).

1.2 Study motivation and problem statement

- Stratospheric-Tropospheric Exchange (STE) is one of the tropospheric O_3 sources that contributes to high O_3 mole fractions observed in the troposphere. Even though a number of studies have used Irene O_3 vertical profiles, statistical analysis of STEs remain a gap that needs further investigation. Moreover, the O_3 vertical profiles are useful to study the atmospheric O_3 changes at different altitudes. Even though there are some studies on O_3 changes in South Africa, this aspect needs further investigation using more statistical analysis. Hence, the first scientific focus of this thesis is to identify STE events and conduct their statistical analysis. In addition, this study investigates O_3 changes at different altitudes over Irene.
- TCO is one of the important parameters to characterize the O_3 layer above a specific region. Hence, the new Stellenbosch Dobson TCO observations are important to understand the status of O_3 layer above Cape Town region. The second focus of this thesis is related to TCO. This thesis evaluates the performance of TCO observations from the recently developed Stellenbosch Dobson spectrophotometer by comparing it with satellite TCO observations.

Furthermore, this thesis determines the bias between Dobson spectrophotometer and satellite observations.

- STE is one of the sources of surface O_3 and contribute to the observed surface O_3 mole fractions. In addition to it, there is a relationship between TCO and tropospheric O_3 because TCO is the total amount of O_3 molecules measured from the surface to the upper atmosphere. Hence, it is important to investigate its relationship with surface O_3 measurements. O_3 production predominantly occur during the day-time where there is enough UV radiation and O_3 precursors. It is important to study O_3 using different datasets with day-time data separated from night-time data in order to find if the observed O_3 increase is related to photochemical production. Increasing tropospheric O_3 mole fractions have become a threat to the environment at large and a concern to the scientific community. Cape Point in particular, is amongst the GAW stations in the Southern Hemisphere that experience increasing O_3 trend. A number of local and international studies have used Cape Point surface O_3 data to study diurnal and seasonal cycles. In addition, long-term trends were previously investigated using Cape Point all data available. However, weekday-weekend, seasonal and annual O_3 changes in all-day, day and night-time datasets were not investigated. The relationship between TCO and Cape Point surface O_3 was previously investigated using TOMS TCO observations only and it will be interesting to investigate the relationship of surface O_3 measurements at Cape Point with other TCO satellite observations. The third focus of this thesis is to investigate if the observed increase surface O_3 increase at Cape Point occurs in both day-time and night-time datasets. Furthermore, to investigate if weekday and weekend trends. This study also investigates the relationship between surface O_3 and TCO observations.

1.3 Aims and objectives of the study

- The current study aims to use Irene O_3 vertical profiles to identify and conduct statistical analysis of STE events. In addition, O_3 vertical profiles were used to investigate O_3 changes at different altitudes.
- This study validates Stellenbosch Dobson spectrophotometer TCO with OMI–Total Mapping Spectrometer (OMI–TOMS), OMI–Differential Optical Absorption Spectroscopy (OMI–DOAS) and Atmospheric Infrared Souder (AIRS) TCO observations. Dobson TCO observations were also compared with Modern-Era Retrospective Analysis for Research and

Applications (MERRA–2) assimilation. The current study is the first to validate and document Dobson TCO with satellite TCO observations over Cape Town.

- The study also investigates the variability and trends (weekday-weekend, seasonal and annual) of surface O_3 by using all-day, day and night-time datasets. Lastly, wind and radon data was used to investigate the effect of local weather and climate on surface O_3 measurements. In addition, this study investigates the relationship between surface O_3 and TCO (OMI-TOMS, OMI-DOAS, AIRS and MERRA-2) observations.

The study objectives include the following:

a) To identify high O_3 events exceeding the monthly 90^{th} and 95^{th} percentile composites by using O_3 vertical profiles.
b) To use Potential Vorticity (PV) of 2PVU together with the monthly 90^{th} and 95^{th} O_3 percentile composites as thresholds to identify stratospheric air masses exchanges over Irene.
c) To calculate O_3 changes at difference altitudes over Irene by using the median, 5^{th} and 95^{th} percentile composites.
d) To calculate the percentage difference, percentage error, root square mean error, mean bias error, mean absolute bias error and correlation coefficient between Stellenbosch Dobson TCO observations and satellites borne instruments that used different methods/algorithms (OMI–TOMS, OMI–DOAS and AIRS) TCO observations.
e) Moreover, the percentage difference, percentage error, root square mean error, mean bias error, mean absolute bias error and correlation coefficient was calculated between Stellenbosch Dobson TCO observations and MERRA–2 assimilation.
f) To calculate the weekday-weekend, seasonal and annual O_3 changes in all–day, day and night–time Cape Point surface O_3 data by using linear regression and Theil-Sen slope.
g) To identify extreme maximum and minimum surface O_3 events at Cape Point.
h) To determine the relationship between TCO observations and surface O_3 at Cape Point.

This study employs data from the following periods:

- Irene O_3 vertical profiles for the period from 2000 to 2007 and 2012 to 2015;
- MERRA-2 PV assimilation for the period from 2000 to 2017;

- Stellenbosch Dobson spectrophotometer TCO observations for the period from 2017 to 2018;
- Stellenbosch OMI–TOMS and OMI–DOAS TCO observations for the period from 2017 to 2018;
- Stellenbosch AIRS TCO observations for the period from 2017 to 2018;
- Stellenbosch MERRA-2 TCO assimilation for the period from 2017 to 2018;
- Cape Point surface O_3 data for the period from 2000 to 2018;
- Cape Point wind data for the period from 2000 to 2018;
- Cape Point radon data for the period from 2000 to 2018.
- Cape Point OMI–TOMS and OMI–DOAS TCO observations for the period from 2005 to 2018;
- Cape Point AIRS TCO observations for the period from 2005 to 2018;
- Cape Point MERRA-2 TCO assimilation for the period from 2005 to 2018.

Table 1 gives a summary of ground-based instruments, location of the stations and data period that was used to fulfil the aim and the objectives of the study.

Table 1: O_3 ground-based instruments used for the study.

Instrument	Period	City
Ozone balloonsondes	2000-2007 and 2012-2015	Irene
Dobson spectrophotometer	2017-2018	Stellenbosch
Thermo Electron analyzer (UV based)	2000-2018	Cape Point

1.4 Study area

1.4.1 Station at Irene

As indicated in Figure 1.2, the Irene station is located approximately sixteen kilometers from Pretoria (-25.9ºS, 28.2°E). The station is one of the fourteen Southern Hemisphere Additional Ozonesondes (SHADOZ) stations worldwide and one of three located in Africa. The SHADOZ network was developed after the Southern African Fire Atmospheric Research Initiative (SAFARI) campaign. The purpose of the SHADOZ network is to monitor O_3 vertical profiles in the Southern Hemisphere using balloon-borne ozonesondes. The O_3 vertical profiles are obtained using electrochemical concentration cell ozonesondes (ECC). The heart of the instrument is the

electrochemical cell that interfaces with a radiosonde and sends back data signals to the ground station receiver. Currently, soundings are conducted every second Wednesday, with the release time as close as possible to 10:00 am local time.

1.4.2 Station at Stellenbosch

As indicated in Figure 1.2, Stellenbosch is located approximately fifty-three kilometers east of the city of Cape Town. (-33.9ºS, 18.3°E). The Dobson spectrophotometer TCO observations are conducted at South African weather service inside the Council for Scientific and Industrial Research (CSIR) premises. Up until 2016, there were two Dobson TCO observations in the country. In November 2016, the third Dobson TCO observations commenced at Stellenbosch, adding to the long–term observations at Irene and Springbok. The Dobson meter was developed in 1924 by Gordon Dobson to measure stratospheric O_3 from the Earth's surface (Dobson, 1968).. The 'Dobson unit' is used worldwide to measure TCO in honor of Gordon Dobson who developed the Dobson spectrometer and carried out the earliest studies of O_3 in the atmosphere. This technique requires manual operation for observations and data logging.

1.4.3 Station at Cape Point

The Cape Point station is located on the Cape Peninsula at the South Africa National Parks (SANParks) nature reserve (-34º35S; 18°48E), which is approximately sixty kilometers south of the City of Cape Town (Figure 1.2). The Cape Point station is one of the forty Global Atmosphere Watch (GAW) stations that are mandated by the World Meteorological Organization (WMO) to monitor trace gases under background conditions. Hence, the station is located far from the anthropogenic activities. The location of the station far from anthropogenic activities makes it a preferred location for background air monitoring. The prevailing air masses at the station are south-easterlies that brings clean air from the ocean. However, at times the station is affected by continental air masses. The Cape Point started trace gas monitoring in 1978 with Carbon monoxide (CO) measurements. In 1983, surface O_3 measurements were added on the program. As time goes on, other parameters such as carbon dioxide (CO_2), methane (CH_4), nitrous oxide (N_2O), total gas mercury (TGM), radon (Rn^{222}) and meteorological parameters (temperature, humidity, wind speed and wind direction) were added on the program.

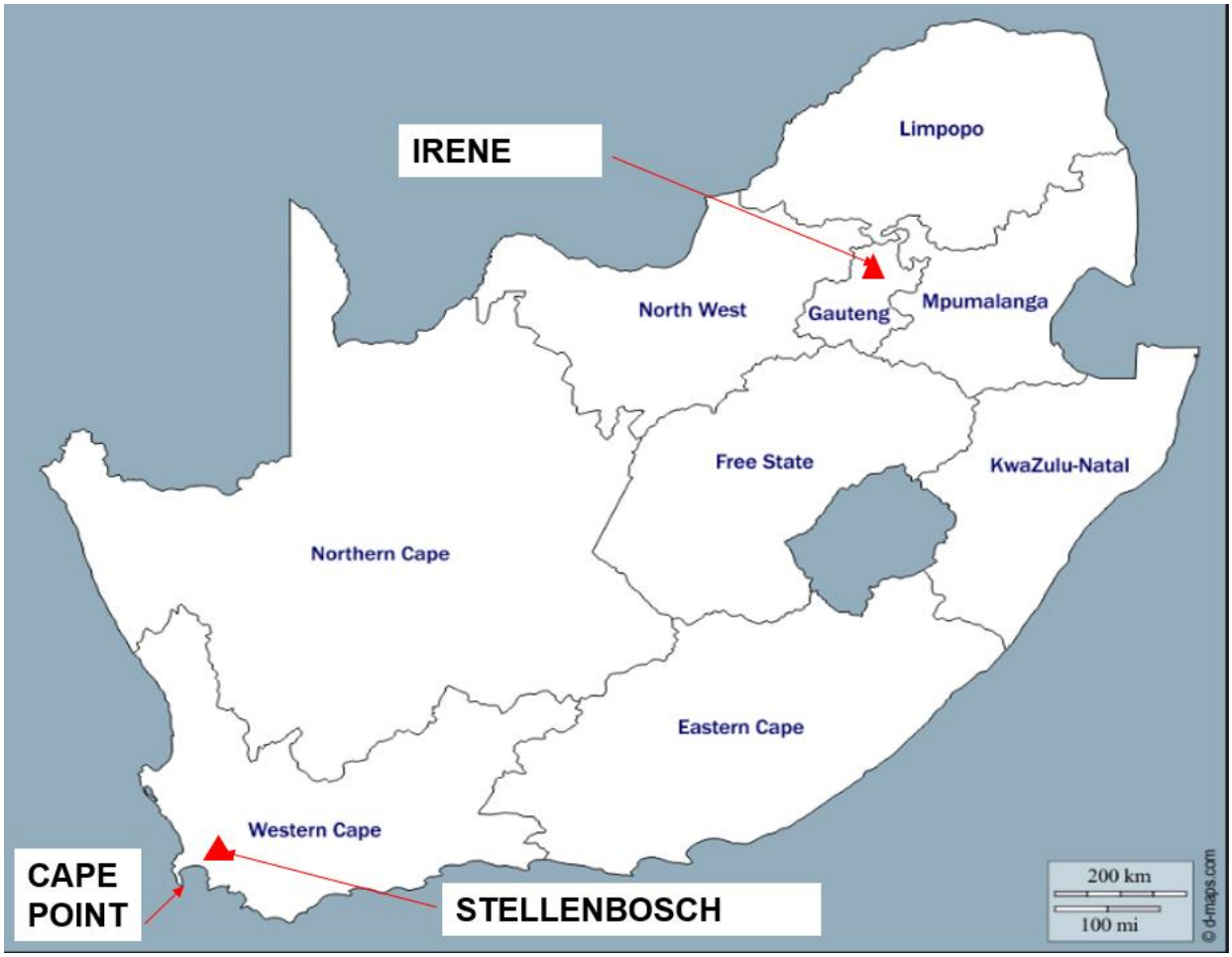

Figure 1.2: Location of Irene, Stellenbosch and Cape Point GAW station.

1.5 Satellite observations

1.5.1 Ozone Monitoring Instrument (OMI)

The OMI was introduced in 2004 after Total Mapping Spectrometer (TOMS) observations to continue the TCO record and other parameters that were observed by TOMS. The OMI is one of the instruments on board the Aura satellite that monitors the O_3 layer. The instrument has some advantages as compared with Global Ozone Monitoring Experiment (GOME) and TOMS. In addition to TCO observations, OMI measures other atmospheric components such as Nitrogen dioxide (NO_2), Sulphur dioxide (SO_2) and aerosols that were not part of TOMS observations. The OMI provides better ground resolution relative to GOME measures O_3 vertical profiles similar to

those measured by Technology Experiment Satellite (TES) and Microwave Limb Sounder (MLS). Moreover, OMI also detects volcanic ash, SO_2 produced in volcanic eruptions at approximately 100 times more sensitivity than TOMS (https://aura.gsfc.nasa.gov). More information on OMI retrieval method is discussed in chapter 4.

1.5.2 Atmospheric Infrared Souder (AIRS) instrument

The AIRS (Figure 3) is one of six instruments on board the National Aeronautics and Space Administration (NASA) Aqua satellite. The instrument was introduced to support climate research and improve weather forecasting. Hence, it monitors the atmospheric composition, greenhouse gases, air quality, humidity profiles, atmospheric profiles and land surface temperature observations. Calibrations are conducted inside the flight during scan period. The AIRS O_3 vertical profiles are on 28 levels from 1100 hPa to 0.1 hPa. More details on AIRS method is given by Susskind et al. (2003) and also discussed in chapter 4. This study uses version 4 level 2 data which are available from Giovanni.

1.5.3 The Modern-Era Retrospective Analysis for Research and Applications, version 2 (MERRA-2)

The MERRA-2 was introduced in October 2004 to improve MERRA assimilation challenges and to continue with the Global Modeling and Assimilation Office (GMAO) commitment in having a continuous near real time climate analysis (Galaro et al., 2017). The MERRA-2 have additional observing system as compared with the former, e.g., MERRA-2 uses MLS O_3 vertical profiles and OMI TCO for assimilation. The MERRA-2 employs version 5.12.4 of the Goddard Earth Observing System (GEOS) atmospheric system (Rienecker et al., 2008; Molod et al., 2015) and the Gridpoint Statistical Interpolation (GSI) analysis scheme (Wu et al., 2002; Kleist et al., 2009b) for assimilation. The model assimilates data from different satellites such as MLS, OMI, Infrared Atmospheric Sounding Interferometer (IASI), Meteorological Operational Satellite-A (MetOP-A) and other satellites. Further information on MERRA-2 is provided in chapter 4.

1.6 Thesis outline

This thesis is made out of six chapters. One of the result chapters (chapter 3) was already published in an international recognized peer-reviewed journal (MDPI Atmosphere). Another chapter (chapter 4) was submitted to local peer-reviewed journal (South African Journal of Geography) for publication. Lastly, chapter 5 was submitted to South African Society for Atmospheric Sciences (SASAS) annual conference proceedings and Clean Air Journal. Therefore, there might be duplications and overlap of this chapter with the subsequent chapters.

Chapter 1 presents the introduction, study's aims and objectives. Chapter 2 introduce the concept and details about 'O_3 layer' destruction, STE and its dynamics and tropospheric O_3 chemistry followed by effects of O_3 in humans and environment. Chapter 3 commences with the balloon-borne ozonesondes measurement technique. Additionally, this chapter uses O_3 vertical profiles to investigate high O_3 events and to conduct statistical analysis of stratosphere-troposphere O_3 exchange events, followed by O_3 changes at different altitudes. Chapter 4 covers the Dobson and Satellite TCO observation techniques, followed by validation of Stellenbosch Dobson TCO with OMI-TOMS, OMI-DOAS and AIRS TCO observations. Furthermore, the relative difference between satellites (OMI-TOMS, OMI-DOAS and AIRS satellites) and Dobson TCO observations was calculated. Lastly, this chapter presents the TCO climatology observed by Dobson and satellites over Stellenbosch. Chapter 5 presents Cape Point weekday-weekend, seasonal and annul O_3 changes by using all-day, day and night-time surface O_3 data. Wind and radon data was also used to investigate the influence of meteorology on O_3 mole fractions. An extreme maximum and minimum observed O_3 values are identified and a case study has been conducted. Chapter 6 provides with summary and conclusions, followed by future work and recommendations.

References

1. Anderson, J. G., Toohey, D. W. and Brune, W. H. Free radicals within the Antarctic vortex: the role of CFCs in Antarctic ozone loss. *Science*, 1991, 251, 4989, 39–46.

2. Andersen, R., Molgaard, C., Skovgaard, L.T., Brot, C., Cashman, K.D., Chabros, E., Charzewska, J., Flynn, A., Jakobsen, J., Karkkainen, M., Kiely, M., Lamberg-allardt, C., Moreiras, O., Natri, A.M., O'brien, M., Rogalska-niedzwiedz, M. and Ovesen. L. Teenage girls and elderly women living in northern Europe have low winter vitamin D status. *Euro. J. Clin. Nutr*., 2005, 59, 533–541.

3. Andersen, S. and Sarma, M. Protecting the Ozone Layer. The United Nations History, 2002, *Earthscan Publicatios* Ltd., Virginia.

4. Angell, J.K. and Korshover, J. Quasi-Biennial and Long-Term Fluctuations in Total Ozone. *Mon. Weather Rev*., 2005, 101, 426-43.

5. Anwar, F., Chaudhry, F.N., Nazeer, S., Zaman, N. and Azam, S. Causes of Ozone Layer Depletion and Its Effects on Human: Review. *ACS*, 2016, 6, 129-134. http://dx.doi.org/10.4236/acs.2016.61011.

6. Dobson, G.M.B. Origin and distribution of polyatomic molecules in the atmosphere. *Proc. R. Soc*., 1956, A236, 187–193.

7. Dobson, G.M.B. Forty years' research on atmospheric ozone at Oxford: a history. *Appl. Optics*, 1968, 7, 387–405.

8. Gelaro, R., McCarty, W., Suárez, M.J., Todling, R., Molod, A. and Takacs, L., Randles, C., Darmenov, A., Bosilovich, M.G., Reichle, R., Wargan, K., Coy, L., Cullather, R., Draper, C., Akella, S., Buchard, V., Conaty, A., da Silva, A., Gu, W., Kim, G.K., Koster, R., Lucchesi, R., Merkova, D., Nielsen, J.E., Partyka, G., Pawson, S., Putman, W., Rienecker,

M., Schubert, S.D., Sienkiewicz, M. and Zhao, B. The Modern-Era Retrospective analysis for Research and Applications, Version 2 (MERRA-2). *J. Clim*. 2017, 30, 14, 5419–5454. https://doi.org/10.1175/JCLI-D-16-0758.1.

9. Hassler, B. Bodeker, G.E. Solomon, S. and Young, P.J. Changes in the polar vortex: Effects on Antarctic total ozone observations at various stations. *Geophys. Res. Lett.*, 2011, 38. 1, ID L01805.

10. Intergovernmental Panel on Climate Change, Climate Change (IPCC). The Scientific Basis – Contribution of Working Group I to the Third Assessment Report of the Intergovernmental Panel on Climate Change, Houghton, J.T., Ding, Y., Griggs, D.J., Noguer, M., van der Linden, P.J., Dai, X., Maskell, K. and Johnson, C.A. (eds), pp. 881, Cambridge University Press, New York, 2001.

11. Kinney, P.L., Thurston, G.D. and Raizenne M. The effects of ambient ozone on lung function in children: A reanalysis of six summer camp studies. *Environ. Health Persp*., 1996, 104, 2, 170-174.

12. Kleist D. T., D. F. Parrish, J. C. Derber, R. Treadon, W.-S. 1531 Wu, and S. Lord, 2009b: Introduction of the GSI into the NCEPs Global Data Assimilation System. Wea. Forecasting, 24, 1691–1705.

13. Liou, K.N. An introduction to atmospheric radiation. Vol. 84, Academic press, 2002.

14. Molina, M.J. and Rowland, F.S.: Stratospheric sink for chlorofluoromethanes: chlorine atomc-atalysed destruction of ozone. *Nature*, 249, 810–812, 1974.

15. Nazir, F. and Zaman, N. Causes of Ozone Layer Depletion and Its Effects on Human: Review, *ACS*., 2016. 129-134, https://www.researchgate.net/publication/292071680.

16. Proffitt, M.H., Margitan, J.J., Kelly, K.K., Loewenstein, M., Podolske, J.R. and Chan, K.R. Ozone loss in the Arctic polar vortex inferred from high-altitude aircraft measurements. *Nature*, 1990, 347, 6288, 31–36.

17. Rienecker and Coauthors, 2011: MERRA - NASA's Modern-Era Retrospective Analysis for Research and Applications. J. Climate, 24, 3624–3648, doi:10.1175/JCLI-D-1641 11-00015.1.

18. Schott, J.R. (2007) REMOTE sensing: The image chain approach. 2nd Edition, Oxford University Press, Oxford, 1.

19. Shindell, D.T., Rind, D. and Lonergan, P. Increased Polar Stratospheric Ozone Losses and Delayed Eventual Recovery Owing to Increasing Greenhouse-Gas Concentration. *Nature*, 1998, 292, 589-592. http://dx.doi.org/10.1038/33385.

20. Solomon, S. Stratospheric ozone depletion: A review of concepts and history. *Rev. Geophys*., 1999, 37, 275–316.

21. Susskind, J., Barnet, C.D. and Blaisdell, J.M. Retrieval of atmospheric and surface parameters from AIRS/AMSU/HSB data in the presence of clouds, IEEE Trans. *Geosci. Remote Sens*., 2003, 41, 390–409, doi:10.1109/TGRS.2002.808236.

22. Tian, J. and Juan, Y. Changes in Ultrastructure and Responses of Antioxidant Systems of Algae (*Dunaliella salina*) during Acclimation to Enhanced Ultraviolet-B Radiation. Journal of Photochemistry and Photobiology B: *Biology*, 2009, **97**, 152-160. http://dx.doi.org/10.1016/j.jphotobiol.2009.09.003.

23. Walton N. (2005). Characterisation of Cape Town Brown Haze, School of Geography, Archaeology and Environmental studies, University of Witwatersrand, Johannesburg. Dissertation.

24. Wargent, J.J. and Jordan, B.R. From Ozone Depletion to Agriculture: Understanding the Role of UV Radiation in Sustainable Crop Production. *New Phytol*., 2013, 197, 1058-1076. http://dx.doi.org/10.1111/nph.12132.

25. Waugh, D.W. and Polvani, L.M. Stratospheric polar vortices. *Geophys. Monogr. Ser.*, 2010, 190, 1, 43–57, 2010.

26. World Meteorological Organization (WMO). Scientific Assessment of Ozone Depletion: 2002. Global Ozone Research and Monitoring Project – Report No. 47, 498 pp, Geneva, 2003.

27. Wu, W.S., Purser, R.J. and Parrish, D.F. Three-dimensional variational analysis with spatially inhomogeneous covariances. *Mon. Wea. Rev*., 2002, 130, 2905–2916.

28. https://aura.gsfc.nasa.gov/omi.html - date retrieved 23 March 2020.

29. https://www.epa.gov/ozone/strathome.html - date retrieved 23 March 2020.

CHAPTER 2: THEORETICAL FRAMEWORK

This chapter presents stratospheric O_3 chemistry, O_3 sources and sinks, vertical and horizontal O_3 distribution, stratospheric-tropospheric O_3 exchange and its dynamic processes, O_3 layer depletion process, effect of meteorology on O_3, environmental impacts of low O_3 mole fractions in the stratosphere and high O_3 mole fractions in the troposphere and ambient O_3 standards.

2 Ozone distribution in the atmosphere

2.1 Total Column Ozone

The Total Column Ozone (TCO) is defined as the total amount of O_3 molecules in a column of air measured from the surface to the top of the atmosphere (https://niasra.uow.edu.au). As indicated in Figure 2.1, the TCO varies according to seasons and geographical location. O_3 production requires sufficient amount of solar radiation. Hence, TCO is mainly produced in the equatorial regions where there is high solar radiation. However, TCO mole fractions are not high in equatorial regions as compared with other regions (Bekki and Lefevre, 2009). Atmospheric circulation and winds play an important role in TCO seasonal cycle. Hence, O_3 accumulates near the poles and far from the equatorial region (Bekki and Lefevre, 2009). In addition, the TCO maximum peak is observed in winter and spring (solar radiation is minimum) in high and mid-latitude. It is observed that the stratospheric O_3 distribution is not only driven by photochemistry. The photochemistry and dynamics in the temporal and spatial variability of O_3 depends on altitude. For example, the photochemical lifespan of O_3 is from few hours to days from 40 km to the stratopause. Due to the short lifespan at these altitude, the transport processes can be neglected because they operate on larger timescales. On the other hand, in the lower stratosphere (between tropopause and 30 km) O_3 lifespan range from few days to a couple of months. Hence, in this region, dynamic movements control the variability of O_3. Due to this reason, high O_3 mole fractions are located in the lower stratosphere and carried to the middle and high latitudes by winds (Bekki and Lefevre, 2009).

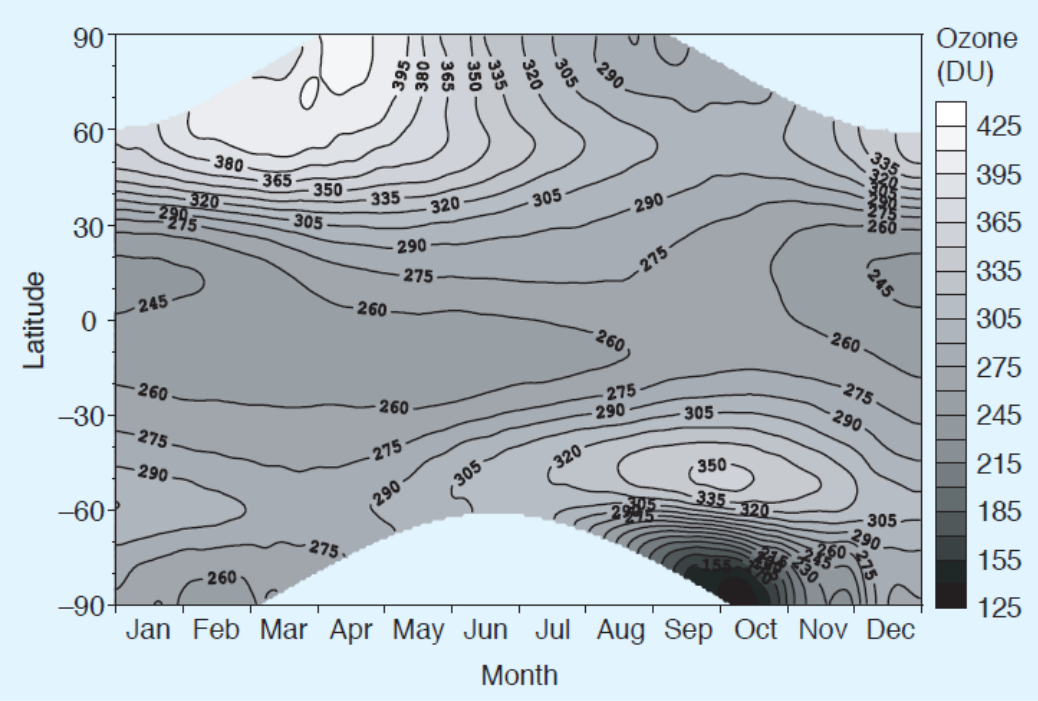

Figure 2.1: TOMS and GOME total column ozone climatology plotted as a function of latitude and month (Obtained from Bodeker et al. 2001).

2.2 Vertical ozone distribution

As mentioned in the above section, O_3 is mostly produced in the tropics because of high solar radiation that is found in the tropics. However, high O_3 mole fractions are found outside the tropical regions (higher latitudes). The vertical distribution indicates low O_3 mole fractions in the troposphere that increases sharply from the tropopause to reach a maximum in the lower stratosphere (15 km to 20 km) and decreases rapidly above 30 km (Figure 2.2). This also indicates the importance of atmospheric movements carrying O_3 from the source region to the poles (Bekki and Lefevre, 2009). Ozone mole fraction is maximum at 15 to 20 km because stratospheric air is carried from the equator to the poles through Brewer-Dobson circulation. The Brewer-Dobson circulation was named after Brewer (1949) and Dobson (1956). The Brewer-Dobson circulation consists of three processes. The first process is the upward movement of O_3 from the tropical troposphere to the stratosphere. The second process is the transport of O_3 from the tropical stratosphere to the poles. The third process is the downward movement of O_3 from the stratosphere in the middle and polar latitudes (Bekki and Lefevre, 2009). In the stratospheric

middle latitudes, descending air is transported into the troposphere. On the other hand, descending air in the polar latitudes is transported into the polar lower stratosphere, where it accumulates. Therefore, the poleward and downward circulation in the middle and high latitudes is the reason for the O_3 increase in the lower stratosphere. Brewer-Dobson circulation results from wave motions in the extratropical stratosphere. One of the atmospheric wave is called Rossby wave. These waves result from a combination of meridional temperature gradients and the rotation of the planet. Another important dynamic process is related to polar vortex. There is lack of sunlight and strong meridional temperature gradients are low in Polar Regions during winter. This result to the formation of westerly jet streams in the stratosphere at the end of the strong meridional temperature gradients. While polar vortex is formed inside the low pressure area inside jet streams. The function of polar vortex is to separate polar stratospheric air masses from its surroundings. Secondly, the reason for high O_3 at 15 to 20 km is related to longer lifespan of O_3 molecule in the middle and high latitudes. Ozone is produced through the photolysis of O_2 mole to two O atoms. This is followed by the reaction of O_2 mole and O atom to produce O_3 molecule. The lower stratosphere is characterised by few O atoms because of less UV radiation in this region (Bekki and Lefevre, 2009). Most of the required UV radiation is absorbed at higher altitudes. Therefore, O_3 is not easily destroyed in the lower stratosphere.

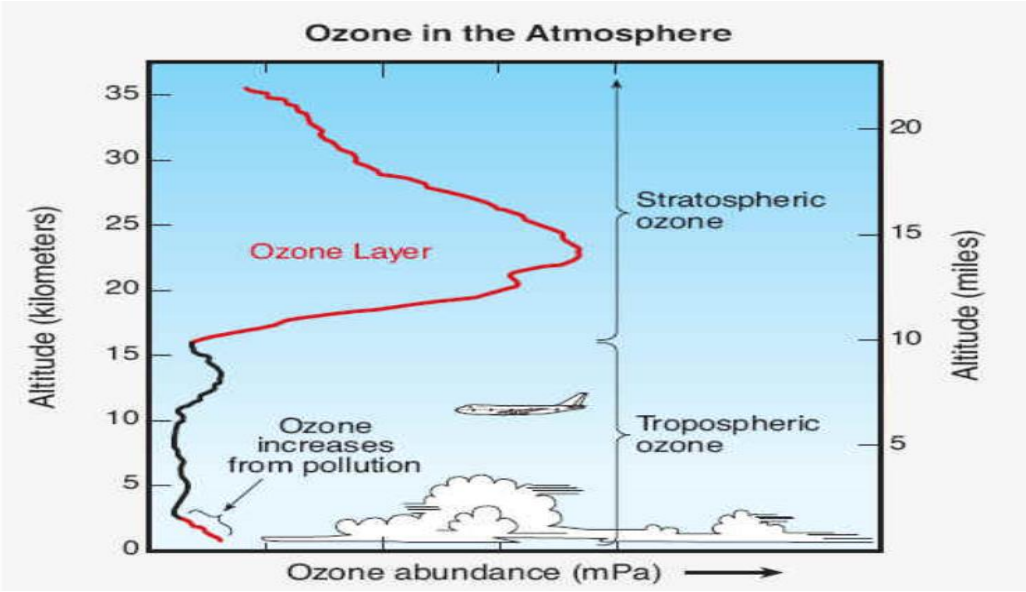

Figure 2.2: Vertical ozone distribution in the atmosphere (Obtained from WMO, 2007).

2.3 Stratospheric Ozone

2.3.1 Stratospheric ozone formation

O_3 is naturally formed in the stratosphere through reactions involving oxygen molecules (O_2). The first reaction (R.1) is the photolysis of oxygen molecule to form two oxygen atoms (O). This reaction only occurs below 242 nm wavelength. The second reaction is the reaction involving two oxygen atoms that reacts with an oxygen molecule to form two O_3 molecules (Figure 4). Where M in reaction R.2 represents main components in the atmosphere (oxygen or nitrogen). The overall process includes three oxygen molecules to form two O_3 molecules (Chapman, 1930).

$O_2 + h\nu \rightarrow O + O \qquad \lambda<242nm \qquad (R.1)$

$O + O_2 + M \rightarrow O_3 + M\ (+\Delta Q) \qquad (R.2)$

2.3.2 Stratospheric ozone photolysis

At wavelength below 310 nm, oxygen atom in excited state O (^1D) and oxygen molecules are formed from O_3 photolysis (R.3). Thereafter, the oxygen atom in excited state reacts with main components in the atmosphere (N_2 and O_2) and form oxygen atom in ground state O (^3P). The wavelength above 310 nm, O_3 photolysis forms oxygen atom in ground state and three oxygen molecules. (R.4) (Chapman, 1930).

$O_3 + h\nu \rightarrow 3O_2 + O(^1D) \qquad \lambda < 310\ nm \qquad (R.3)$

$O(^1D) + N_2 \rightarrow O(^3P) + N_2$

$O(^1D) + O_2 \rightarrow O(^3P) + O_2$

$O_3 + h\nu \rightarrow 3O_2 + O(^3P) \qquad \lambda > 310\ nm \qquad (R.4)$

2.4 Ozone layer depletion

According to Kowalok (1993), the total O_3 of approximately 90% is found in the stratosphere (approximately 10 to 50 km) while the remaining 10% is found in the troposphere. The term 'ozone hole' is used when normal total O_3 concentration (300 to 350 DU) decrease to 220 DU. According to Gardiner (1988), the observed O_3 decrease over Antarctica occurs in winter (begins in late August and reach a minimum in mid-October). A number of studies have been conducted

to understand the underlying reason for the occurrence of 'O_3 hole' over Antarctica. Studies such as Bekkie et al. (1991) associated O_3 decline with solar cycle and radiation. While Jana and Nandi (2005) reported that O_3 is not depleted rather distributed in the atmosphere. Other studies associated O_3 depletion with different chemical reactions such as O_x (Chapman, 1930), Cl_x and ClO_x (Molina and Rowland, 1974), Br and BrO_x (Wofsy et al, 1975), ClO_x and BrO_x (Mc Elroy et al, 1986), NO_x (Crutzen and Arnold, 1986) and HO_x (Thomposon, 1992). Halogens are emitted at earth surfaces all over the stratosphere. Most of these gases have no natural removal processes in the lower atmosphere. Halogens enter the stratosphere through the tropical tropopause and transported in the stratosphere and Polar Regions by atmospheric motions. Ozone hole requires low temperatures in order to occur and that's the reason for its occurrence in Antarctica and Arctic regions. These low temperatures are suitable for the formation of polar stratospheric clouds (PSC). Antarctica low temperatures last for approximately five to six months while in Arctic regions they last for few days (ten to sixty days). This is the reason that O_3 hole predominantly occur in Antarctica as compared to Arctic regions. Another important unique atmospheric condition in Polar Regions is that polar stratospheric air is isolated from other stratospheric air. This isolation is observed in winter due to strong winds that surrounds the poles and result to the formation of polar vortex. The polar vortex prevents air movement in and out of polar stratosphere. The formation of polar vortex strengthens in winter when temperatures are low. More discussion of stratospheric O_3 depletion related to hydroxyl radical, hydroperoxyl radical, chlorine, bromine and nitrous oxide is provided in section 2.4.1 to 2.4.4.

2.5 Ozone destruction

O_3 destruction in the stratosphere involves a number of destructive substances such as hydroxyl radical, hydroperoxyl radical, chlorine, bromine and nitrous oxide. The following cycles describes the O_3 destruction:

2.5.1 Cycle X

The following reactions (R.5 and R.6) occur above 30 km. In the stratosphere, X represents hydroxyl radical (OH), nitrogen oxide (NO), chlorine (Cl) or bromine (Br). The first reaction is the destruction of O_3 molecule (O_3) by either OH, NO, Cl or Br to form oxygen molecule (O_2) and hydroperoxyl radical (HO_2), nitrogen dioxide (NO_2), chlorine oxide (ClO) or bromine oxide

(BrO). The formed products reacts with oxygen atom (O) to form oxygen molecule. Cycle X summarizes different catalytic O_3 loss cycles. The following cycles indicate similar steps except that X is replaced with either OH, NO, Cl or Br (Chapman, 1930).

$X + O_3 \rightarrow XO + O_2$ (R.5)

$XO + O \rightarrow OX + O_2$ (R.6)

Net: $O_3 + O \rightarrow 2O_2$

2.5.2 Hydrogen cycle

Two hydroxyl radicals (OH) are formed from the reaction of water vapour (H_2O) and oxygen atom in excited state (R.7). Reaction R.8 indicates the formation of the hydroperoxyl radical (HO_2) from the destruction of O_3 molecule by hydroxyl radical. The hydroperoxyl radical in reaction R.9 reacts with oxygen atom to form the hydroxyl radical and two oxygen molecules. The overall reaction is the formation of two oxygen molecules from the reaction of an O_3 molecule and oxygen atom (Bates and Nicolet 1950; Nicolet, 1970). Hydroxyl radical is formed through the oxidation of methane (CH_4) and other hydrogenated compounds.

$O(^1D) + H_2O \rightarrow OH + OH$ (R.7)

$OH + O_3 \rightarrow HO_2 + O_2$ (R.8)

$HO_2 + O \rightarrow OH + O_2$ (R.9)

Net: $O_3 + O \rightarrow 2O_2$

As indicated in reaction 11, hydroperoxyl radical formed in reaction R.10 reacts directly with O_3 molecules in the lower altitudes to form two oxygen molecules and hydroxyl radical.

$OH + O_3 \rightarrow HO_2 + O_2$ (R.10)

$HO_2 + O_3 \rightarrow OH + O_2 + O_2$ (R.11)

Net: $O_3 + O_3 \rightarrow 3O_2$

2.5.3 Chlorine cycle

The following reactions describe the depletion of O_3 layer by chlorofluorocarbons (CFCs). The main sources of chlorine are methyl chloride (CH_3Cl), trichlorofluoromethane ($CFCl_3$ (CFC-11)) and dichlorofluoromethane (CF_2Cl_2 (CFC-12)). As indicated in reaction R.12, the CFC molecule absorbs ultra violet radiation to form chlorine (Cl) atoms. The formed reactive chlorine breaks down O_3 molecule to form chlorine oxide (ClO) and oxygen molecule (reaction R.13). Due to the slow movement of CFCs and their long lifespan in the atmosphere, O_3 destruction is not observed immediately after CFCs are released in the atmosphere (reaction R.14). Figure 2.3 shows the release of chlorine in the atmosphere and the destruction of O_3 molecule resulting in more ultra violet (UV) radiation reaching the troposphere and cause negative effects on humans and environment (Molina and Molina, 1987).

$CCl_3F + h\nu \rightarrow CCl_2F + Cl$ (R.12)

$Cl + O_3 \rightarrow ClO + O_2$ (R.13)

$ClO + O \rightarrow Cl + O$ (R.14)

Net: $O_3 + O \rightarrow 2O_2$

Figure 2.3 indicates the natural formation of chlorine over Antarctica. In austral summer, there is no light, temperatures are very low and Polar Stratospheric Clouds (PSC) are formed over Antarctica. The PSC activate chlorine as chlorine radical (Cl^-) and chlorine oxide (ClO). Ice crystals destroy O_3 and CFC accumulate in the atmosphere (Bekki and Lefevre, 2009). Reactive chlorine atoms are formed in the presence of light and destroys the O_3 layer.

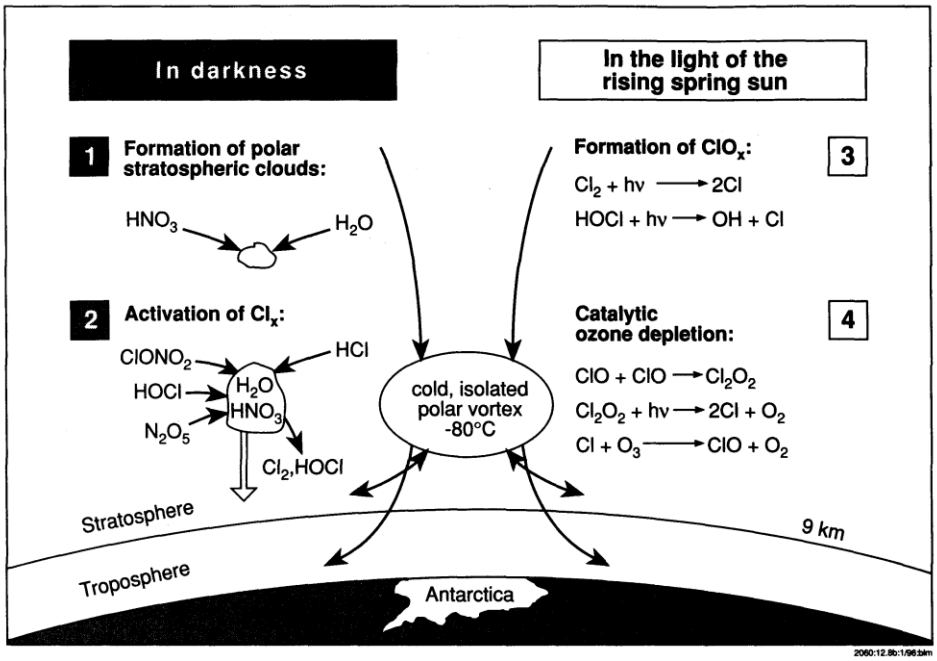

Figure 2.3: Natural destruction of stratospheric ozone. (Obtained from https://earth.esa.int).

2.5.4 Bromine cycles

Bromine is formed in the stratosphere from the photolysis and oxidation of brominated compounds by hydroxyl radical. Even though the brominated compounds are emitted from the surface, they have a long lifespan and reach the stratosphere. Brominated compounds are emitted in the atmosphere naturally or through industrial activities. The most abundant bromides are the methyl bromide with a lifespan of approximately one year that gives it enough time to reach the lower stratosphere. In addition to the brominated compounds, brominated hydrocarbon compounds such as halons also reach the stratosphere. The most abundant brominated hydrocarbon compounds are CF_2ClBr (H-1211) and CF_3Br (H-1301) with a lifespan of 16 years and 65 years, respectively. Reaction R.15, R.16, R.17 and R.18 indicates the sequential destruction of O_3 by bromine (Tung et al., 1986; McElroy et al., 1986).

$BrO + ClO \rightarrow Br + ClO_2$ (R.15)

$ClO_2 + M \rightarrow Cl + O_2$ (R.16)

$Br + O_3 \rightarrow BrO + O_2$ (R.17)

$Cl + O_3 \rightarrow ClO + O_2$ (R.18)

Net: $2O_3 \rightarrow 3O_2$

2.5.5 Nitrogen cycle

Nitrous oxide (N_2O) is the main source of nitrogen oxides in the stratosphere. Reaction R.19 indicates the formation of two nitrogen oxides (NO) through the reaction of nitrous oxide and oxygen atom in the excited state (Hampson, 1964). This reaction represent less than 5% of nitrous oxide destruction in the atmosphere.

$N_2O + O(^1D) \rightarrow NO + NO$ (R.19)

Nitrogen oxide reacts directly with O_3 to form nitrogen dioxide (NO_2) and oxygen molecule (reaction R.20). Reaction R.21 indicates the reaction of nitrogen dioxide with oxygen atom to form nitrogen oxide and oxygen molecule. The overall reaction is the formation of two oxygen molecules from O_3 destruction.

$NO + O_3 \rightarrow NO_2 + O_2$ (R.20)

$NO_2 + O \rightarrow NO + O_2$ (R.21)

Net: $O_3 + O \rightarrow 2O_2$

2.6 Tropospheric Ozone

O_3 is not emitted directly in the atmosphere. In the troposphere, O_3 is the secondary pollutant formed through the reactions of nitrogen oxides (NO_x), volatile organic compounds (VOCs), methane (CH_4), and carbon monoxide (CO) in the presence of sunlight (Seinfeld and Pandis, 1998; Crutzen, 1974; Atkinson, 2000). In addition, air containing high O_3 mole fractions can be transported from the stratosphere to the troposphere, through a process called stratosphere-troposphere exchange (Olsen et al., 2002). Figure 2.4 indicates sources and sinks of tropospheric O_3. Approximately 4500 Tg per year of O_3 is formed from chemical production on a global scale. O_3 affects the global radiation of the atmosphere (Forster et al., 2007).

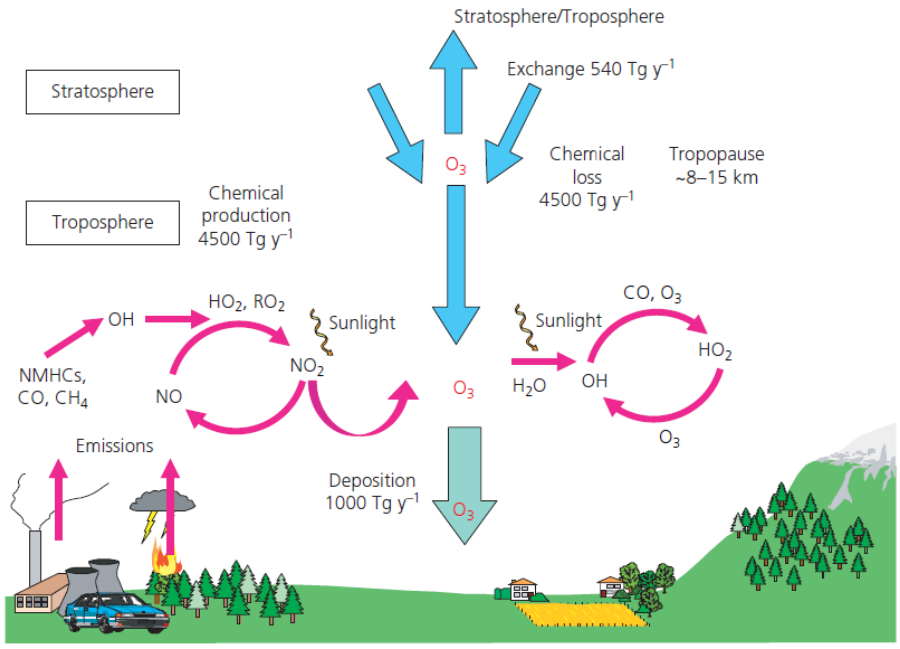

Figure 2.4: Scheme of the sources and sinks of tropospheric ozone (Obtained from Denman et al., 2007).

2.7 Stratospheric-Tropospheric Exchange

The stratosphere and troposphere have different chemical and dynamic processes. The troposphere is characterized by low O_3, low potential vorticity, high carbon monoxide and humidity while high O_3, high potential vorticity, low carbon monoxide and humidity exists in the stratosphere. During STE, air can either ascends from the troposphere to the stratosphere (TST) or descends from the stratosphere to the troposphere (STT). The TST events are observed in the tropics and also at high latitudes through the extratropical tropopause (Dessler et al., 1995). On the other hand, the STT events are observed everywhere but dominant in the mid-latitudes. The air movement from the troposphere to the stratosphere and from stratosphere to troposphere is irreversible (Hintsa et al., 1998; Papayannis et al., 2005). Newell, (1963) and Danielsen, (1968) associated STEs events with the occurrence of jet streams and tropopause folds and large-scale overturning of the stratosphere (Brewer, 1949; Holton et al., 1995). These jet streams are the polar jets that occur approximately 9 to 12 km above sea level while subtropical jets occurs at approximately 10 to 16 km above sea level. While other studies associated the occurrence of STEs with cut of lows (Ancellet et al., 1994), thunderstorms (Tremblay and Servranckx, 1993),

breaking of gravity waves (Lamarque et al., 1996) and mesoscale convective complexes (Poulida et al., 1996). Jet streams are the polar jets that occur approximately 9 to 12 km above sea level while subtropical jets occurs at approximately 10 to 16 km above sea level. According to Holton (1992) and Bluestein (1993), the subtropical jet streams are found at the pole ward edge of the Hardley circulation while polar jet streams are found in the region above the polar front (Figure 2.5). Stratospheric intrusion events can be identified by a rapid decrease of relative humidity and an increase in O_3 mole fractions (Cui et al., 2009). Stratosphere-troposphere exchange plays an important role in atmospheric chemistry by changing the oxidative capacity of the troposphere (Kentarchos and Roelofs, 2003) and potentially affect the climate system because O_3 and water vapour are potent greenhouse gases (Forster et al. 2007). The STE contributes approximately 550±140 Tg per year to the net global O_3 budget (Olsen et al., 2001; McLinden et al., 2000). On the other hand, Denman et al. (2007) reported that STEs contribute 540 Tg per year to the tropospheric O_3 budget.

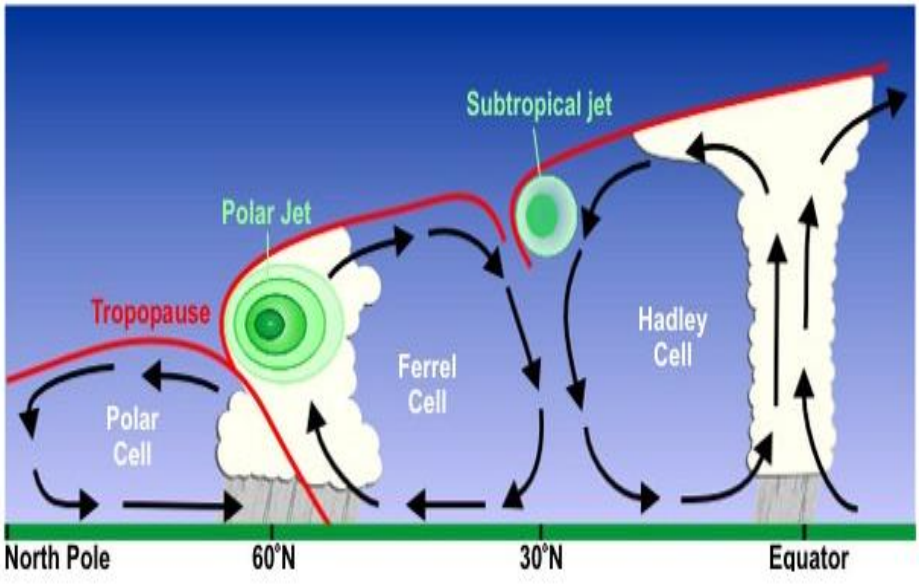

Figure 2.5: Location of subtropical and polar jets (Obtained from http://www.srh.noaa.gov).

2.8 Ozone Sinks

Ozone sinks in the atmosphere include the following:

- Dry and wet deposition

Dry deposition is defined as the direct uptake of trace gases by soil, water or vegetation and wet deposition is defined as absorption of trace gases followed by droplet precipitation or fog precipitation (Seinfeld and Pandis, 2012). Dry deposition of O_3 occurs in water surfaces and land. However, there are uncertainties in quantifying ocean dry deposition. O_3 dry deposition is found to be 98.4 ± 4.5 Tg O_3 per year for the ocean and a total of 722.8 ± 20.9 Tg O_3 per year globally (Luhar et al., 2017). Dry deposition affects forests more than vegetation (Fowler et al., 1999). O_3 dry deposition may disturb the hydrological cycle and key biogeochemical cycles, including carbon and nitrogen cycles (Schreuder et al., 2001; Paoletti and Grulke, 2010; Hoshika et al., 2015; Franz et al., 2017). In general, O_3 exposure might affect the global terrestrial biodiversity (Fuhrer et al., 2016).

- Ozone photolysis

Reaction R.22 indicates the photolysis of O_3 by ultraviolet radiation. The second step of O_3 photolysis (reaction R.23) is the formation of two hydroxyl radicals (Chapman, 1930).

$$O_3 + h\nu \rightarrow O_2 + O\ (< 340\ nm) \qquad (R.22)$$

$$O + H_2O \rightarrow 2OH \qquad (R.23)$$

- Ozone destruction

Reaction R.24 and R.25 indicate O_3 destruction by hydroxyl radical (OH) and hydroperoxyl radical (HO_2). The formation of OH and HO_2 was previously discussed in section 2.4.2.

$$O_3 + OH \rightarrow O_2 + HO_2 \qquad (R.24)$$

$$O_3 + HO_2 \rightarrow 2O_2 + OH \qquad (R.25)$$

The lifetime of O_3 is greater in the middle and upper troposphere due to a drier atmosphere than in the continental or marine boundary layer where O_3 molecules survive for 2 to 5 days.

2.9 The effects of meteorology on tropospheric ozone

Meteorological parameters such as wind direction, wind speed, humidity, solar radiation, temperature and cloud cover plays important role in O_3 reactions and its transport to surrounding areas. Winds with low speed, high solar radiation, high temperatures, and low humidity generally promote O_3 increase. Carvalho et al. (2010) and Shan et al. (2009) observed a positive correlation between O_3 mole fractions with temperature while a negative correlation was observed with relative humidity. Furthermore, Shan et al. (2009) also reported a positive correlation between O_3 mole fractions with solar radiation and wind speed. In addition, wet, rainy weather with high

relative humidity is typically associated with the low O_3 concentrations provided by wet O_3 deposition on the water droplets (Tarasova and Karpetchko, 2003). Whereas, Zhang et al. (2017); Shan et al. (2009); Pires et al. (2012) and Chen et al. (2011) observed lower O_3 mole fractions on periods of high NO, NO_2 concentrations and lower temperatures.

2.10 Negative effects of low stratospheric and high tropospheric ozone in human

High O_3 mole fractions in the troposphere have negative effects on human and environment. Previous studies have reported O_3 related morbidities such as bronchitis, asthma, appendicitis (Anenberg et al., 2010; Anenberg et al., 2011; Anenberg at al., 2013), appendicitis (Kaplan et al., 2013),venous thromboembolic disease, and pulmonary embolisms(Dales et al., 2010). Some of the studies have predicted a global increase of 0.75 million per year in premature deaths due to surface O_3 by 2050 (OECD, 2012). Modelling studies on tropospheric O_3 suggests that O_3 increase in developing countries by 2050 while studies in O_3 precursors and climate change suggest O_3 decrease in developed countries by 2050 due to differences in future emissions (Lei et al., 2012). High surface O_3 mole fractions of 70 to 100 ppb cause reduction in plant yields (Leisne et al., 2012). In general, productivity and yields of crops may decrease due to high surface O_3 mole fractions**.** High levels of UV due to low O_3 in the stratosphere increases the possibility of skin cancer, causes sunburns and eye damage to humans.

2.11 Summary

It can be summarized that dynamic factors are very important in O_3 vertical and horizontal distribution. Brewer-Dobson circulation play an important role in the transportation of O_3. Stratosphere-troposphere exchange contributes to the observed troposphere O_3 budget. Moreover, dynamic factors such as Rossby waves, polar vortex play an important role in stratosphere-troposphere exchange. There are many factors that control O_3 mole fractions in the atmosphere. These include the influence of industrial and vehicular emissions, lightning, biomass burning, biogenic release, stratospheric-tropospheric exchange, photolytic destruction and dry deposition. These factors can affect both the short and long-term O_3 trends. Therefore, it is very important to consider these factors when conducting O_3 studies. High mole fractions of O_3 exceeding 60 ppb have a negative effect on human and environment.

References

1. Ancellet, G., Beekman, M., Papayannis, A., 1994. Impact of a cut off low development on downward transport of ozone in the troposphere. *J. Geophys. Res.,* 99, 3451-3468.

2. Anenberg, S.C., Horowitz, L.W., Tong, D.Q. and West, J.J. An estimate of the global burden of anthropogenic ozone and fine particulate matter on premature human mortality using atmospheric modelling. *Environ. Health Perspect*., 2010, 118, 1189–1195.

3. Anenberg, S.C., Schwartz, J., Shindell, D., Amann, M., Faluvegi, G., Klimont, Z., Janssens-Maenhout, G., Pozzoli, L., Van Dingenen, R., Vignati, E., Emberson, L., Muller, N.Z., West, J.J., Williams, M., Demkine, V., Hicks, W.K., Kuylenstierna, J., Raes, F. and Ramanathan, V. Global air quality and health co-benefits of mitigating near-term climate change through methane and black carbon emission controls. *Environ. Health Perspect*., 2012, 120, 831–839.

4. Anenberg, S.C., West, J.J., Horowitz, L.W. and Tong, D.Q. The global burden of air pollution on mortality: Anenberg et al. respond. *Environ. Health Perspect*., 2011, 119, 4, A158– A159.

5. Atkinson, R. Atmoshperic chemistry of VOCs and NOx. *Atmos. Environ*., 34, 2063–2101, 2000.

6. Bates, D.R. and Nicolet, M. The photochemistry of atmospheric water vapor, *J. Geophys. Res.* 1950, 55, 301–327.

7. Bekki, S., Towmi, R., Pyle, J.A. and Jones, A.E. Future aircraft and global ozone. *Nature (UK)*, 1991, 354, 193-194.

8. Bekki, S and Lefevre, F. Stratospheric ozone. History and concepts and interactions with climate. *Eur. Phys. J. Conferences*, 2009, 1, 113–136 (2009). doi: 10.1140/epjconf/e2009-00914-y.

9. Bluestein, H.B. Synoptic-Dynamic Meteorology in Midlatitudes, Vol. 2, Observations and Theory of Weather Systems, 594 pp., Oxford Univ. Press, New York, USA, 1993.

10. Bodeker, G.E., Scott, J.C., Kresher, K. and McKenzie, R.L. Global Ozone Trends in Potential Vorticity Coordinates Using TOMS and GOMEE Inter–Compared Against the Dobson network, *J. Geophys. Res*., 2001, 106, 23029–23042.

11. Brewer, A.W. Evidence for a world circulation provided by the measurements of helium and water vapour distribution in the stratosphere, *Q. J. R. Meteorol. Soc*., 1949, 75, 326, 351–363.

12. Carvalho, A., Monteiro, A., Ribeiro, I., Tchepel, O., Miranda, A.I., Borrego, C., Saavedra, S., Souto, J.A. and Casares, J.J. High ozone levels in the northeast of Portugal: Analysis and characterization. *Atmos. Environ*., 2010, 44, 1020–1031.

13. Chapman, S. A theory of upper atmospheric ozone. *Mem. Roy. Soc*., 1930, 3, 103–109.

14. Chen, H.H., Stanier, C.O., Young, M.A., Grassian, V.H. A kinetic study of ozone decomposition on illuminated oxide surfaces. *J. Phys. Chem*., 2011, 115, 11979–11987.

15. Crutzen P.J. Photochemical reaction initiated by and influencing ozone in unpolluted tropospheric air. *Tellus*, 1974, 26, 45-55.

16. Crutzen, P.J. and Arnold, F. Nitric acid cloud formation in the cold Antarctic stratosphere : A major cause for the springtime ozone hole. *Nature*, 1986, 324, 651-655.

17. Cui, J., Sprenger, M., Staehelin, J., Siegrist, A., Kunz, M., Henne, S., and Steinbacher, M.: Impact of stratospheric intrusions and intercontinental transport on ozone at Jungfraujoch in 2005: comparison and validation of two Lagrangian approaches, *Atmos. Chem. Phys*., 9, 3371–3383, doi:10.5194/acp-9-3371-2009, 2009.

18. Dales, R.E., Cakmak, S. and Vidal, C.B. Air pollution and hospitalization for venous thromboembolic disease in Chile. *J. Thromb. Haemost*., 2010, 8, 669–674.

19. Danielsen, E.F. Stratospheric-tropospheric exchange based on radioactivity, ozone and potential vorticity, *J. Atmos. Sci*. 1968, 25, 502–518.

20. Dessler, A.E., Hintsa, E.J., Weinstock, E.M., Anderson, J.G. and Chan, K.R. Mechanisms controlling water vapor in the lower stratosphere: "A tale of two stratospheres". *J. Geophys. Res*., 1995, 100(D11), 23167–23176.

21. Denman, K.L., Brasseur, G., Chidthaisong, A., Ciais, P., Cox, P.M., Dickinson, R.E., Hauglustaine, D., Heinze, C., Holland, E., Jacob, D., Lohmann, U., Ramachandran, S., da Silva Dias, P.L., Wofsy, S.C. and Zhang, X. 2007: Couplings Between Changes in the Climate System and Biogeochemistry. In: Climate Change 2007: The Physical Science Basis. Contribution of Working Group I to the Fourth Assessment Report of the Intergovernmental Panel on Climate Change [Solomon, S.,D. Qin, M. Manning, Z. Chen, M. Marquis, K.B. Averyt, M. Tignor and Miller, H.L. (eds.)]. Cambridge University Press, Cambridge, United Kingdom and New York, NY, USA.

22. Dobson, G.M.B. Origin and distribution of polyatomic molecules in the atmosphere. *Proc. R. Soc*., 1956, A236, 187–193.

23. Forster, P., Ramaswamy, V., Artaxo, P., Berntsen, T., Betts, R., Fahey, D.W., Haywood, J., Lean, J., Lowe, D.C., Myhre, G., Nganga, J., Prinn, R., Raga, G.M.S. and Van Dorland, R. Changes in atmospheric constituents and rediative forcing. Climate change 2007: The

physical Scientific Basis, Cambridge University Press, Cambridge, United Kingdom and New York, NY, USA, 6pp, 2007.

24. Fowler, D., Cape, J.N., Coyle, M., Flechard, C., Kuylenstierna, J., Hicks, K., Derwent, D., Johnson, C. and Stevenson, D. Water, Air, and Soil Pollution volume 116, pages5–32(1999)The global exposure of forests to air pollutants. *Water Air Soil Pollut*., 1999, 116, 5–32. doi: 10.1023/A:1005249231882.

25. Franz, M., Simpson, D., Arneth, A. and Zaehle, S. Development and evaluation of an ozone deposition scheme for coupling to a terrestrial biosphere model. *Biogeosciences*, 2017, 14, 45–71. doi: 10.5194/bg-14-45-2017.

26. Fuhrer, J., Val Martin, M.V., Mills, G., Heald, C.L., Harmens, H., Hayes, F., Sharps, K., Bender, J. and Ashmore, M.R. Current and future ozone risks to global terrestrial biodiversity and ecosystem processes. *Ecol. Evol*., 2016, 6, 8785–8799. doi: 10.1002/ece3.2568.

27. Gardiner, B.G. Comparative morphology of the vertical ozone profile in the Antarctic spring. *Geophys. Res. Lett*., 1998, 15, 901-904.

28. Hampson, J. Photochemical behaviour of the ozonelayer. Tech. rep., Canadian Armament Research and Development Establishment, CARDE technical note, 1964, 1627.

29. Hintsa, E.J. Troposphere-to-stratosphere transport in the lower most stratosphere from measurements of H2O, CO2, N2O and O3. *Geophys. Res. Lett*., 1998, 25(14), 2655–2658.

30. Holton, J.R. An Introduction to Dynamic Meteorology, 511 pp., Elsevier, New York, USA, 1992.

31. Holton, J.R., Hayenes, P.H., McInyre, M.E., Douglass, R.A., Roodand, R.B., Pfister, L. Stratosphere–Troposphere exchange. *Rev. Geophys*., 1995, 33, 403–439.

32. Hoshika, Y., Katata, G., Deushi, M., Watanabe, M., Koike, T. and Paoletti, E. Ozone-induced stomatal sluggishness changes carbon and water balance of temperate deciduous forests. *Sci. Rep*., 2015, 5, 9871. doi: 10.1038/srep09871.

33. Jana, P.K. and Nandi, S C. Effect of solar parameters on Antarctic, arctic and tropical ozone during the last solar cycle. *Ind. J. radio and space Phys*., 2005, **34**, 114-118.

34. Kaplan, G.G., Tanyingoh, D., Dixon, E., Johnson, M., Wheeler, A.J., Myers, R.P., Bertazzon, S., Saini, V., Madsen, K., Ghosh, S. and Villeneuve, P.J. Ambient ozone concentrations and the risk of perforated and nonperforated appendicitis: a multicity case-crossover study, *Environ. Health Perspect*., 2013, 121, 939–943.

35. Kentarchos, A.S. and G.J. Roelofs. A model study of stratospheric ozone in the troposphere and its contribution to tropospheric OH formation. *J. Geophys. Res*., 2003, 108(D12), 8517, doi:10.1029/2002JD002598.

36. Kowalok, M.E. Common threads - Research lessons from acid rain, ozone depletion, and global warming, *Environ*, 1993, 35, 6, 13-38.

37. Lamarque, J.F., Langford, A.O., Proffitt, M.H. 1996. Cross tropopause mixing of ozone through gravity wave breaking: observation and modeling. *J. Geophys. Res*., 1996, 101, 22969-22976.

38. Lei, H., Wuebbles, D.J. and Liang, X.Z. Projected risk of high ozone episodes in 2050. *Atmos. Environ*., 2012, 59, 567–577.

39. Leisner, C.P and Ainsworth, E.A. Quantifying the effects of ozone on plant reproductive growth and development. *Glob. Change Biol*., 2012, 18, 606–616.

40. Luhar, A.K., Woodhouse, M. and Galbally, I.E. Revising global ozone dry deposition estimates based on a new mechanistic parameterisation for air-sea exchange and the multiyear MACC composition reanalysis. *Atmos. Chem. Phys. Discuss*., https://doi.org/10.5194/acp-2017-768.

41. Macdonald, A.M., Anlauf, K.G., Leaitch, W.R., Chan, E. and Tarasick, D.W. Interannual variability of ozone and carbon monoxide at the Whistler high elevation site: 2002–2006. *Atmos. Chem. Phys*., 2011, 11, 11431–11446, https://doi.org/10.5194/acp-11- 11431-2011.

42. McElroy, M.B., Salawitch, R.J., Wofsy, S.C. and Logan, J.S. Reductions of Antarctic ozone due to synergistic interactions of chlorine and bromine. *Nature*, 1986, 321, 759–762.

43. McLinden, C., Olsen, S., Hannegan, B., Wild, O., Prather, M. and Sundet, J. Stratospheric ozone in 3-D models: a simple chemistry and the cross-tropopause flux. *J. Geophys. Res*. 2000, 105, 14653-14665.

44. Molina, M.J. and Rowland, F.S. Stratospheric sink of chlorofluromethanes: Chlorine atom catalysed sink of ozone. *Nature*, 1974, 249, 5460, 810-812.

45. Molina, L.T. and Molina, M.J. Production of Cl2O2 from the selfreaction of the ClO radical. *J. Phys. Chem*., 1987, 91, 433–436.

46. https://niasra.uow.edu.au/cei/webprojects/UOW175994.html retrieved 22 of March 2020.

47. https://www.srh.noaa.gov/jetstream/global/circ.htm retrieved on the 25 of March 2020.

48. Newell, R.E. Transfer through the tropopause and within the stratosphere, *Q. J. R. Meteorol. Soc*., 1963, 89(380), 167–204.

49. Nicolet M. Ozone and hydrogen reactions. *Annl Geophys*., 1970, 26, 531.

50. OECD, OECD Environmental Outlook to 2050: The Consequences of Inaction: Key Findings on Health and Environment, Organization for Economic Cooperation and Development Report No., Paris, 2012. http://www.oecd.org/environment/outlookto2050.

51. Olsen, M.A., and J.L. Stanford, Evidence of stratosphere-to-tropospheretransport within a mesoscale model and Total Ozone Mapping Spectro-meter total ozone, *J. Geophys. Res.*,106, 27,323–27,334, 2001.

52. Olsen, M.A., Douglass, A.R. and Schoeberl, M.R. Estimating downward cross-tropopause ozone flux using column ozone and potential vorticity. J. *Geophys. Res*., 2002, 107, 4636, doi:10.1029/2001JD002041.

53. Paoletti, E. and Grulke, N.E. Ozone exposure and stomatal sluggishness in different plant physiognomic classes. *Environ. Pollut*., 2010, 158, 2664–2671. doi: 10.1016/j.envpol.2010.04.024.

54. Papayannis, A., Balis, D., Zanis, P., Galani, E., Wernli, H., Zerefos, C., Stohl, A., Eckhardt, S. and Amiridis, V. Sampling of an STT event over the Eastern Mediterranean region by lidar and electrochemical sonde. *Ann. Geophys*., 2005, 23, 2039–2050.

55. Poulida, O., Dickerson, R.R. and Heyms"eld, A. Stratosphere-troposphere exchange in a midlatitude mesoscale convective complex. 1-Observations. *J. Geophys. Res*., 1996, 101, 6823-6836.

56. Pires, J.C.M., Alvim-Ferraz, M.C.M. and Martins, F.G. Surface ozone behaviour at rural sites in Portugal. *Atmos. Res*., 2012, 104, 164–171.

57. Schreuder, M.D.J., van Hove, L.W.A. and Brewer, C.A. Ozone exposure affects leaf wettability and tree water balance. *N. Phytologist*, 2001, 152, 443–454. doi: 10.1046/j.0028-646X.2001.00272.

58. Seinfeld, J.H. and Pandis, S.N. From Air Pollution to Climate Change. *Atmos. Chem. Phys*., 1998, Wiley and Sons, New York.

59. Seinfeld J.H. and Pandis S.N. From Air Pollution to Climate Change. *Atmos. Chem. Phys*., 2012, Wiley-Interscience, John Wiley & Sons, Inc.

60. Shan, W.P., Yin, Y.Q., Zhang, J.D., Ji, X. and Deng, X.Y. Surface ozone and meteorological condition in a single year at an urban site in central-eastern China. *Environ. Monit. Assess*., 2009, 151, 127–141.

61. Tarasova, O.A. and Karpetchko, A.Y. Accounting for local meteorological effects in the ozone time-series of Lovozero (Kola Peninsula). *Atmos. Chem. Phys. Discus.*, 2003, 3, 655–676.

62. Thompson, A.M. The oxidising capacity of the earth's atmosphere : probable past and future changes. *Science (USA), 1992,* 256, 1157-1165.

63. Tremblay, J. and Servranckx, R. Beryllium-7 as a tracer of stratospheric ozone: a case study. *J. Radioanal. Nucl. Chem*., 1993, 172, 49-56.

64. Tung, K.K., Ko, M.K. W., J. and Sze, N.D. Are Antarctic ozone variations manifestations of dynamics or chemistry? *Nature*, 1986, **333**, 811–814.

65. Waugh, D.W. and Polvani, L.M. Climatology of intrusions into the tropical upper troposphere. *Geophys. Res. Lett*., 2000, 27, 3857–3860.

66. Wofsy, S. C., McElroy, M. B. and Yung, Y. L., 1975, “The chemistry of atmospheric bromine”, *Geophys. Res. Lett (USA),* **2**, 215-218.

67. World Meteorological Organization (WMO). Scientific assessment of ozone depletion: 2006, global ozone research and monitoring project—report No. 50, 572 pp, Geneva, Switzerland, 2007.

68. World Meteorological Organization (WMO), Scientific Assessment of Ozone Depletion: 2010, Global Ozone Research and Monitoring Project-Report No. 52, 516 pp, Geneva, Switzerland, 2011.

69. Zhang, R., Cohan, A., Biazar, A.P., and Cohan, D.S. Source apportionment of biogenic contributions to ozone formation over the United States. *Atmos. Environ*., 164, 8–19, https://doi.org/10.1016/j.atmosenv.2017.05.044, 2017.

CHAPTER 3: STRATOSPHERE–TROPOSPHERE EXCHANGE AND O_3 VARIABILITY IN THE LOWER STRATOSPHERE AND UPPER TROPOSPHERE OVER THE IRENE SHADOZ SITE, SOUTH AFRICA

This chapter is based on a published manuscript: Stratosphere–troposphere exchange and O_3 variability in the lower stratosphere and upper troposphere over the Irene SHADOZ site, South Africa, Thumeka Mkololo, Nkanyiso Mbatha, Venkataraman Sivakumar, Nelson Bègue, Gerrie Coetzee and Casper Labuschagne (2020) Atmosphere **2020**, 11(6), 586. doi.10.3390.atmos/1060586.

3.1 Abstract

This study aims to investigate the Stratosphere-Troposphere Exchange (STE) events and ozone changes over Irene (25.5°S, 28.1°E). Twelve years of ozonesondes data (2000–2007, 2012–2015) from Irene station operating in the framework of the Southern Hemisphere Additional Ozonesodes (SHADOZ) was used to study the troposphere (0–16 km) and stratosphere (17– 28 km) ozone (O_3) vertical profiles. Ozone profiles were grouped into three categories (2000–2003, 2004–2007 and 2012–2015) and average composites were calculated for each category. Fifteen O_3 enhancement events were identified over the study period. These events were observed in all seasons (one event in summer, four events in autumn, five events in winter and five events in spring); however, they predominantly occur in winter and spring. The STE events presented here are observed to be influenced by the Southern Hemisphere polar vortex. To strengthen the investigation into STE events, advected potential vorticity maps were used, which were assimilated using Modélisation Isentrope du transport Méso–échelle de l'Ozone Stratosphérique par Advection (MIMOSA) model for the 350 K (~12–13 km) isentropic level. These maps indicated transport of high latitude air masses responsible for the reduction of the O_3 mole fractions at the lower stratosphere over Irene which coincides with the enhancement of ozone in the upper troposphere. In general, the stratosphere is dominated by higher Modern Retrospective Analysis for Research Application (MERRA-2) potential vorticity (PV) values compared to the troposphere. However, during the STE events, higher PV values from the stratosphere were observed to intrude the troposphere. Ozone decline was observed from 12 km to 24 km with highest decline occurring from 14 km to 18 km. An average decrease of 6.0% and 9.1% was

calculated from 12 to 24 km in 2004–2007 and 2012–2015 respectively, when compared with 2000–2003 average composite. The observed decline occurred in the upper troposphere and lower stratosphere with winter and spring showing more decline compared with summer and autumn.

Keywords: ozone enhancement; Irene; ozone decline; potential vorticity; ozonesondes

3.2 Introduction

The stratosphere and troposphere have different characteristics that are useful in identifying air movement from the stratosphere to the troposphere and vice versa. The stratosphere is characterized by high ozone (O_3) and potential vorticity (PV). On the other hand, the troposphere is characterized by low O_3 and PV. Approximately 90% of O_3 is found in the stratosphere and only 10% in the troposphere. Most of the O_3 in the stratosphere is situated within the O_3 layer (e.g. Bekki et al., 2009) where it plays a critical role in shielding the environment and protecting human health from dangerous ultra violet (UV) rays. The O_3 hole was discovered over Antarctica in late 1980's (e.g. Farman et al., 1985; Morrisette, 1989) and its dynamics with O_3 Depleting Substances (ODS) are well documented (Rowland et al., 1975; Mäder et al., 2010; WMO, 2011). The appearance of O_3 hole was a big concern because of the relationship that increased UV can have on various processes in the lower troposphere. In 1998, the Montreal protocol was successfully implemented to phase out the use of ODS. Subsequently, O_3 was expected to increase in the stratosphere after ODS were phased out. Since 1985, a decreasing trend of 30 DU in total column O_3 was reported for stations over the southern mid–latitudes (Bodeker et al., 2011). A positive trend was only observed in the upper stratosphere above 10 hPa (WMO, 2018; Ball et al., 2017). A continuous O_3 decline (even though statistically non–significant) was reported in the lower stratosphere from 1998 until present for the stations lying between 60°N and 60°S (Ball et al., 2018).

Tropospheric O_3 mole fractions are controlled by chemical and physical processes, and its precursors originate from both natural and anthropogenic activities. In the troposphere, O_3 is a secondary pollutant formed through a number of reactions containing nitrogen oxides (NO_x), volatile organic compounds (VOCs), methane (CH_4), and CO in the presence of sunlight (Seinfeld and Pandis, 1998) or through the transportation of O_3–rich air from the stratosphere. This process of O_3 movement from the stratosphere to the troposphere and vice versa is known as stratosphere–

troposphere O_3 exchange (STE). After the Los Angeles photochemical smog, studies revealed that O_3 can either be transported from the stratosphere or produced from chemical reactions involving O_3 precursors in the troposphere (Haagen-Smit, 1952). Stratosphere intrusion (SI) are expected to transport high O_3 and PV to the troposphere. Hence, high O_3, high PV and dry atmospheric air are used to identify stratosphere intrusion events in the troposphere. The STE plays an important role in the chemical budget of O_3 and water vapour of the upper troposphere and lower stratosphere (Amraoui et al., 2010). Stratospheric Intrusion studies are poorly documented in the Southern Hemisphere, hence, it is challenging to find the threshold that could be used to study these events in the literature. O_3 vertical profiles are useful in identifying and studying STE. A number of studies have been undertaken using Irene ozonesondes data. These studies include: a) study of O_3 climatology over Irene by Diab et al. (2004) using 1990 to 1994 and 1998 to 2004 dataset, b) satellite validation of global transport models (Ziemke et al., 2006; Ziemke et al., 2011), c) a study on stratospheric profile and water vapour in Southern Hemisphere (Sivakumar et al., 2011), and d) the study on the Southern Hemisphere tropopause (Thompson et al., 2012). In their study, Diab et al. (2004) reported O_3 enhancement in Irene above 10 km (upper troposphere) which can be related to STEs during late winter. Similar to this study, they also noted the absence of seasonal consistency in the occurrence of these events at a height above 10 km level. The frequency of occurrence of STEs in the Irene SHADOZ data set has never been studied due to limited data availability and the frequency of the launching of ozonesondes. However, according to Diab et al. (2004), the STEs events are dominant in winter and spring in the Irene station. In support to these observations, a study by Poulida et al. (1996) also found high O_3 mole fractions in the upper troposphere dominating in winter and spring months.

There are limited studies conducted over Southern Africa on STEs. A recent study on high O_3 events was conducted by Mulumba in Nairobi, Congo Basin and Irene using ozonesondes data (Mulumba et al., 2015). However, the focus was more on Nairobi and Congo Basin and little was done with Irene data. Hence, this study focuses on O_3 data observed from Irene station. It is crucial to investigate O_3 enhancement events in the troposphere and determine if such episodes were related to stratosphere–troposphere exchange. Also, events such as cut–off lows (CoL), Rossby waves, Quasi–Biennial Oscillation (QBO) and El Niño–Southern Oscillation (ENSO) are all factors that could potentially play a critical role in STEs (Ndarana and Waugh, 2010; Sun et al., 2014). For example, QBO affects the troposphere by direct effect of QBO on the tropical or

subtropical troposphere (Garfinkel et al., 2011). A downward movement of easterly winds is more dominant and much stronger compared to westerlies. Easterlies are represented as negative on the QBO index while positive signal represents westerlies. Another way that QBO affects the troposphere is through polar vortex (Holton et al., 1980; Hamilton, 1998; Baldwin and Dunkerton, 2001) processes. Most researchers have defined the polar vortex as a region of high PV. The stratosphere polar vortex develops in autumn when there is no solar heating in polar regions, strengthens in winter and breaks down in spring as sunlight returns to polar regions (Waugh and Polvani, 2000). The breakdown of stratospheric polar vortex especially plays an important role in O_3 distribution in high latitudes (Sun et al., 2014). Several studies have investigated the role of the southern polar vortex w.r.t. the middle atmosphere of the southern hemisphere (e.g. Semane et al., 2006; Bencherif et al., 2011; Orte et al., 2019 and others)

A comprehensive study on STEs was recently conducted at three Southern Hemisphere stations (Davis (69°S, 78°E), Macquarie Island (55°S, 159°E) and Melbourne (38°S, 145°E)) by looking at the statistical analysis of STEs and their impact on tropospheric O_3 (Greenslade et al., 2016). This study has coupled observed STEs with meteorological conditions such as low pressure fronts, cut–off low pressure system, indeterminate meteorology and smoke plumes. A total number of 45, 47 and 72 events were detected in Davis, Macquarie and Melbourne stations, respectively, from ozonesondes data. The majority of events were related to low pressure fronts with fire plumes contributing the least.

A number of researchers have investigated O_3 trends in the lower troposphere O_3 (Helmig et al., 2007; Cooper et al., 2014; Oltmans et al., 2013; Lin et al., 2015b; Xu et al., 2016 and others) and only a few studies have conducted trends analyses at different altitudes of troposphere and the lower stratosphere (e.g. Ball et al., 2017; Sivakumar and Ogunniyi, 2017). A study by Granados–Munoz and Leblanc (2016) investigated tropospheric trends at different altitudes over California using a procedure similar to that described by Cooper et al. (2014). In their study, linear fits of medians, 5^{th} percentiles and 95^{th} percentiles were done using least squares method. Statistical significant negative trends were observed in the lower troposphere (4-7 km) in winter for the medians and 5^{th} percentiles. On the other hand, a positive significant trend of 0.3 ppb/year was reported for the upper troposphere (7 to 10 km) for the period of 2000 to 2015. A non-significant trend was reported for layers closer to the tropopause whilst negative trends were observed in the lower stratosphere (17 to 19 km). A recent study by Ball et al. (2017) reported a

continuous decrease of O_3 in the lower stratosphere in the region between 60°N and 60°S, while O_3 recovery was observed in the upper stratosphere.

The aim of this study is to utilise the available Irene ozonesonde vertical profile to investigate the STE events that are known to lead to SI occurrence. Thus, this study identifies O_3 enhancement events exceeding monthly 90^{th} percentile composite in the upper troposphere, and investigate whether such episodes were due to SI events. Another objective of this study is to investigate O_3 changes in the upper troposphere and lower stratosphere using Irene ozonesondes data and linear regression for medians, 5^{th} percentiles and 95^{th} percentiles.

3.3 Method and data

3.3.1 Ozonesondes

Irene station soundings started in 1998 during the Southern African Fire Atmospheric Research Initiative (SAFARI) campaign in the African region. Currently, the station operates within the framework of the Southern Hemisphere Additional Ozonesodes (SHADOZ). The main aim of the project was to determine O_3 mole fractions in the troposphere and stratosphere, and also to have a full coverage of O_3 measurements over Southern Hemisphere. Since then, balloon launching continued in Irene with ozonesondes launched every second Wednesday of each month circumstances allowing. Ozone vertical profiles are obtained using electrochemical concentration cell (ECC). The heart of the instrument is the electrochemical cell that interfaces with a radiosonde that transmits back data signals to the ground station receiver. The method used by the electrochemical cell to detect O_3 was discussed extensively by Sivakumar Ogunniyi, (2017). A total number of 250 ozonesondes were launched over the study period. Irene ozonesondes data was retrieved from SHADOZ website: http://croc.gsfc.nasa.gov/shadoz. It is important to note that there is a data gap of approximately four years (2008 to September 2012) in the Irene data due to budget constraints and technical problems with the ground receiver. The program was resumed in 2012 when these issues were resolved.

3.3.2 MERRA-2 Potential Vorticity

The stratosphere has static stability and is known to contain higher potential vorticity (PV) compared with the troposphere. During the stratosphere intrusion episode, an air mass rich in O_3

and high PV enters the lower stratosphere and upper troposphere. Hence, PV can be used to identify troposphere air mass having a stratosphere origin. The tropopause is defined using a PV value as 2 PVU (Holton et al., 1995; Newell et al., 1997). Therefore, any higher PV events located in the troposphere are associated with stratosphere origin. Other studies, have used PV values of 1.5 PVU as a threshold to identify stratosphere air (WMO, 1985; Shapiro, 1980). In this study, a PV value of 2 PVU was used as a threshold for stratospheric air. This study employs PV data from the Modern Retrospective Analysis for Research Application version 2 (MERRA-2) with a spatial resolution of 0.5 x 0.625°. MERRA-2 model is an Earth System reanalysis model by National Aeronautics Space Administration (NASA) Global Modeling and Assimilation Office (GMAO). More details about MERRA-2 can be found in the website: https://gmao.gsfc.nasa.gov/reanalysis/MERRA-2/. Although the units of PV are $Km^2kg^{-1}s^{-1}$, PV Units (PVU) (where 1 PVU = $1x10^{-6}$ $Km^2kg^{-1}s^{-1}$) will be used for convenience in this study. To view the vertical slices of PV over Irene, the NASA instrument Panoply software was applied (see https://www.giss.nasa.gov) in this study.

3.3.3 Data Processing

The ozonesonde data is recorded every two seconds from 1.5 km to approximately 28 km. Ozone averages were calculated from 2 seconds data for each kilometre (km) ascended (e.g. 1 km, 2 km, 3 km to 28 km). As the ozonesonde ascends, pressure, temperature, humidity and O_3 (both ppm and DU units) are also recorded. The current study used the available ozonesondes data to investigate high O_3 events. The ozonesonde data was grouped into months in order to calculate averages, standard deviations, medians, 5^{th} and 95^{th} percentiles from 1 to 28 km. Monthly averaged data was used in conjunction with individual high O_3 event profiles to determine how individual profiles differ from their respective monthly composite profiles. Monthly averaged data was used in conjunction with individual high O_3 event profiles to determine how individual profiles differ from their respective monthly composite profiles. This study defines high O_3 event as the event where O_3 exceeds the monthly 90^{th} and 95^{th} percentile composites. Events exceeding these percentile composites were selected as an observed high O_3 events. However, these events might originate from different sources such as plumes, stratospheric-troposphere exchange (STE) and other man made activities that generate O_3 precursors. Due to this reason, potential vorticity (PV) of 2PV was added as another criteria to

identify events of stratospheric origin. PV was used in this study because it is one of the characteristics to differentiate between the stratosphere and troposphere air masses. Monthly 90th and 95th percentile composites were calculated from the available data of all ozonesondes launched during the study period. Any profile exceeding the monthly 90th and 95th percentile composites at a height between 6 and 11 km was considered for further investigation. The main reason to focus between 6 km and 11 km is to eliminate tropospheric pollution and to select events that occurred below the tropopause. Our method differs from previous studies that identified Stratospheric Intrusion (SI) events as an event where O_3 exceeds 80 ppb and then decreases by 20 ppb within 3 km or more to a value less than 120 ppb (Tang and Prather, 2010). This method was not used because it may miss some of the events observed over Irene due to lower O_3 mole fractions in the Southern Hemisphere. Another study used the 99^{th} percentile as a threshold to study SI O_3 events and their impact on tropospheric O_3 (Greenslade et al., 2016). Similar percentile threshold was not applied in this study for similar reason stated above. We attempted to use the 95^{th} percentile as a threshold, however, we missed five events. Consequently, we opted to use 90^{th} percentile as a threshold.

Average O_3 composite profiles were calculated for three categories (2000–2003, 2004–2007 and 2012–2015) using the available ozonesondes data. In the case of annual and seasonal O_3 changes, monthly averaged composites were calculated from the available ozonesondes data. Monthly averaged composites were used to compensate data gaps that occurred in summer and autumn. Hence, only summer and autumn composites were used to fill 2015 data gaps. This exercise was done to prevent the bias that may be caused by months with data gaps in calculating O_3 changes at different altitudes. Data gaps were covered only for 2015, not for the years where there was no ozonedondes data for the complete year. Annual changes were studied by averaging monthly data into yearly averages at different layers such as 13–15 km, 16–18 km, 19–21 km and 22–24 km. Furthermore, the medians, 5th and 95th percentiles were calculated at each layer. The slope was determined by fitting a linear trend to yearly averaged data plotted on the scatter plot. The standard error corresponding to the slope was calculated at each layer for median values, and both the 5th and 95th percentile. Similar approach was used to calculate seasonal O_3 changes.

3.4 Results and Discussion

Figure 3.1 indicates the monthly (a) and yearly (b) ozonesondes data launched from year 2000 to year 2015 at Irene station. Over the study period, a total number of 250 ozonesondes were launched with 2008 to September 2012 showing a significant data gap. However, 12.4% of the launched ozonesondes did not reach 28 km. A maximum of 25 ozonesondes were launched in October and November, respectively whilst a total of 12 ozonesondes were launched in January over the study period. On a per annual basis, the highest number (39) of ozonesondes were launched in 2000 while 2015 reflects the lowest number (11) of ozonesondes launched. The discrepancy in the annual number of ozonesondes launched was a factor of budgetary constraints as well as some operational issues encountered. In general, the target for this SHADOZ station is to launch at least two ozonesondes per month, which makes a total of 24 launches per year.

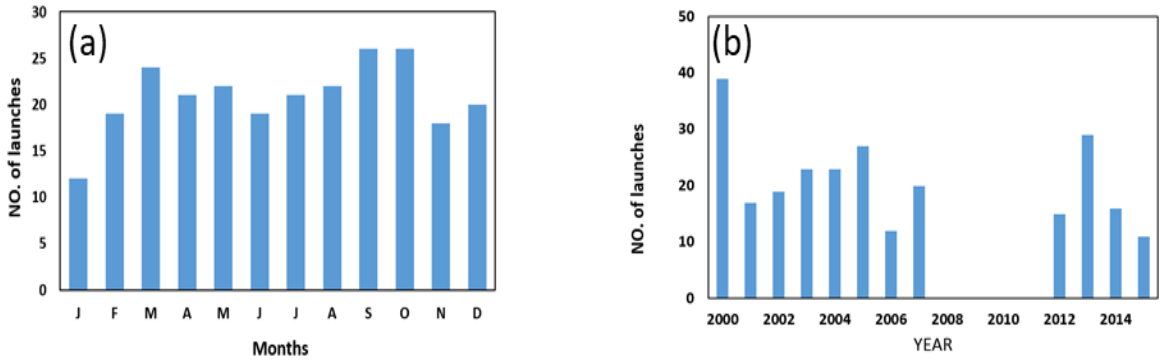

Figure 3.1: Number of ozonesondes launched at Irene from 2000 to 2015, expressed (a) monthly and (b) annually.

Figure 3.2 shows O_3 vertical profiles for the troposphere (Figure 3.2a) and stratosphere (Figure 3.2b). The data was grouped into three categories namely 2000–2003, 2004–2007, 2012–2015, and the O_3 composite was calculated at kilometre intervals from 1 km to 28 km. The data used in figure 3.2 also include 12.4% of ozonesondes that didn't reach 28 km. Therefore, 87.6% of ozonesondes launched over the study period reached 28 km. Three vertical profiles (2000–2003, 2004–2007 and 2012–2015) were compared and the difference between 2000–2003 and 2004–2007 and between 2000–2003 and 2012–2015 was calculated to determine O_3 variation over the years. The percentage decrease for 2004–2007 profiles were calculated from O_3 difference between 2000–2003 and 2004–2007, similarly, the percentage decrease for 2012–2015

was calculated from 2000–2004 and 2012–2015 O_3 difference. A continuous decrease from 2004–2007 and 2012–2015 was apparent at the height between 12 km and 28 km, with highest decrease occurring at a height between 14 km and 18 km. An average decrease of 6.0% and 9.1% was observed at a height between 12 km and 26 km for 2004–2007 and 2012–2015, respectively, when compared to the 2000–2003 period. These results are in agreement with a study by Ball et al. (2018) which reported evidence from multiple satellite measurements that O_3 in the lower stratosphere between 60° S and 60° N has indeed continued to decline since 1998.

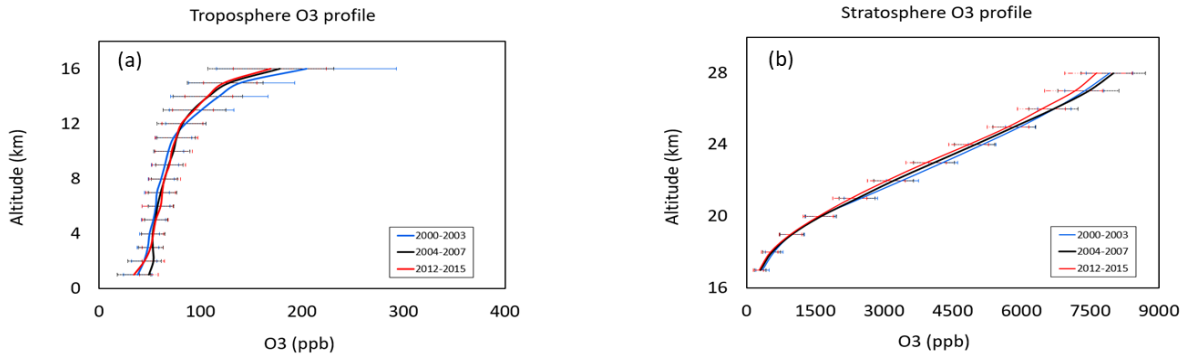

Figure 3.2: Ozone troposphere (a) and stratosphere (b) profiles. The blue line indicates 2000–2003 averages, black line indicates 2004–2007 averages and red line indicates 2012–2015 averages. The error bars indicate the standard deviation.

Figure 3.3 shows the O_3 seasonal vertical profiles averages for the troposphere and stratosphere. In the year 2012–2015, summer experienced high O_3 increase from 5 km to 12 km (Figure 3.3a). On the other hand, 2004–2007 experienced high O_3 mole fractions in the lower troposphere (Figure 3.3a, 3.3c, 3.3e and 3.3g), with the increase noted up to 8 km during the winter (Figure 3.3e). On the other hand, O_3 decrease was observed in the upper troposphere and lower stratosphere, with 2012–2015 experiencing lower mole fractions compared to 2004–2007 and 2000–2003 (Figure 3.3b, 3.3d, 3.3f and 3.3h). In general, a continuous non–consistent O_3 decrease occurred from the upper troposphere (above 16 km) to lower stratosphere (28 km) for all seasons. These results suggest that the observed O_3 decrease in the lower stratosphere is independent of season. Whereas, O_3 increase between 1.5 and 4 km could be related to increase in urban influence boundary layer precursors (Thompson et al., 2014). Such O_3 precursors could

originate from domestic heating and power stations. Maximum standard deviation is observed at altitudes closer to tropopause region. Such increase could be related to STE and other dynamic changes occurring in the tropopause region. This variation was observed to be lesser in summer when compared to other seasons. Sivakumar and Ogunniyi (2017) reported similar observations of higher standard deviation closer to the tropopause height.

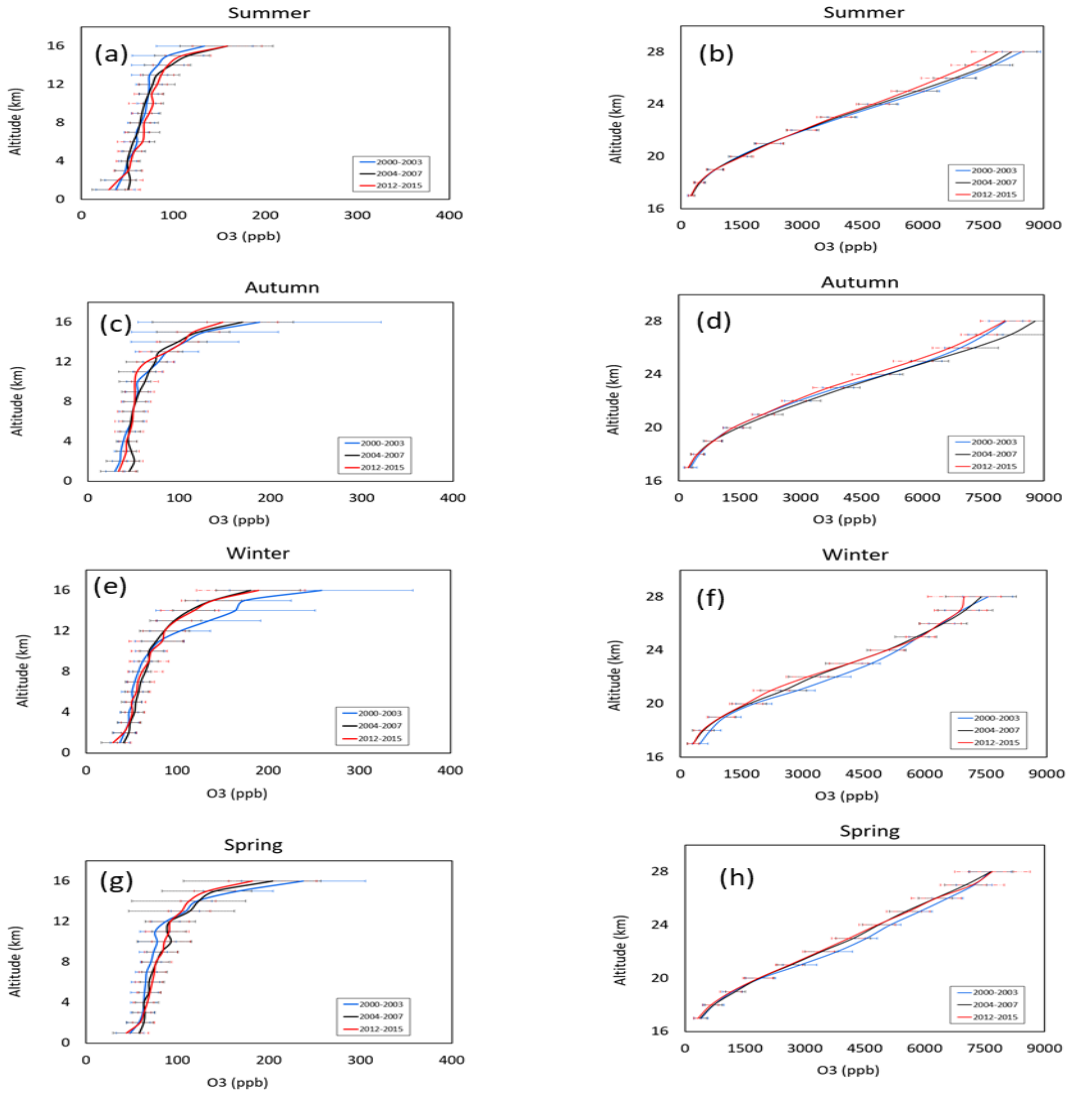

Figure 3.3: Ozone seasonal profiles for the troposphere (a, c, e and g) and stratosphere (b, d, f and h). Blue line indicates 2000–2003 averages, black line indicates 2004–2007 averages and red line indicates 2012–2015 averages. The error bars indicate the standard deviation.

Table 3.1 and 3.2 summarizes statistic of high O_3 events that were obtained by using the 95th and 90th percentile composites and potential vorticity of 2 PVU as thresholds. All episodes that exceed the monthly 95th percentile composite and 2 PVU were automatically classified as high O_3 events (Table 3.1). However, it was noted that more episodes could be identified when 90th percentile composite is used instead of 95th percentile (Table 3.2). The monthly average composites, 90th percentile and 95th percentile composites were calculated by using 2000 – 2015 Irene ozonesondes data. The maximum of the peak was defined as the highest O_3 observed from a particular O_3 profile at a particular altitude. In this case, it is the maximum of the profile dated on the first column. Delta O_3 was defined as the difference between the maximum of a particular event observed at a particular altitude and 90th or 95th percentile composite profile. The altitude of the event was defined as an altitude where maximum values of O_3 occurred. Based on observations indicated in Table 3.2, it is noted that stratospheric intrusions can reach 7 km altitude over Irene. Similar results of the occurrence of deep intrusions at 7 km altitude were reported at Reunion Island (Clain et al., 2010). Clain et al. (2010) used different PV thresholds (1.0, 1.5 and 2.0 PVU) on the study of STEs in Reunion Island. Their findings revealed that the number of detected STEs depends on the PV value and duration of back trajectories. About 9.9% STEs were detected using 2 PVU and 2 days back trajectories relative to 28.5% STEs detected using 1 PVU and 10 days back trajectories. In this study, 6.8% STEs were detected using 2 PVU and 90th percentile composite as a threshold. While 4.6% STEs were detected using 2 PVU and 95th percentile composite as a threshold. Figures 3.4 to 3.10b show more events of high PV propagation from the stratosphere to the troposphere. However, in most cases there was no data gap of ozonesondes.

Table 3.1: Summary of high ozone (ppb) events statistics) using 95th percentile and potential vorticity (2 PVU) as thresholds.

Date of the event	Monthly composite	Monthly 95th Percentile composite	Maximum peak of the event	Delta Ozone	Altitude of the event
07/08/2002	70.00	99.00	160.50	61.50	11
07/07/2004	55.68, 67.62	74.00, 147.00	146.73, 215.51	72.73, 68.51	9, 11
15/09/2004	79.15	103.00	144.02	41.02	9
26/08/2005	71.98	99.00	171.37	72.37	11
12/04/2006	58.03	110.80	120.00	9.20	11
08/08/2007	58.18	99.00	105.71	6.71	9
10/01/2007	74.65	93.00	110.91	17.91	11

31/07/2013	60.41	90.50	121.67	31.17	10
16/04/2014	50.42	72.00	81.46	9.46	9
25/11/2015	91.67	134.00	162.03	28.03	10

Table 3.2: Summary of high ozone (ppb) events statistics using 90th percentile and potential vorticity (2 PVU) as thresholds.

Date of the event	Monthly composite	Monthly 90th Percentile composite	Maximum peak of the event	Delta Ozone	Altitude of the event
07/08/2002	70.00	96.00	160.50	64.50	11
27/11/2002	87.33	99.00	117.13	18.13	9
03/03/2004	64.91	82.00	87.13	5.13	9
07/07/2004	55.68, 67.62	70.00, 86.00	146.73, 215.51	76.73, 129.51	9, 11
15/09/2004	79.15	99.00	144.02	45.02	9
26/08/2005	71.98	96.00	171.37	75.37	11
12/04/2006	58.03	71.00	120.00	49.00	11
01/03/2007	58.45	74.00	81.27	7.27	7
08/08/2007	58.18	76.00	105.71	29.71	9
10/01/2007	74.65	87.00	110.91	23.91	11
03/10/2012	89.50	112.00	110.94	2.94	10
17/10/2012	89.50	112.00	137.00	25.00	10
31/07/2013	60.41	72.00	121.67	49.67	10
16/04/2014	50.42	66.00	81.46	15.46	9
25/11/2015	91.67	113.00	162.03	49.03	10

3.4.1 High O_3 events

In this study, events with high O_3 mole fractions exceeding monthly 90th percentile composites were selected and discussed in terms of PV retrieved using MERRA-2 reanalyses system. As indicated on a PV chart (PV plotted on an isotropic surface) in Figure 3.4, values outside the contour lines appear relatively low with PV values of about -1.9x10^{-12} Km^{-2}kg^{-1}s^{-1} compared with values inside the contour lines, which have PV values ranging between -4.7x10^{-6} to 1.9x10^{-6} Km^{-2}kg^{-1}s^{-1}. Higher PV values in the troposphere indicate air mass of stratospheric origin due to increased static stability. PV is generally negative in the Southern Hemisphere (SH) and is usually multiplied by negative one (–1) to appear positive (Stan and Randall, 2007; Hoang et al., 2016). In general, higher values of PV are found in the stratosphere than in the troposphere.

Stratosphere polar vortex forms during autumn in Southern Hemisphere (Waugh and Polvani, 2010). And, in regards to the geographic position of Irene, this location experiences anticyclonic gyre due to midlatitude westerly waves that occur in autumn and winter (Tyson and Preston–Whyte, 2000). These anticyclonic gyres are responsible for increase in pollutant concentrations for a long period (Diab et al., 2000). Two possible stratosphere–troposphere O_3 autumn events (12 April 2006 and 16 April 2014) were selected for discussion.

For the purpose of this study, three possible stratosphere–troposphere O_3 winter events (7 July 2004, 26 August 2005 and 31 July 2013) were selected for discussion. Generally, one may conclude that activities such as anticyclone patterns, domestic usage of biofuels for heating, power generating plants and STEs are the cause of higher O_3 enhancement during this period in Irene (Tyson and Preston–Whyte, 2000). Furthermore, during this season, stratospheric polar vortex starts to be very active in polar region (Waugh and Polvani, 2010).

Also, in this study, two high O_3 events (15 September 2004 and 25 November 2015) were selected in spring and discussed. It is well known that the spring O_3 enhancement events can either be caused by biogenic emissions, biomass burning and lightning production or a combination of them all (Seinfeld and Pandis, 1998). However, the occurrence of STEs is dominant in winter and spring over the study area (Diab et al., 2000), and during this time, the stratospheric polar vortex is more active. According to Clain et al. (2010), it is possible that O_3 mole fractions related to stratosphere intrusion can be influenced by climatological O_3 background.

3.4.2 Case studies on high ozone events

Figure 3.4a, 3.5a, 3.6a, 3.7a, 3.8a, 3.9a and 3.10a show events that were selected for the case study. These events are part of the fifteen high O_3 events that were identified over the study period. Since these events took place in the month of April, July, August and September, 90th percentile composites for these months were used as thresholds. On these days, high O_3 peaks exceeding the monthly 90^{th} percentile composites were observed between 9 km and 11 km. Figure 3.4b, 3.5b, 3.6b, 3.7b, 3.8b, 3.9b and 3.10b show ECMWF-ERA potential vorticity plotted against the Isobaric surface between 70 hPa and 400 hPa. These vertical PV slices are for the whole month for the selected events, and averaged to the closest latitude and longitude to Irene SHADOZ site. As indicated on the PV slices, there are several episodes observed in these months where air

masses with higher PV of approximately 3.0 PVU propagated from the lower stratosphere (70 hPa) to the upper troposphere (400 hPa). These events are shown as the downward tongues on the PV slices. However, for the purpose of this study, we focus on the time scale closer to the event dates. As indicated by O_3 vertical profiles, the observed high O_3 events coincides with high PV observed in the higher troposphere. Therefore, it can be reasonably concluded that, the observed high O_3 in the upper troposphere could be of stratospheric origin.

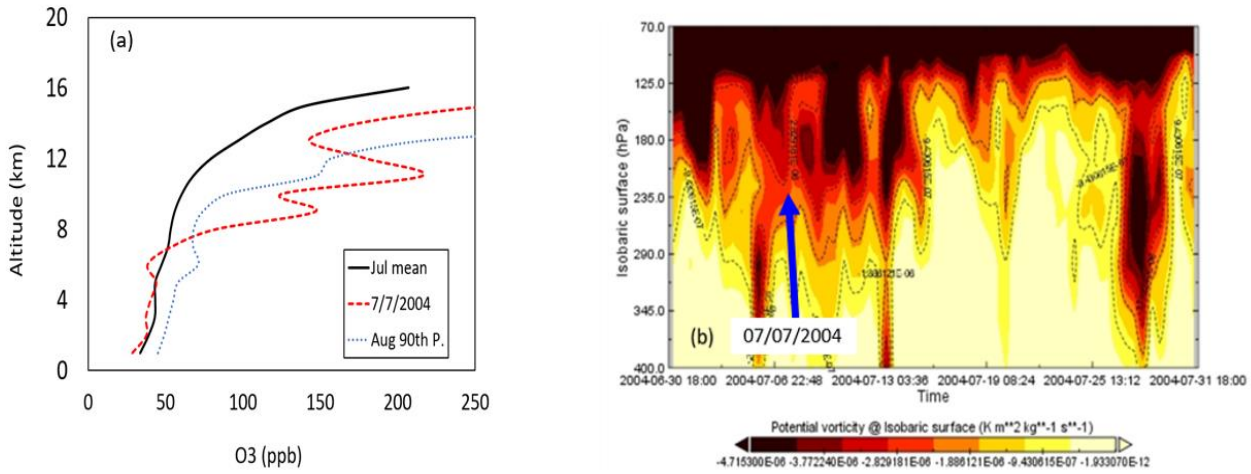

Figure 3.4: (a) Ozone troposphere profile over Irene on 07 July 2004. (b) Potential vorticity at Isobaric surface over Irene on July 2004 (from MERRA 2). Solid line in Figure 3.4a indicates monthly O_3 average composite, broken line indicates O_3 event and dotted line indicate 90^{th} percentile composite. Colours in Figure 3.4b indicates the level of potential vorticity, black indicates high potential vorticity of more than 3 $Km^{-2}kg^{-1}s^{-1}$ while yellow indicates potential vorticity of less than 2 $Km^{-2}kg^{-1}s^{-1}$. Blue arrow in Figure 3.4b indicates the event that is associated with O_3 profile in Figure 3.4a.

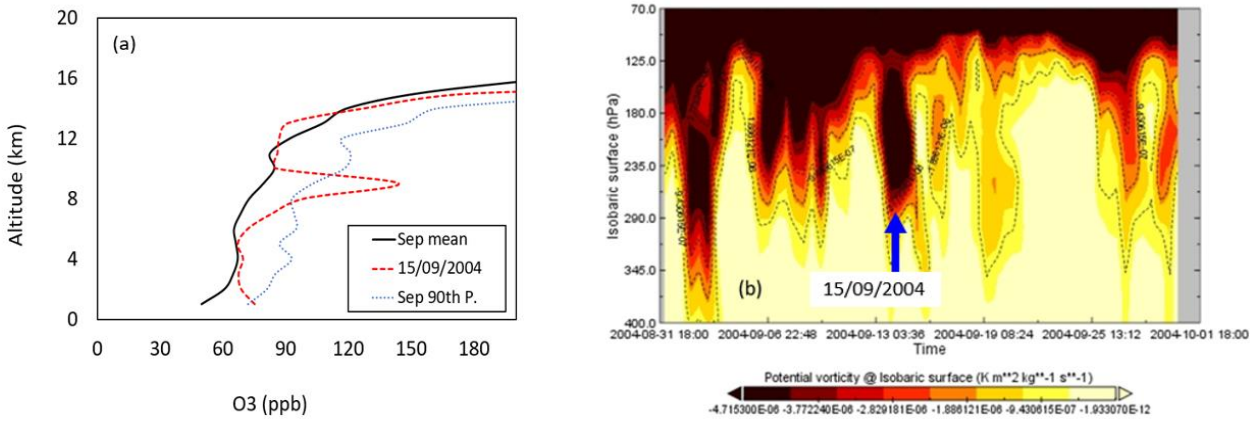

Figure 3.5: (a) Ozone troposphere profile over Irene on 15 September 2004. (b) Potential vorticity at Isobaric surface over Irene on July 2004 (from MERRA-2). Solid line in Figure 3.5a indicates monthly O_3 average composite, broken line indicates O_3 event and dotted line indicate 90th percentile composite. Colours in Figure 3.5b indicates the level of potential vorticity, black indicates high potential vorticity of more than 3 $Km^{-2}\,kg^{-1}s^{-1}$ while yellow indicates potential vorticity of less than 2 $Km^{-2}\,kg^{-1}s^{-1}$. Blue arrow in Figure 3.5b indicates the event that is associated with O_3 profile in Figure 3.5a.

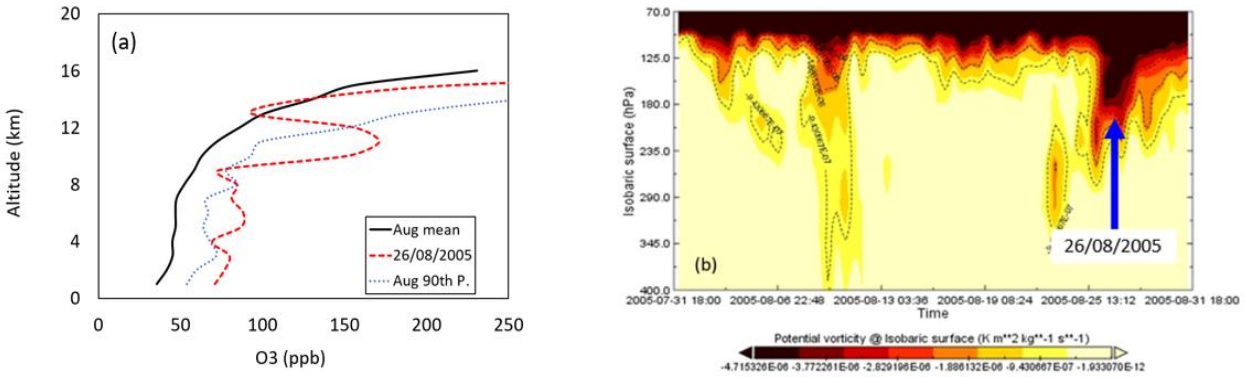

Figure 3.6: (a) Ozone troposphere profile over Irene on 26 August 2005. (b) Potential vorticity at Isobaric surface over Irene on July 2004 (from MERRA-2). Solid line in Figure 3.6a indicates monthly O_3 average composite, broken line indicates O_3 event and dotted line indicate 90th percentile composite. Colours in Figure 3.6b indicates the level of potential vorticity, black indicates high potential vorticity of more than 3 $Km^{-2}\,kg^{-1}s^{-1}$ while yellow indicates potential vorticity of less than 2 $Km^{-2}\,kg^{-1}s^{-1}$. Blue arrow in Figure 3.6b indicates the event that is associated with O_3 profile in Figure 3.6a.

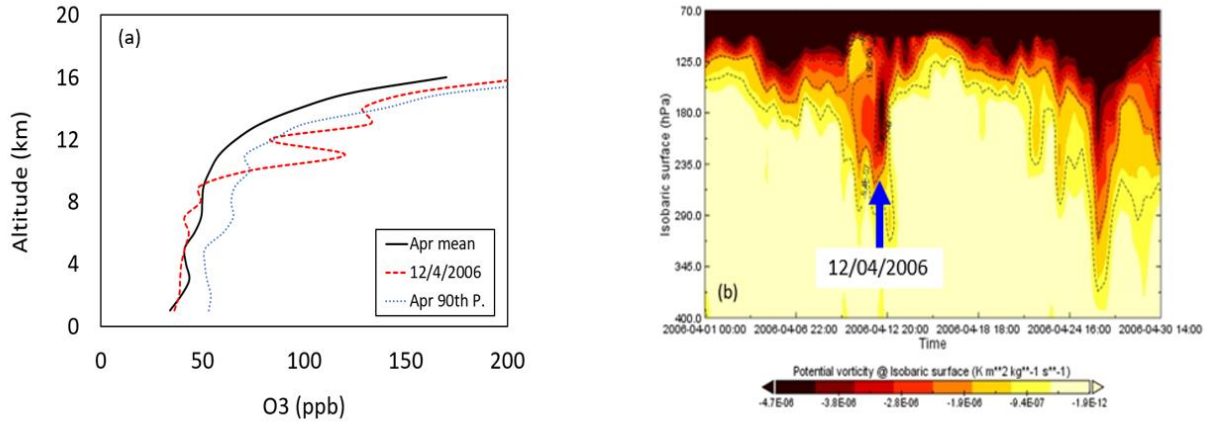

Figure 3.7: (a) Ozone troposphere profile over Irene on 12 April 2006. (b) Potential vorticity at Isobaric surface over Irene on July 2004 (from MERRA-2). Solid line in Figure 3.7a indicates monthly O_3 average composite, broken line indicates O_3 event and dotted line indicate 90th percentile composite. Colours in Figure 3.7b indicates the level of potential vorticity, black indicates high potential vorticity of more than 3 $Km^{-2}\,kg^{-1}s^{-1}$ while yellow indicates potential vorticity of less than 2 $Km^{-2}\,kg^{-1}s^{-1}$. Blue arrow in Figure 3.7b indicates the event that is associated with O_3 profile in Figure 3.7a.

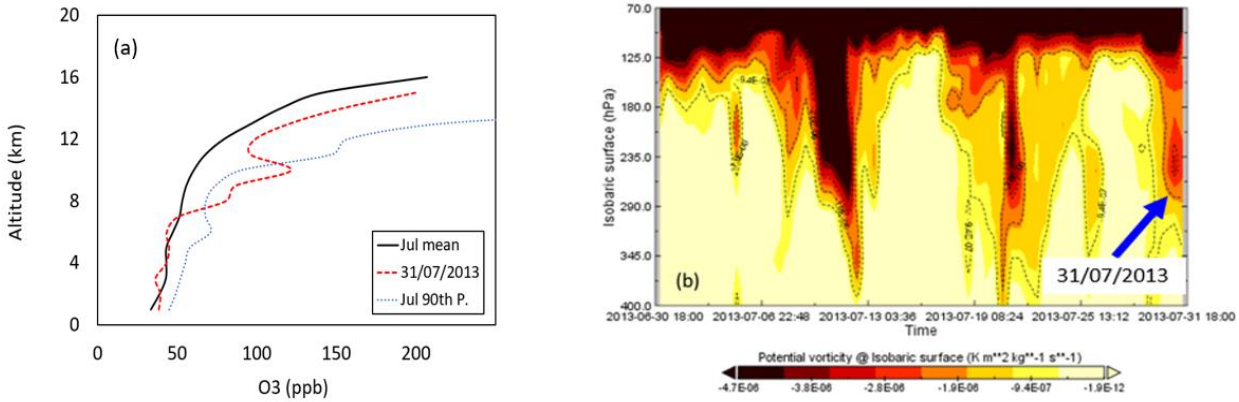

Figure 3.8 (a) Ozone troposphere profile over Irene on 31 July 2013. (b) Potential vorticity at Isobaric surface over Irene on July 2004 (from MERRA-2). Solid line in Figure 3.8a indicates monthly O_3 average composite, broken line indicates O_3 event and dotted line indicate 90th percentile composite. Colours in Figure 3.8b indicates the level of potential vorticity, black indicates high potential vorticity of more than 3 $Km^{-2}\,kg^{-1}s^{-1}$ while yellow indicates potential vorticity of less than 2 $Km^{-2}\,kg^{-1}s^{-1}$. Blue arrow in Figure 3.8b indicates the event that is associated with O_3 profile in Figure 3.8a.

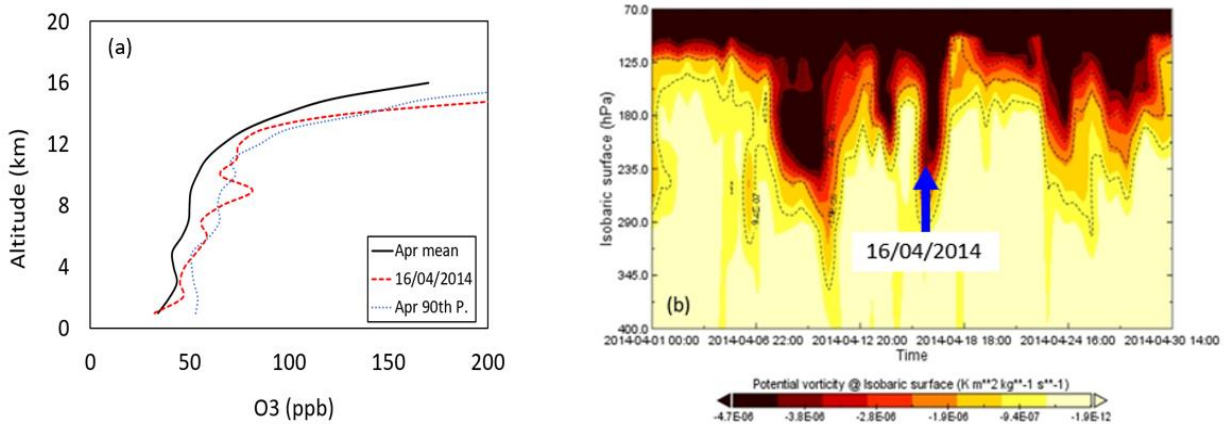

Figure 3.9: (a) Ozone troposphere profile over Irene on 16 April 2014. (b) Potential vorticity at Isobaric surface over Irene on July 2004 (from MERRA-2). Solid line in Figure 3.9a indicates monthly O_3 average composite, broken line indicates O_3 event and dotted line indicate 90th percentile composite. Colours in Figure 3.9b indicates the level of potential vorticity, black indicates high potential vorticity of more than 3 $Km^{-2}\,kg^{-1}s^{-1}$ while yellow indicates potential vorticity of less than 2 $Km^{-2}\,kg^{-1}s^{-1}$. Blue arrow in Figure 3.9b indicates the event that is associated with O_3 profile in Figure 3.9a.

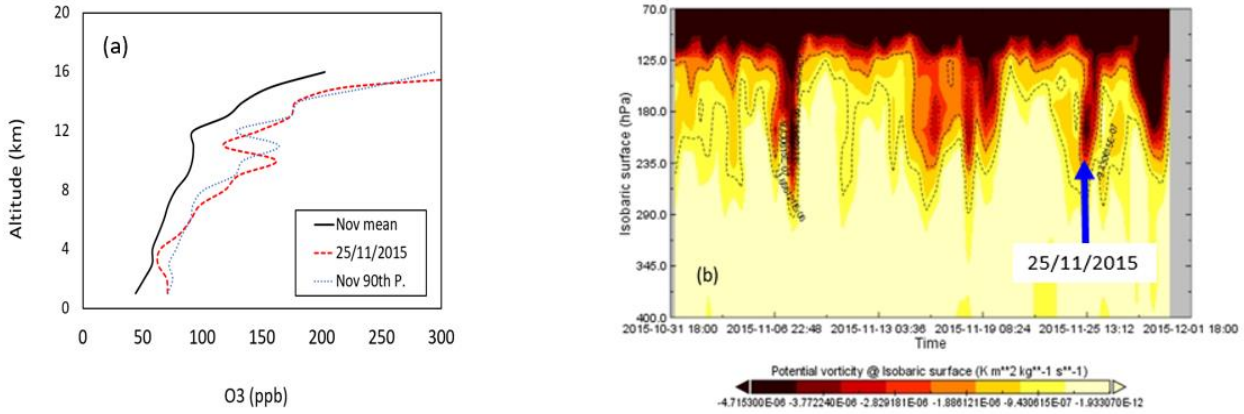

Figure 3.10: (a) Ozone troposphere profile over Irene on 25 November 2015. (b) Potential vorticity at Isobaric surface over Irene on July 2004 (from MERRA-2). Solid line in Figure 3.10a indicates monthly O_3 average composite, broken line indicates O_3 event and dotted line indicate 90th percentile composite. Colours in Figure 3.10b indicates the level of potential vorticity, black indicates high potential vorticity of more than 3 $Km^{-2}\,kg^{-1}s^{-1}$while yellow indicates potential vorticity of less than 2 $Km^{-2}\,kg^{-1}s^{-1}$. Blue arrow in Figure 3.10b indicates the event that is associated with O_3 profile in Figure 3.10a.

3.4.3 Dynamical context using MIMOSA model

There are several studies that have shown that the dynamics of the Southern Hemisphere polar vortex has an influence in the nearby surrounding structures (upper troposphere and stratosphere) of the Southern Hemisphere (Semane et al., 2006; Bencherif et al., 2011; Orte et al., 2019). A useful method that can assist in profiling the isentropic transport across the dynamical barriers in the stratosphere is the MIMOSA (Modélisation Isentrope du transport Méso–échelle de l'Ozone Stratosphérique par Advection) model. MIMOSA model is a high-resolution advection contour model that is based on Ertel's potential vorticity which was developed at the Service d'Aeronomie by Hauchecorne et al. (2002). The advection is driven by ECMWF meteorological analyses at a resolution of 0.5°x0.5°. In the case of the PV, its slow diabatic evolution is taken into account by relaxing the model PV towards the PV calculated from the ECMWF fields with a relaxation time of 10 days. Using this procedure, it is possible to run the model continuously and follow the evolution of PV filaments during several months. This model system enables the investigation of the contribution of the horizontal transport mechanism in the vertical distribution of O_3 over high latitudes, mid-latitudes and subtropics. The model gives as an output the advected potential vorticity (APV) with a resolution of 0.3°x 0.3° which is measured in potential vorticity units (PVU) which corresponds to $1x10^{-6}Km^{-2}kg^{-1}s^{-1}$.

In their recent study, Orte et al. (2019) successfully showed the influence of the polar vortex over Rio Gallegos, Argentina by using the APV calculated from the MIMOSA high–resolution advection model. Having adopted a similar approach in this study, the influence of the dynamics of the polar vortex over Irene during the days where the STE was observed is also investigated using the APV outputs from the MIMOSA model. The APV maps assimilated using MIMOSA model for the 350 K isentropic level plotted for the 07 July 2004 (a), 15 September 2004 (b), 26 August 2005 (c), 12 April 2006 (d), 30 July 2013 (e), 31 July 2013, 16 April 2014 (f), and 25 November 2015 (g) are shown in Figure 3.11. The location of Irene is indicated by a black dot in the maps. The slices of APV for 350 K isentropic level which is equivalent to 12-13 km were selected because this is the good pressure level to investigate an STE event.

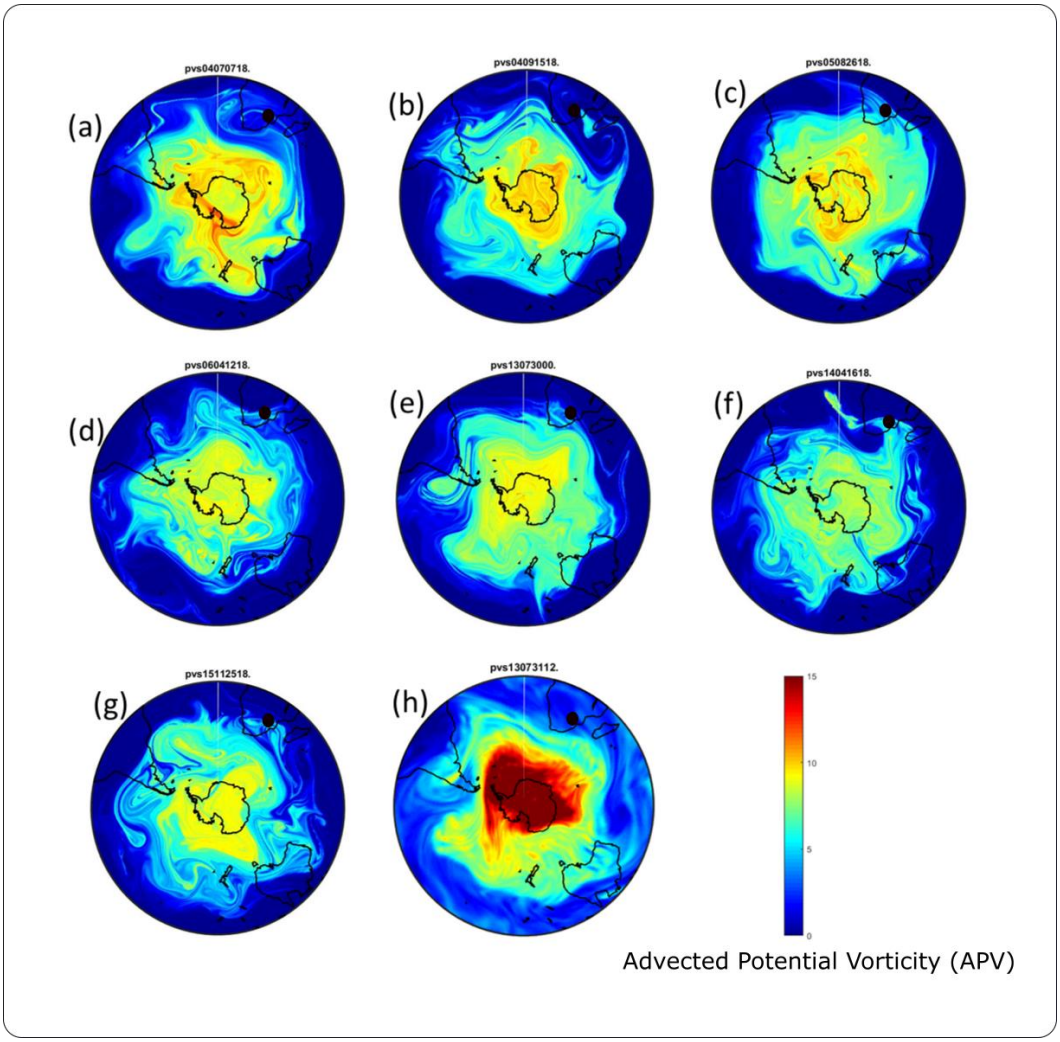

Figure 3.11: Advected Potential Vorticity (APV) maps assimilated with the MIMOSA model for the 350 K isentropic level (in PVU) and for 07 July 2004 (a), 15 September 2004 (b), 26 August 2005 (c), 12 April 2006 (d), 30 July 2013 (e), 31 July 2013 (f), 16 April 2014 (g), and 25 November 2015 (h). The black dot represents the location of the Irene site.

In general, during all these days which experienced STE process there is obvious passing of APV values with an averaged value of 8 PVU over Irene, South Africa. This is confirmed by blue tongue at the 350 K isentropic level that reflect higher PV values passing over Irene during the days of the STE that were profiled in this study. It can thus be reasoned that this isentropic transport seems to be responsible for the observed reduction of the O_3 mole fractions at the lower stratosphere over Irene which takes place at the same time with the enhancement of O_3 in the upper troposphere. The possible dynamical event which is well simulated by the MIMOSA model

during the STEs presented here could be that the high APV values are transported from the high latitudes towards the tropics bringing air masses that contain lower O_3 concentrations. There is an upward propagation of the middle atmosphere planetary waves in the high and mid-latitudes regions which results to downward propagation around the lower latitudes of the lower stratosphere (e.g. Semane et al., 2006). The O_3 mole fractions in the lower stratosphere are transported to the upper troposphere, and hence the observed STEs. The influence of the high latitude stratospheric air masses over Irene were also reported on by Semane et al. (2006) via their study of the dynamics of the middle atmosphere during the winter of year 2002. Besides, this was a special winter in the southern hemisphere because of the unprecedented year 2002 major stratospheric warming (Dowdy et al., 2004; Mbatha et al., 2010 and others).

Diab et al. (2000) reported a tropopause folding event that occurs during the winter and spring transition period in Irene. The tropopause folding is a good indicator of a STE physical process (Diab et al., 2000). Thus, with an improvement of SHADOZ data collection at Irene site since then, it is always important to investigate such a physical process in this study. Figure 3.12 shows monthly averaged composite of O_3 vertical profiles measured at Irene for the year period from 2000 to 2015. These profiles were plotted for the height region between 1 km to 15 km for January (Jan) to December (Dec). There is a general significant intrusion of higher O_3 mole fractions which are sourced from the stratosphere which is observed in late winter and spring months. In their study, Diab et al. associated this O_3 injection to middle troposphere with westerly winds, which marks the end of maritime season (Diab et al., 2000). Also, the subtropical jet was reported to play a role in permitting high stratospheric O_3 air to penetrate into the troposphere (Baray et al., 1998). While most of the free troposphere over Irene was characterised by O_3 mole fraction of approximately 55–60 ppb, the late winter months experience an increase of O_3 concentration to approximately 80 ppb just above the planetary boundary layer. It is also worth noting that the spring season is the period where there are activities such as anthropogenic pollutants sourced from the Congo region and Highveld region biomass burning, and natural activities such as lightning from rainy season and biogenic activities (Thompson et al., 2002). On the other hand, a similar observation to that which was reported by Diab et al. (2000), the tropical tropopause layer (TTL) with O_3 mole fraction ranging between 95 ppb and 100 ppb at a height above 14 km from January to February, while it noticeably declined throughout the year, and approached its minimum altitude of 11 km in October.

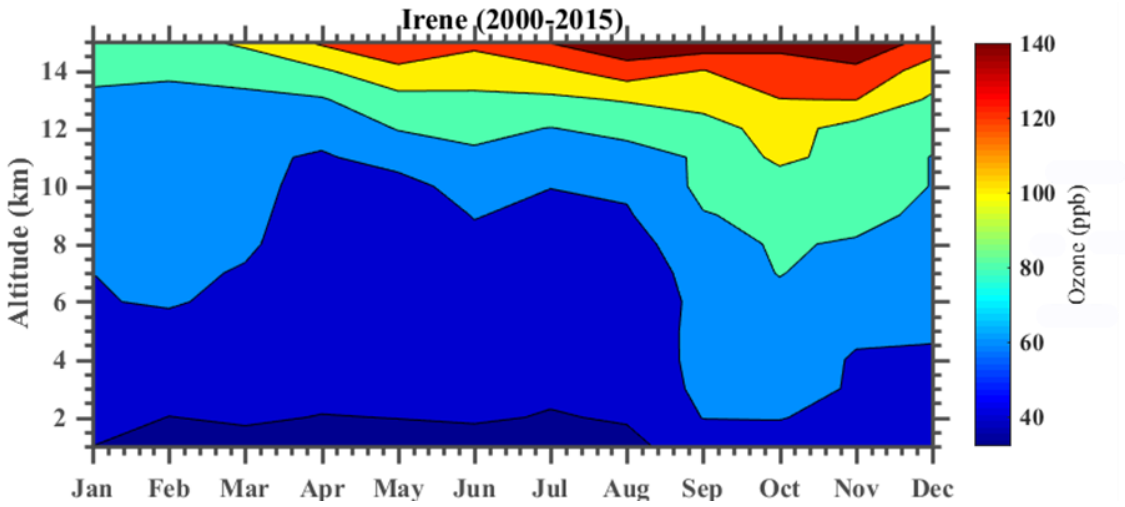

Figure 3.12: Contour plot of Irene O_3 mole fraction (in ppb) for the period, 2000 to 2015.

3.4.4 Ozone decline in Lower Stratosphere

The recovery of O_3 in the upper stratosphere has been well discussed (Ball et al., 2017; Bourassa et al., 2017; Sofieva et al., 2017; Steinbrecht et al., 2017; WMO, 2018; Petropavlovskikh et al., 2019). However, the investigation of O_3 recovery at different altitude starting from the lower stratosphere upwards still needs attention. This also arise because some recent studies seem to have reported that there may be a continuous decline of O_3 at the lower stratosphere (Ball et al., 2018; Wargan et al., 2018). A recent study by Sivakumar and Ogunniyi (2017) divided ozonesondes data into two categories, namely tropospheric (0 -15 km) and stratospheric region (15 -30 km) and reported O_3 maximum occurrence between 22-27 km. Thus, in this study, we also investigate the O_3 decline in the lower stratosphere by using Irene ozonesondes data. Ozone decline is calculated by using medians, 5^{th} and 95^{th} percentiles. Moreover, a composite was calculated at different altitudes (e.g. 13–15 km, 16–18 km and 19–21 km) of the upper troposphere and stratosphere. Rate of change was then calculated by fitting a linear trend on the graphs.

3.4.5 Annual changes at different altitudes

Table 3.3 summarises the statistics calculated for the medians, 5^{th} and 95^{th} percentiles. Layers corresponding to the upper troposphere (7–9 km) show a positive change of 0.33±0.57, 0.19±0.56 and 0.38±0.88ppb/year for the median, 5^{th} and 95^{th} percentiles respectively. Similarly, at 10–12

km height, a positive change of 0.29±0.58 and 0.24±1.25 ppb/year was observed for the median and 95th percentile respectively. In contrast, a negative change of 2.58±3.90, -0.59±3.17 and -9.63±9.27 ppb/year was observed at 16–18 km for the median, 5th and 95th percentile respectively. Similarly, negative changes were observed at 19–21 and 22–24 km for median, 5th and 95th percentiles. In summary, the results presented here indicate that there are negative changes in the lower stratosphere, while the upper troposphere shows a positive change. Similar observations of O_3 decline in the lower stratosphere were reported by Granados–Munoz and Leblanc (2016) when studying tropospheric O_3 seasonal and long-term variability at the JPL–Table Mountain. Furthermore, Ball et al. (2018) suggested that lower stratosphere decline contributes to the observed total column O_3 decline. Therefore, the results presented here are consistent with the previous observations reported in literature (Ball et al., 2018; Granados–Munoz and Leblanc, 2016).

Table 3.3: Statistical analysis of ozone at different altitudes.

Altitude	Median [ppb/year]	5th Percentile [ppb/year]	95th Percentile [ppb/year]
7-9 km	0.33±0.57	0.19±0.56	0.38±0.88
10-12 km	0.29±0.58	-0.08±0.78	0.24±1.25
13-15 km	0.21±1.04	0.47±1.13	-2.38±3.28
16-18 km	-2.58±3.90	-0.59±3.17	-9.63±9.27
19-21 km	-6.95±13.07	-7.04±9.83	-9.46±18.31
22-24 km	-16.16±21.83	-21.19±27.39	-14.81±21.82

3.4.6 Seasonal changes at different altitudes

Figure 3.13 indicates O_3 changes calculated using linear regression at different altitudes during summer, autumn, winter and spring season. Table 3.4 (a,b,c,d) provide summery statistics (Median, 5th and 95th percentiles) of these changes. Standard deviation values close to zero indicate O_3 observed over the years was close to the calculated mean. The observations in these tables can be summarised as follows:

7–9 km layer: there was a negative change identified in autumn (-0.11±0.53 ppb/year). While there was a positive change observed in summer (0.53±0.40 ppb/year), winter (0.85±0.72 ppb/year) and spring (0.04±0.57 ppb/year) for the medians. Similarly, there was a positive change

observed for the 5th percentiles in summer (0.60±0.58 ppb/year), autumn (0.40±0.34 ppb/year) and winter (0.02±0.17 ppb/year). While spring (-0.02±0.22 ppb/year) showed a negative change. There was a negative change observed in spring (-0.54±1.00 ppb/year), while a positive change was observed in summer (0.23±0.78 ppb/year), autumn (0.68±0.79 ppb/year) and winter (1.14±0.94 ppb/year) for the 95th percentiles. Therefore, it can be concluded that an overall positive change is dominant in this layer for most of the seasons.

10–12 km layer: there was a negative change observed in autumn for the medians (-0.03±0.81 ppb/year) and for the 5th percentiles in summer (-0.07±0.66 ppb/year), autumn (-0.13±0.61ppb/year) and winter (-1.00±0.85 ppb/year). Similarly, there was a negative change observed in winter (-0.96±2.03 ppb/year) and spring (-0.36±1.19 ppb/year) for the 95th percentiles. Whilst on the other hand, a positive change was observed in summer (1.09±0.72 ppb/year) and autumn (1.17±1.04 ppb/year) for the 95th percentiles.

13–15 km layer: with the exception of winter (-0.18±1.34 ppb/year) and spring (-0.50±0.88 ppb/year), a positive change was observed in summer (0.91±1.26ppb/year) and autumn (0.62±0.67 ppb/year) for the medians. Similarly, a positive change was also observed in summer (0.59±1.47 ppb/year), autumn (1.02±0.81 ppb/year), winter (0.03±0.93 ppb/year) and spring (0.24±1.31 ppb/year) for the 5th percentiles. Contrasting with the 10–12 km layer, the 95th percentiles yielded negative change in all of the seasons.

16–18 km layer: with the exception of autumn (0.93±2.53 ppb/year), negative changes were observed in summer (-0.28±1.84 ppb/year), winter (-3.85±6.26ppb/year) and spring (-7.11±4.99 ppb/year) for the medians. Similarly, there was a negative change observed in autumn (-0.87±1.69 ppb/year), winter (-0.88±3.31 ppb/year) and spring (-1.15±5.73 ppb/year) for the 5th percentiles except in summer (0.56±1.96 ppb/year). The 95th percentiles again showed negative changes in all of the seasons. Standard deviations of more than 1.5 ppb were observed in all seasons.

19–21 km layer: with the exception of autumn (1.40±8.90 ppb/year), negative changes were observed for the medians in summer (-1.28±8.96 ppb/year), winter (-13.30±23.48 ppb/year) and spring (-14.61±10.94ppb/year). In addition to this, negative changes were also observed in all seasons for the 5th and 95th percentiles. With the exception of 5th percentiles in autumn, standard deviations in excess of 8.0 ppb were calculated in this layer with more variation observed during winter and spring.

22–24 km layer: There was a negative change observed in all seasons for the medians, 5th and 95th percentiles. A standard deviation of more 14.0 ppb was calculated in this layer with more variation in winter and spring. The observed high standard deviations, suggests greater significance of changes within this layer.

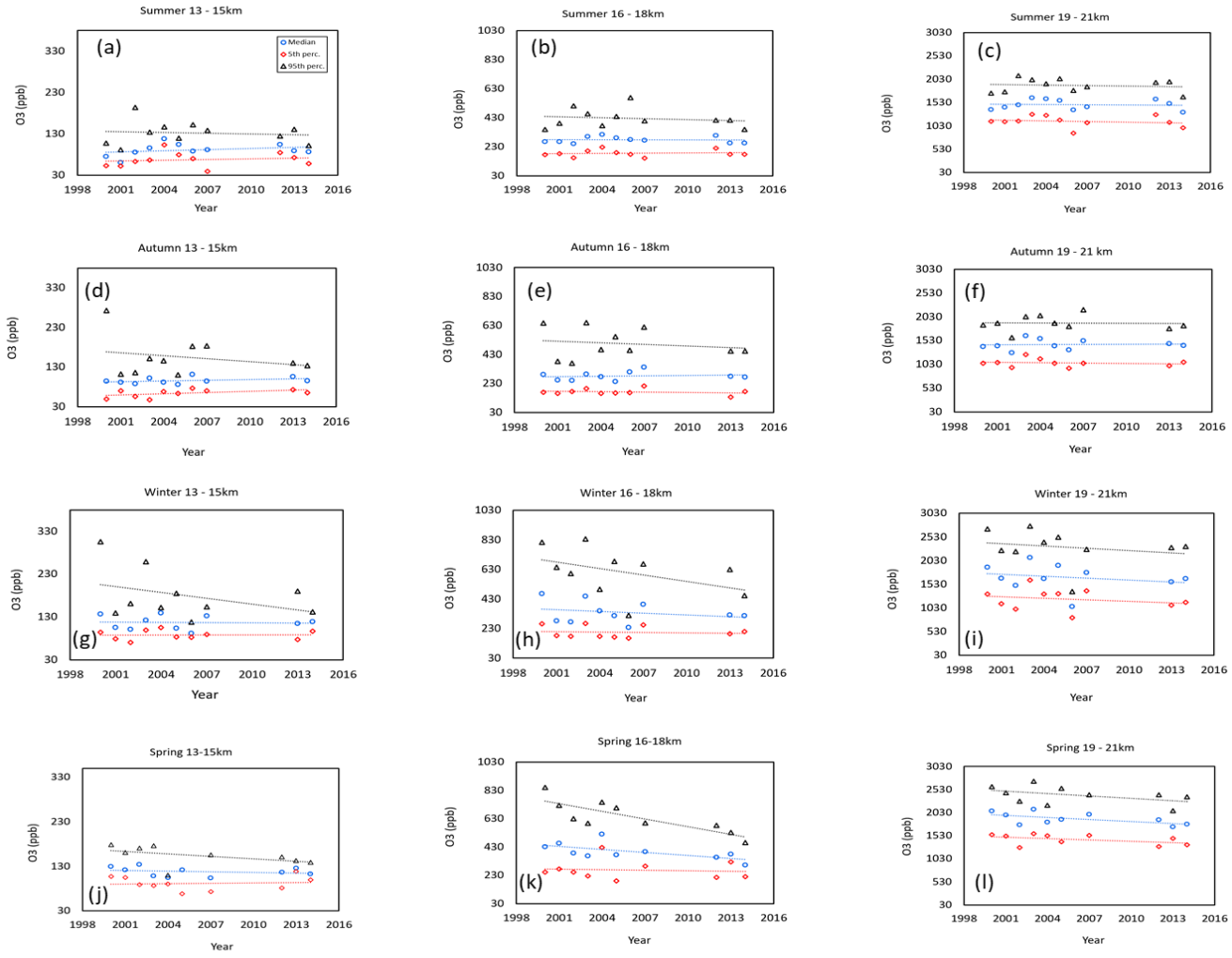

Figure 3.13: Ozone time series (2000–2015) of the 5th (red), median (blue) and 95th (black) percentile ozone mole fractions at different altitude, (a) summer 13-15 km, (b) summer 16-18 km and (c) summer 19-21 km, (d) autumn 13-15 km, (e) autumn 16-18 km, (f) autumn 19-21 km, (g) winter 13-15 km, (h) winter 16-18 km, (i) winter 19-21 km, (j) spring 13-15 km, (k) spring 16-18 km and (l) spring 19-21 km. Dashed lines represent the linear fit for each time series.

Table 3.4: Ozone statistical summary at different altitudes and seasons.

Table 3.4 (a): Summer (± indicates the standard deviation)

Altitude	Median [ppb/year]	5th Percentile [ppb/year]	95th Percentile [ppb/year]
(a). Summer (± indicates the standard deviation)			
7–9 km	0.53 ± 0.40	0.60 ± 0.58	0.23 ± 0.78
10–12 km	0.48 ± 0.49	−0.07 ± 0.66	1.09 ± 0.72
13–15 km	0.91 ± 1.26	0.59 ± 1.47	−0.59 ± 2.36
16–18 km	−0.28 ± 1.84	0.56 ± 1.96	−2.08 ± 5.58
19–21 km	−1.28 ± 8.96	−4.69 ± 10.01	−3.39 ± 12.09
22–24 km	−21.78 ± 17.53	−25.66 ± 29.31	−18.00 ± 14.98
(b). Autumn (± indicates the standard deviation)			
7–9 km	−0.11 ± 0.53	0.40 ± 0.34	0.68 ± 0.79
10–12 km	−0.03 ± 0.81	−0.13 ± 0.61	1.17 ± 1.04
13–15 km	0.62 ± 0.67	1.02 ± 0.81	−2.50 ± 4.07
16–18 km	0.93 ± 2.53	−0.87 ± 1.69	−3.77 ± 8.74
19–21 km	1.40 ± 8.90	−2.94 ± 1.06	−0.99 ± 13.61
22–24 km	−12.54 ± 19.67	−13.77 ± 20.90	−13.59 ± 19.54
(c). Winter (± indicates the standard deviation)			
7–9 km	0.85 ± 0.72	0.06 ± 0.56	1.14 ± 0.94
10–12 km	0.14 ± 0.61	−1.00 ± 0.85	−0.96 ± 2.03
13–15 km	−0.18 ± 1.34	0.03 ± 0.93	−4.57 ± 4.89
16–18 km	−3.85 ± 6.26	−0.88 ± 3.31	−14.46 ± 13.17
19–21 km	−13.30 ± 23.48	−10.60 ± 18.75	−16.47 ± 31.56
22–24 km	−10.14±31.64	−25.50±34.14	−8.47 ± 33.79
(d). Spring (± indicates the standard deviation)			
7–9 km	0.04 ± 0.57	-0.30 ± 0.76	-0.54 ± 1.00
10–12 km	0.57 ± 0.42	0.90 ± 1.00	-0.36 ± 1.19
13–15 km	-0.50 ± 0.88	0.24 ± 1.31	-1.85 ± 1.80
16–18 km	-7.11 ± 4.99	-1.15 ± 5.73	-18.19 ± 9.57
19–21 km	-14.61 ± 10.94	-9.93 ± 9.50	-17.00 ± 15.99
22–24 km	-20.18 ± 18.49	-19.83 ± 25.19	-19.19 ± 18.97

3.5 Summary and Conclusions

This study examined Irene O_3 profile data from 2000–2015 in order to identify high O_3 events and to study O_3 decline at different altitudes of the stratosphere. Monthly 90^{th} percentile

composites were used as a threshold to identify high O_3 events. Furthermore, PV charts at isobaric level were used to identify high PV air mass of stratospheric origin (more than 2 PVU). Based on the observations, high O_3 events were found to occur in all seasons. However, they were most prevalent in winter and spring. The results showed that high O_3 of stratospheric origin can propagate down to 7 km over Irene. However, very few events were found to reach this altitude. The majority of events occurred between 9 km and 10 km from the earth surface. Based on the results obtained from the PV charts, high PV values of approximately 3 PVU were observed over Irene.

Furthermore, O_3 data was grouped into three categories: 2000–2003, 2004–20007 and 2012–2015 to investigate possible long-term changes using monthly 5^{th} percentile composites, monthly 95^{th} percentile composites and monthly median composites. Troposphere and stratosphere O_3 vertical profiles were generated for the three datasets (2000–2003, 2004–20007 and 2012–2015). Based on the vertical profile graphs, it was noted that the maximum standard deviation occur in altitudes closer to the tropopause (approximately 17 km). This could be related to STE and other dynamic changes occurring in the tropopause region.

The annual changes presented in Table 3.3 show an O_3 decline at 13–15 km for the 95^{th} percentiles (–2.38±3.28 ppb/year) while median and 5^{th} percentile O_3 decline started at the 16–18 km layer. A maximum decline was observed at 22–24 km for the medians (-16.16±21.83 ppb/year), 5^{th} (-21.19±27.39 ppb/year) and 95^{th} percentile (-14.81±21.82 ppb/year). High O_3 decline was observed at 19–21 km and 22–24 km in all seasons. The 95^{th} percentiles show O_3 decline at 13–15 km. While O_3 decline was observed in winter and spring at 10–12 km layer for medians and 95^{th} percentiles. In conclusion, high O_3 of stratospheric origin can occasionally reach down as low as 7 km above Irene. However, 68.8% of these events were observed within the 9 km to 10 km region.

PV charts proved a very useful tool and showed the propagation of stratospheric air masses to the troposphere as further evidence of stratosphere O_3 intrusion for the selected high O_3 episodes in this study. These observations seem to indicate that STE events which are observed in over Irene are strongly driven by the dynamics of the Southern Hemisphere polar vortex.

O_3 decline was observed mainly in the lower stratosphere (16–28 km). However, it was more dominant in winter and spring. While, few events were observed in summer and autumn. Contrary to this, O_3 increase was observed in the lower troposphere. These observations of O_3 increase in

the lower troposphere are in line with literature reports and were associated with an increase pollution in the lower troposphere.

References

1. Baldwin, M.P. and Dunkerton, T.P. Stratospheric harbingers of anomalous weather regimes. *Science*, 2001, 294, 581–584, doi:10.1126/ science.1063315.

2. Ball, W.T., Alsing, J., Mortlock, D.J., Rozanov, E.V., Tummon, F. and Haigh, J.D. Reconciling differences in stratospheric ozone composites. *Atmos. Chem. Phys*., 2017, 17, 12269– 12302, https://doi.org/10.5194/acp–17–12269–2017.

3. Ball, W.T., Alsing, J., Mortlock, D.J., Staehelin, J., Haigh, J.D., Peter, T., Tummon, F., Stübi, R., Stenke, A., Anderson, J., Bourassa, A., Davis, S.M., Degenstein, D., Frith, S., Froidevaux, L., Roth, C., Sofieva, V., Wang, R., Wild, J., Yu, P., Ziemke, J. R. and Rozanov, E.V. Evidence for a continuous decline in lower stratospheric ozone offsetting ozone layer recovery. *Atmos. Chem. Phys*., 2018, 18, 1379–1394.

4. Baray, J. L., Ancellet, G., Taupin, F. G., Bessafi, M., Baldy, S. and Keckhut, P. Subtropical tropopause break as a possible stratospheric source of ozone in the tropical troposphere, *J. Atmos. Sol. Terr. Phys*., 1998, 60, 27– 36.

5. Bekki, S and Lefevre, F. Stratospheric ozone. History and concepts and interactions with climate. *Eur. Phys. J. Conferences*, 2009, 1, 113–136 (2009). doi: 10.1140/epjconf/e2009-00914-y.

6. Bencherif, H., Amraoui, L.E., Kirgis, G., Leclair De Bellevue, J., Hauchecorne, A., Mzé, N., Portafaix T., Pazmino A. and Goutail, F. Analysis of a rapid increase of stratospheric ozone during late austral summer 2008 over Kerguelen (49.4° S, 70.3° E). *Atmos. Chem. Phys*., 2011, 11, 1, 363-373.

7. Bodeker, G.E., Scott, J.C., Kreher, K. and McKenzie, R.L. Global ozone trends in potential vorticity coordinates using TOMS and GOME intercompared against the Dobson network: 1978–1998. *J. Geophys. Res. Atmos*., 2001, 106, D19, 23,029–23,042.

8. Bourassa, A.E., Roth, C.Z., Zawada, D.J., Rieger, L.A., McLinden, C.A. and Degenstein, D.A. Drift corrected Odin-OSIRIS ozone product: algorithm and updated stratospheric ozone trends, *Atmos. Meas. Tech. Discuss*., 2017, doi:10.5194/amt-2017-229.

9. Clain, G., Baray, J.L., Delmas, R., Keckhut, P., Cammas, J.P. A lagrangian approach to analyse the tropospheric ozone climatology in the tropics: Climatology of stratosphere-troposphere exchange at Reunion Island. *Atmos. Environ*., 2010, 44, 968-975.

10. Cooper, O.R., Parrish, D.D., Ziemke, J., Balashov, N.V.M. Cupeiro, M., Galbally, I.E., Gilge, S., Horowitz, L., Jensen, N.R., Lamarque, J.F., Naik, V., Oltmans, S.J., Schwab, J., Shindell, D.T., Thompson, A.M., Thouret, V., Wang, Y. and Zbinden, R.M. Global distribution and trends of tropospheric ozone: An observation-based review. *Elementa Sci Anthrop.,* 2014, 2: 000029, doi: 10.12952/journal.elementa.000029.

11. Diab, R.D., Thompson, A.M., Mari, K., Ramsay, L., Coetzee, G.J.R. Tropospheric ozone climatology over Irene, South Africa from 1990 to 1994 and 1998 to 2000. *J. Geophys. Res*. 2004, 109, JD00479.

12. Dowdy, A.J., Vincent, R.A., Murphy, D.J., Tsutsumi, M., Riggin, D.M. and Jarvis, M.J. The large-scale dynamics of the mesosphere–lower thermosphere during the Southern Hemisphere stratospheric warming of 2002. *Geophys. Res. Lett*., 2004, 31, 14.

13. El Amraoui, L., Atti´e, J. L., Semane, N., Claeyman, M., Peuch, V.H., Warner, J., Ricaud, P., Cammas, J.P., Piacentini, A., Josse, B., Cariolle, D., Massart, S. and Bencherif, H. Midlatitude stratosphere – troposphere exchange as diagnosed by MLS O3 and MOPITT CO assimilated fields. *Atmos. Chem. Phys*., 2010, 10, 2175–2194, doi:10.5194/acp–10–2175–2010.

14. Farman, J.C., Gardiner, B.G. and Shanklin, J.D. Large losses of total ozone in Antarctica reveal seasonal CLOX/NOX interaction. *Nature*, 1985, 315(6016), 207–210.

15. Garfinkel, I., Hartmann, D.L. The influence of the quasi-biennial oscillation on the troposphere in winter in a Hierachy of Models. Part 1: simplified dry GCMs. *AM. Meteol. Soc*., 2011, doi: 10.1175/2011JAS3665.1.

16. Granados–Muñoz, M.J., Leblanc, T. Tropospheric ozone seasonal and long–term variability as seen by LIDAR and surface measurements at the JPL–Table Mountain Facility, California. *Atmos. Chem. Phys*., 2016, 16, 9299–9319.

17. Greenslade, J.W., Alexander, S.P., Schofield, R., Fisher, J.A. and Klekociuk, A.K. Stratospheric ozone intrusion and their impacts on tropospheric ozone. *Atmos. Chem. Phys. Disc*., 2017, doi: 10.5194/acp–2016 1124.

18. Haagen-Smit, A.J. Chemistry and physiology of Los Angeles smog. *Ind. Eng. Chem*., 1952, 44, 1342–1346.

19. Hamilton, K. Effects of an imposed quasi-biennial oscillation in a comprehensive troposphere–stratosphere–mesosphere general circulation model. *J. Atmos. Sci*., 1998, 55, 2393–2418.

20. Hauchecorne, A., Godin, S., Marchand, M., Heese, B. and Souprayen, C. Quantification of the transport of chemical constituents from the polar vortex to midlatitudes in the lower stratosphere using the high-resolution advection model MIMOSA and effective diffusivity. *J. Geophys. Res*.: *Atmospheres*, 2002, 107, D20, SOL-32.

21. Helmig, D., Oltmans, S.J., Carlson, D., Lamarque, J-F., Jones, A., Labuschagne, C., Anlauf, K. and Hayden, K. A review of surface ozone in the polar regions. *Atmos. Environ*., 2007, 41, 5138–5161.

22. Hoang, L.P., Reeder, M.J., Berry, G.J., Schwendike, J. Coherent Potential Vorticity Maxima and Their Relationship to Extreme Summer Rainfall in the Australian and North African Tropics. J. SO. *Hemisph. Earth*., 2016, 66, 424–441. DOI: 10.22499/3.6604.004.

23. Holton, J.R. and Tan, H. C. The influence of the equatorial quasi–biennial oscillation on the global circulation at 50 mb. J. *Atmos. Sci*., 1980, 37, 2200–2208.

24. Holton, J.R., Hayenes, P.H., McInyre, M.E., Douglass, R.A., Roodand, R.B., Pfister, L. Stratosphere–Troposphere exchange. *Rev. Geophys*., 1995, 33, 403–439.

25. Lin, M., Horowitz, L.W., Cooper, O.R., Tarasick, D., Conley, S., Iraci, L.T., Johnson, B., Thierry Leblanc, T., Petropavlovskikh, I. and Yates, E.L. Revisiting the evidence of increasing springtime ozone mixing ratios in the free troposphere over western North America. *Geophys. Res. Lett*., 2015b, 8719–8728, https://doi.org/10.1002/2015GL065311.

26. Mäder, J.A., Staehelin, J., Peter, T., Brunner, D., Rieder, H. E., Stahel, W. A. Evidence for the effectiveness of the Montreal Protocol to protect the ozone layer. *Atmos. Chem. Phys*., 2010, 10, 12,161–12,171.

27. Mbatha, N., Sivakumar, V., Malinga, S. B., Bencherif, H. and Pillay, S.R. Study on the impact of sudden stratosphere warming in the upper mesosphere-lower thermosphere regions using satellite and HF radar measurements. *Atmos. Chem. Phys*., 2010, 10, 7, 3397-3404.

28. Morrisette, P.M. The evolution of policy responses to tratospheric ozone depletion. *Nat Resources J*. 1989, 29, 3.

29. Mulumba, J.P., Sivakumar, V. and Afullo, T. J. O. Modelling Tropospheric ozone climatology over Irene (South Africa) using retrieved (Submitted for peer review and published at– J. Geosci). *Remote Sens*., 2015, doi.rg/10.4172/2169–0049.1000151.

30. Ndarana T. and Waugh, D.W. The link between cut–off lows and Rossby wave breaking in the Southern Hemisphere. *Q. J. R. Meteorol. Soc*., 2010, April 2010 Part B, 136, 869–885.

31. Newell, R.E., Browell, E.V., Davis, D.D. and Liu, S.C. Western Pacific tropospheric ozone and potential vorticity: Implications for Asian pollution. *Geophys. Res. Lett*., 1997, 24(22), 2733–2736, doi:10.1029/97GL02799.

32. Oltmans, S.J., Lefohn, A.S., Shadwick, D., Harris, J.M., Scheel, H.E., Galbally, I., Tarasick, D.W., Johnson, B.J., Brunke, E.G., Claude, H., Zeng, G., Nichol, S., Schmidlin, F., Davies, J., Cuevas, E., Redondas, A., Naoe, H., Nakano, T. and Kawasato, T. Recent tropospheric ozone changes A pattern dominated by slow or no growth. *Atmos. Environ.*, 2013, **67**, 331-351.

33. Orte, P.F., Wolfram, E., Salvador, J., Mizuno, A., Bègue, N. and Bencherif, H., Bali, J.L., D'Elia, R., Pazmiño, A., Godin-Beekmann, S., Ohyama, H. and Quiroga, J. Analysis of a southern sub-polar short-term ozone variation event using a millimetre-wave radiometer. *Ann. Geophys*., 2019, 37, 613-629.

34. Petropavlovskikh, I., Godin-Beekmann, S., Hubert, D., Damadeo, R.;,Hassler, B. and Sofieva, V. SPARC/IO3C/GAW report on Long-term Ozone Trends and Uncertainties in the Stratosphere, SPARC/IO3C/GAW, SPARC Report No. 9, WCRP-17/2018, GAW Report No. 241, doi:10.17874/f899e57a20b, 2019.

35. Poulida, O.; Dickerson, R. R.; Heymsfield, A. Stratosphere– troposphere exchange in a midlatitude mesoscale con– vective complex. 1. Observations. J. *Geophys. Res*., 1996, 101, 6823–6836.

36. Rowland, F.S. and Molina, M.J. Chlorofluoromethanes in environment. *Rev. Geophys*., 1975, 13, 1, 1–35.

37. Seinfeld, J.H., Pandis, S.N. From Air Pollution to Climate Change. *Atmos. Chem. Phys*., 1998, Wiley and Sons, New York.

38. Semane, N., Bencherif, H., Morel, B., Hauchecorne, A. and Diab, R. D. An unusual stratospheric ozone decrease in the Southern Hemisphere subtropics linked to isentropic air-mass transport as observed over Irene (25.5 S, 28.1 E) in mid-May 2002. *Atmos. Chem. Phys*., 2006, 6, 7, 1927-1936.

39. Shapiro, M.A. Turbulent mixing within tropopause folds as a mechanism for the exchange of chemical constituents between the stratosphere and the troposphere. *J. Atmos. Sci*., 1980, 37, 994– 1004.

40. Sivakumar, V. and Ogunniyi, J. Ozone climatology and variability over Irene, South Africa determined by ground based and satellite observations. Part 1: Vertical variations in the troposphere and stratosphere. *Atmosfera*, 2017, 30, 4, doi.org/10.20937/atm.2017.30.04.05.

41. Sivakumar, V., Bencherif, H., Begue, N. and Thompson, A.M. Tropopause characteristics and variability from 11 years of SHADOZ Observations in the Southern Tropics and Subtropics. J. *Appl. Meteorol. Clim*., 2011, 50, 1403–1416.

42. Sofieva, V., Kyrölä, E., Laine, M., Tamminen, J., Degenstein, D. and Bourassa, A., Roth, C., Zawada, D., Weber, M., Rozanov, A., Rahpoe, N., Stiller, G., Laeng, A., von Clarmann, T., Walker, K.A., Sheese, P., Hubert, D., van Roozendael, M., Zehner, C. Merged SAGE II, Ozone_cci and OMPS ozone profiles dataset and evaluation of ozone trends in the stratosphere. *Atmos. Chem. Phys. Discuss*., 2017, doi:10.5194/acp-2017-598.

43. Stan, C. and Randall, D.A. Potential vorticity as Meridonal coordinate. *B. AM. Meteol. Soc*., 2007, 64.

44. Steinbrecht, W., Froidevaux, L., Fuller, R., Wang, R., Anderson, J., Roth, C., Bourassa, A., Degenstein, D., Damadeo, R., Zawodny, J., Frith, S., McPeters, R., Bhartia, P., Wild, J., Long, C., Davis, S., Rosenlof, K., Sofieva, V., Walker, K., Rahpoe, N., Rozanov, A., Weber, M., Laeng, A., von Clarmann, T., Stiller, G., Kramarova, N., Godin-Beekmann, S.,

Leblanc, T., Querel, R., Swart, D., Boyd, I., Hocke, K., Kämpfer, N., Barras, E.M., Moreira, L., Nedoluha, G., Vigouroux, C., Blumenstock, T., Schneider, M., García, O., Jones, N., Mahieu, E., Smale, D., Kotkamp, M., Robinson, J., Petropavlovskikh, I., Harris, N., Hassler, B., Hubert, D. and Tummon. F. An update on ozone profile trends for the period 2000 to 2016. *Atmos. Chem. Phys. Discuss*., 2017, 1–24, doi:10.5194/acp-2017-391.

45. Sun., L., Chen, G. and Robinson, W.A. The Role of Stratospheric Polar Vortex Breakdown in Southern Hemisphere Climate Trends. *B. AM. Meteol. Soc*., 2014, doi: 10.1175/JAS–D–13–0290.1.

46. Thompson, A.M., Balashov, J.C., Coetzee, J.R.C., Thouret, V., Posny, F. Tropospheric ozone increases over the southern Africa region: bellwether for rapid growth in Southern Hemisphere pollution? *Atmos. Chem. Phys*., 2014, 14, 9855-9869.

47. Thompson, A.M., Miller, S.K., Tilmes, S., Kollonige, D.W., Witte, J. C., Oltmans, S. J., Bryan J. Johnson, B.J., Fujiwara, M., Schmidlin, F.J., Coetzee, G.J.R., Komala, N., Maata, M., bt Mohamad, M., Nguyo, J., Mutai, C., Ogino, S.Y., Raimundo Da Silva, F., Paes Leme, N.M., Posn, F., Scheele, R., Selkirk, H.B., Shiotani, M., Stübi, R., Levrat, G., Calpini, B., Thouret, V., Tsuruta, H., Canossa, J.V., Vömel, H., Yonemura, S., Diaz, J.A., Tan Thanh, N.T. and Thuy Ha, H.T. Southern Hemisphere Additional Ozonesondes (SHADOZ) ozone climatology (2005–2009): Tropospheric and tropical tropopause layer (TTL) profiles with comparisons to OMI–based ozone products. *J. Geophys. Res. Atmos*., 2012, 17, (D23301), doi:10.1029/2011jd016911.

48. Thompson, A.M., Witte, J.C., Freiman, M.T., Phahlane, N.A. and Coetzee, G.J.R. Lusaka, Zambia, during SAFARI–2000: Convergence of local and imported ozone pollution. *Geophys. Res. Lett*., 2002, 29, 20, 1976, doi:10.1029/2002GL015399.

49. Tyson, P.D. and Preston–Whyte, R.A. The Weather and Climate of Southern Africa. Oxford Univ. Press. 2000, New York.

50. Wargan, K., Orbe, C., Pawson, S., Ziemke, J. R., Oman, L. D. and Olsen, M. A., Coy, L. and Emma Knowland, K. Recent decline in extratropical lower stratospheric ozone attributed to circulation changes. *Geophys. Res. Lett*., 2018, 45. https://doi.org/10.1029/2018GL077406.

51. Waugh, D.W. and Polvani, L.M. Climatology of intrusions into the tropical upper troposphere. *Geophys. Res. Lett*., 2000, 27, 3857–3860.

52. Waugh, D.W. and Polvani, L.M. Stratospheric polar vortices, in the stratosphere: Dynamics, Transport, and Chemistry, Geophys. Monogr. Ser., 2010, vol. 190, edited by L. M. Polvani, A. H. Sobel, and D. W. Waugh, 43–57, AGU, Washington, D. C., doi:10.1029/2009GM000887.

53. WMO: Scientific Assessment of Ozone Depletion: 2018, Global Ozone Research and Monitoring Project–Report, World Meteorological Organization, Geneva, Switzerland, 588, 2018.

54. WMO: Atmospheric Ozone 1985, vol. I., Report No. 16, World Meteorological Organization, Geneva, Switzerland, 478, 1986.

55. WMO: Scientific Assessment of Ozone Depletion, Global Ozone Research and Monitoring Project Report, World Meteorological Organization, Geneva, Switzerland, 416, 2014.

56. Xu, W., Lin, W., Xu, X., Tang, J., Huang, J., Wu, H. and Zhang. X. Long-term trends of surface ozone and its influencing factors at the Mt Waliguan GAW station, China – Part 1: Overall trends and characteristics. *Atmos. Chem. and Phys*., 2016, 16, 6191-6205.

57. Ziemke, J.R., Chandra, S., Duncan, B.N., Froidevaux, L., Bhartia, P.K., Levelt, P.F. and Waters, J.W. Tropospheric ozone determined from Aura OMI and MLS: Evaluation of measurements and comparison with the Global Modeling Initiative's Chemical Transport

Model. *J. Geophys. Res. Atmos*. 2006, 111, D19303, https://doi.org/10.1029/2006JD007089.

58. Ziemke, J.R., Chandra, S., Labow, G.J., Bhartia, P.K., Fridevaux, L. and Witte, J.C. A global Climatology of Tropospheric and Stratospheric Ozone Derived from AURA OMI and MLS Measurements. *Atmos. Chem. Phys*., 2011, 11, 9237–9251.

59. http://www.cpc.ncep.noaa.gov/data/indices/qbo.u50.index, date retrieved 13 September 2018.
60. http://croc.gsfc.nasa.gov/shadoz , date retrieved 20 April 2016.
61. https://www.giss.nasa.gov/tools/panoply, date retrieved 22 November 2018.

CHAPTER 4: VALIDATION OF STELLENBOSCH DOBSON TOTAL COLUMN OZONE OBSERVATIONS WITH SATELLITE OBSERVATIONS

This chapter is based on to be submitted manuscript: Validation of Stellenbosch Dobson total column ozone observations with satellite observations. T. Mkololo, V. Sivakumar, N. Mbatha, H. Bencherif, G. Coetzee, E. Mbambalala and D. vanderSpuy, that is prepared for submission in South African Journal of Geography.

4.1 Abstract

This study aims to compare 2017 and 2018 Dobson#035 Total Column Ozone (TCO) with Ozone Monitoring Instrument (OMI) and Atmospheric Infrared Sounder (AIRS) satellites that overpass Stellenbosch (33.9°S; 18.3°E). OMI satellite data used for validations was obtained from Total Mapping Spectrometer (OMI-TOMS) and Differential Optical Absorption Spectroscopy (OMI-DOAS). Furthermore, Dobson#035 TCO data was compared with Modern-Era Retrospective Analysis for Research and Applications (MERRA-2) assimilation. A maximum of 373.3 DU, 373.4 DU, 382.7 DU, 383.0 DU and 358.5 DU was obtained from Dobson#035, OMI-TOMS, OMI-DOAS, AIRS and MERRA-2, respectively. While a minimum of 232.7 DU, 236.3 DU, 233.5 DU, 260.1 DU and 234.0 DU was obtained from Dobson#035, OMI-TOMS, OMI-DOAS, AIRS and MERRA-2, respectively. The percentage difference, percentage error and correlation coefficient between Dobson#035 and satellite TCO observations was also calculated. The daily percentage difference between Dobson#035 and satellites ranged between -2% and 2%. A correlation coefficient of 0.97 (OMI-TOMS), 0.92 (OMI-DOAS) and 0.85 (AIRS) was obtained between Dobson#035 and satellite observations while a correlation of 0.96 was obtained between Dobson#035 and MERRA-2 assimilation. These observations indicate that OMI-TOMS and MERRA-2 correlates better with Dobson#035 as compared with OMI-DOAS and AIRS. In addition, the root square mean error (RMSE), mean bias error (MBE) and mean absolute bias error (MABE) between Dobson and satellites observation was calculated.

Keywords: Total Column Ozone, Stellenbosch, OMI-TOMS, OMI-DOAS, AIRS, MERRA-2 model.

4.2 Introduction

Ozone (O_3) is a colourless gas that occurs natural in the stratosphere through the reaction of oxygen molecule with an oxygen atom in the presence of sunlight. Approximately 10% of O_3 is located in the troposphere while the bulk of O_3 (approximately 90%) is located in the lower stratosphere (ozone layer) at approximately 10 to 50 km above the Earth's surface (Bekki and Lefevre, 2009).

In different parts of the atmosphere, and at specific concentrations, O_3 can have positive or negative impacts on human health and environment. In the stratosphere, O_3 plays positive role by absorbing incoming ultraviolet solar radiation. Decrease of the O_3 layer has negative effects on human health and the environment at large (Bekki and Lefevre, 2009). On the other hand, Kinney et al. (1996) reported that O_3 acts as a strong greenhouse gas in the lower troposphere and its higher concentrations affects the respiratory system, causing lung infections, asthma symptoms and premature mortality. Moreover, high O_3 concentrations can affect human and plants directly or through the formation of poisonous gases such as peroxyacetyl nitrate (Lacis et al., 1990; Darrall, 1989; Bertman and Roberts, 1991; Derwent, 1995). Finkelstein (2004) reported that young children are at high risk of being affected by high O_3 concentrations as compared with adults because their lung development is incomplete and they have a higher breathing rate than adults. In addition, National Research Council (NRC) reported that high O_3 concentrations of more than 60 ppb have negative effects to forests, natural vegetation and agricultural crops (NRC, 1999). Moreover, negative effects of high O_3 concentrations were reported in plants (Morgan et al., 2006), vegetation (Gimeno et al., 1995; Penuelas et al., 1999), cultivate crops (Treshow and Steward, 1973), aquatic ecosystem and affect air quality (Sivasakthivel and Reddy, 2011). O_3 also affects global radiative forcing and climate change over long timescales (Cho et al., 2003; Martens, 1998; WMO, 2014).

A number of researchers (e.g. Kim et al., 2017; Vaz Peres et al., 2017; Cizkova et al., 2019) have used ground-based instruments such as Dobson and Brewer to validate TCO satellite observations. Bramstedt et al. (2003) reported that Total Mapping Spectrometer (TOMS) V7 overestimates Southern Hemisphere ground-based observations by more than 2% while Kroon et al. (2006) reported a bias of 1% between TOMS and Dobson TCO observations. Kim et al. (2017) reported a correlation coefficient of 0.96 for TOMS and 0.95 for Differential Optical

Absorption Spectroscopy (OMI-DOAS). Atmospheric Infrared Sounder (AIRS) was mostly used to validate ozonesondes dataset (Monahan et al., 2007; Bian et al., 2007), while other studies used AIRS to examine the quality of O_3 profiles, water vapour and temperature (Susskind et al., 2003; Susskind et al., 2006; Strow et al., 2006; Fetzer et al., 2006). Susskind et al. (2003) reported that the performance of AIRS depends on altitude. As a result, a positive bias was reported at lower atmosphere (400 to 300 hPa) while a negative bias was obtained in the lower and middle stratosphere (100 to 70 hPa). Bian et al. (2007) also reported a positive bias (80%) of AIRS in the region of 700 hPa to 200 hPa and a negative bias (0 to -20%) in the region of 100 hPa to 30 hPa. AIRS bias is more in the Southern Hemisphere relative to the Northern Hemisphere and the observed bias was mostly in the upper troposphere and lower stratosphere region (Monahan et al., 2007). TOMS observations and MERRA-2 assimilation were used to study global tropospheric O_3 trends (Ziemke et al., 2017). On the other hand, Millan and Manney (2017) used MERRA-2 reanalyses data to study mini-hole in the Northern Hemisphere and found that MERRA-2 O_3 data represents O_3 mini-hole events better than the other reanalyses.

The current study used satellite TCO observations to validate Stellenbosch Dobson#035 TCO observations. Satellite TCO data used in this study was obtained from OMI-TOMS, OMI-DOAS and AIRS instruments. In addition to satellite observations, Modern-Era Retrospective Analysis for Research and Applications (MERRA-2) reanalysis data was compared with Dobson#035 TCO observations. Statistical analysis such as percentage difference, percentage error, root square mean error (RMSE), mean bias error (MBE), mean absolute bias error (MABE) and correlation coefficient was calculated between Dobson#035 TCO and satellite TCO observations using 2017 and 2018 datasets. Similar statistical analysis was performed using MERRA-2 reanalyses dataset.

4.3 Methodology

4.3.1 Dobson Spectrophotometer

Stellenbosch Dobson TCO observations started in November 2016 as part of the South African Weather Service Global Atmosphere Watch (GAW) regional programme. This is the third Dobson instrument in South Africa, after the long-term Dobson TCO observations over Irene and Springbok. This technique measures TCO by measuring the relative intensity of the UVB radiation that reaches the earth and compare to UVA radiation at ground level. Observations

are taken either under Direct Sun (DS), Zenith Blue (ZB) or Zenith Cloudy (ZC) depending on the weather conditions. However, direct sun data gives better comparisons with satellites as compared with zenith-sky data (Balis et al., 2007).

Dobson method is strongly affected by aerosols and pollutants in the atmosphere because they absorb light at the same wavelength (Vanicek et al., 2003). More details on the operation of Dobson spectrophotometers can be found in a study by Komhyr et al. (1989).

4.3.2 Satellite observations

The current study used Ozone Monitoring Instrument (OMI), Atmospheric Infrared Sounder (AIRS) observations and Modern-Era Retrospective Analysis for Research and Applications (MERRA-2) reanalysis data. OMI observations data used in this study was obtained from OMI-Total Mapping Spectrometer (OMI-TOMS) and OMI-Differential Optical Absorption Spectroscopy (OMI-DOAS). This study used 0.25° spatial resolution data for OMI-TOMS, OMI-DOAS and AIRS satellite observations.

OMI was launched on the 15 of July 2004 on the NASA Earth Observing System Aura (EOS-Aura) platform to replace TOMS. OMI-TOMS and OMI-DOAS observations began in October 2004. The OMI instrument measures the solar radiation backscattered by the surface and the Earth's atmosphere in three wavelengths (264-311 nm, 307-383 nm and 349-504 nm). OMI uses two algorithms to compute TCO, a TOMS like (OMI-TOMS) algorithm and DOAS (OMI-DOAS) algorithm. OMI-TOMS measuring technique was extensively discussed in other studies (Kim et al., 2017; Balis et al., 2007). OMI-TOMS algorithm uses two sets of wavelengths (317.5 nm / 331.2 nm, and 331.2 nm / 360 nm). The 331.2 nm / 360 nm wavelength set is used for high O_3 and high solar zenith angles, while the 317.5 nm / 331.2 nm set is used in most observations. Moreover, this technique requires the aerosol index for O_3 observations. The function of the aerosol index is to measure the absorption of UV radiation by desert dust and smoke (Vanicek et al., 2003). OMI-DOAS technique uses OMI-DOAS algorithm that was developed by the Royal Dutch Meteorological Institute (KNMI) (Veefkind et al., 2006). In OMI-DOAS, O_3 vertical column is determined in three phases. Firstly, OMI-DOAS fitting is performed to form slant column density. Secondly, the air mass factor is calculated. This phase is required to convert slant column density to a vertical column. The last phase is the correction of clouds. The last phase is

critical because the OMI-DOAS spectral uses a window that is very low sensitive to temperature. The spectral of OMI-DOAS uses 5 nm wide fit window centered on 334.1 nm. The air mass factor is determined by applying the OMI-DOAS fit to assimilate OMI spectra (Veefkind et al., 2006).

Atmospheric Infrared Sounder (AIRS) is a National Aeronautics and Space Administration (NASA) satellite that was launched in May 2002. This satellite makes vertical observations of atmospheric dynamics and atmospheric chemistry from 1000 hPa to 0.1 hPa. The methodology of AIRS was previously discussed in literature (Susskind et al., 2003; Aumann et al., 2003). According to Aumann (2003), the AIRS is a cross-track scanning grating spectrometer with 2378 channels from 3.7 to 15.4 μm and a field of view at nadir of 13.5 km. AIRS uses retrieval algorithm information from a companion microwave sounder (Advanced Microwave Sounding Unit (AMSU)) to retrieve data in the presence of clouds on a horizontal scale of one AMSU and field of view (45×45 km at nadir) that is equivalent to 3×3 AIRS footprints (Susskind et al., 2003).

4.3.3 Reanalysis data

Modern-Era Retrospective Analysis for Research and Applications (MERRA-2) is the second version of MERRA and one of NASA's products. It was launched in the beginning of 1980 to replace the old MERRA dataset (Rienecker et al., 2011). MERRA-2 uses a spatial resolution of 0.5 x 0.625° with a time resolution of three hours. Gelaro et al. (2017) reported that the current model is advanced relative to the previous MERRA. The current model has new assimilation system for data analysis, model constraints and parameterization. Some of these new additions include temperature and O_3 profiles from the Microwave Limb Sounder (MLS) and TCO from OMI. Furthermore, MERRA-2 assimilates OMI and MLS satellite measurements (Millán and Manney, 2017). More details about MERRA-2 including information about updates from MERRA system previously discussed in literature (Rienecker et al., 2011; Bosilovich et al., 2015; Molod et al., 2015; Takacs et al., 2016; Bosilovich et al., 2016).

4.4 Data analysis

The current study used 2017 and 2018 Dobson#035 satellite TCO data. Dobson observations are conducted under direct sun, zenith blue and zenith cloud. However, this study used direct sun observations because they compare better with satellites. Zenith-sky data and zenith-blue readings

were flagged out during data quality control. Consistency of dataset was monitored. For example, within an hour there shouldn't be much difference. Satellite data obtained from OMI-TOMS, OMI-DOAS and AIRS observations was used to validate Dobson#035 TCO observations. The percentage difference between Dobson#035 and satellites TCO observations was calculated by using equation 4.1 while the percentage error between Dobson#035 and satellite TCO observations was calculated by using equation 4.2. In addition, MERRA-2 assimilation data was compared with Dobson#035 using similar calculations described for Dobson#035 and satellite validations.

$$\text{Percentage Difference} = 100 \cdot \frac{(\text{Satellite} - \text{Dobson})}{((\text{Satellite}+\text{Dobson})/2)} \quad (4.1)$$

$$\text{Percentage Error} = 100 \cdot \frac{(\text{Satellite} - \text{Dobson})}{(\text{Dobson})} \quad (4.2)$$

Satellite TCO data was obtained from the Giovanni platform: https://giovanni.gsfc.nasa.gov/giovanni.

The root square mean error (RMSE), mean bias error (MBE) and mean absolute bias error (MABE) were calculated by using equations 4.3, 4.4 and 4.5, respectively. Similar methods were used in previous studies (e.g. Antón et al., 2009, 2010b; Toihir et al., 2015) to compare satellite observations with Dobson and Brewer spectrophotometers. The number of the paired samples is represented by n in equation 4.3, 4.4 and 4.5 below. A positive MBA indicates the overestimation of Dobson observations while a negative MBA indicates the underestimation of Dobson observations by satellites.

$$\text{RMSE} = \sqrt{\frac{\sum_{i-1}^{n}(Satellite - Dobson)^2}{n}} \quad (4.3)$$

$$\text{MBE} = \frac{100}{n}\sum_{i-1}^{n}\frac{Satellite - Dobson}{Dobson} \quad (4.4)$$

$$\text{MABE} = \frac{100}{n} \sum_{i-1}^{n} \frac{|Satellite - Dobson|}{Dobson} \quad (4.5)$$

4.5 Results and discussion

4.5.1 Daily TCO comparisons

The comparison of satellites vs. Dobson was conducted by comparing datasets obtained from OMI-TOMS vs. Dobson, OMI-DOAS vs. Dobson, AIRS vs. Dobson and MERRA-2 vs. Dobson from January 2017 to December 2018. Table 4.1 indicates the statistical analyses obtained between daily Dobson and satellite observations. A small root square mean error (RMSE) of 2.14%, 2.19%, 1.68% and 1.71% was observed in OMI-TOMS vs. Dobson, OMI-DOAS vs. Dobson, AIRS vs. Dobson and MERRA-2 vs. Dobson, respectively. This is in line with other similar studies conducted using southern tropics and subtropics TCO observations, where Toihir et al. (2015) compared Dobson and satellite observations. The small percentage of the MBE indicates a non-significant overestimation or underestimation of the Dobson TCO observations by satellites and MERRA-2 model. With the exception of OMI-TOMS vs. Dobson (-0.20%), a positive MBE percentages was observed for satellites vs. Dobson. Similar observations of negative MBE percentage was reported by Toihir et al. (2015) for OMI-TOMS vs. Dobson spectrophotometers over Irene (-0.90%) and Springbok (-1.28%). In general, all satellites show mean absolute bias error (MABE) values of less than 2.0% when compared with Dobson spectrophotometer. With OMI-DOAS vs. Dobson showing a slightly high MABE percentage of 1.90%. While MERRA-2 vs. Dobson, AIRS vs. Dobson and TOMS vs. Dobson show a MABE percentage of 1.40%, 1.38% and 1.77%, respectively. These results suggest that the daily differences between Dobson and satellite data are small and are in better agreement.

Table 4.1: Comparison of TCO between Dobson and satellite observations from January 2017 to December 2018.

	RMSE (DU)	**MBE (%)**	**MABE (DU)**
OMI–TOMS vs. Dobson 035	6.13 (2.14%)	-0.20	5.09 (1.77%)

OMI–DOAS vs. Dobson 035	6.29 (2.19%)	0.52	5.44 (1.90%)
AIRS vs. Dobson 035	4.81 (1.68%)	0.27	3.97 (1.38%)
MERRA–2 vs. Dobson 035	4.90 (1.71%)	0.30	4.00 (1.40%)

Figure 4.1 shows Dobson#035 and satellites TCO observations time series obtained by using January 2017 to December 2018 data. High standard deviations were observed during austral winter (June-July-August) in all observations while low standard deviations were observed during summer (December-January-February). Bencherif et al. (2000 and 2007) associated the occurrence of high standard deviations with increase of dynamical activity in the winter hemisphere due to the reverse of the zonal wind in the stratosphere. Moreover, the occurrence of stratosphere-troposphere exchange is dominant in winter and spring (Diab et al., 2004). Similar observations were reported in previous study (Thompson et al., 2003).

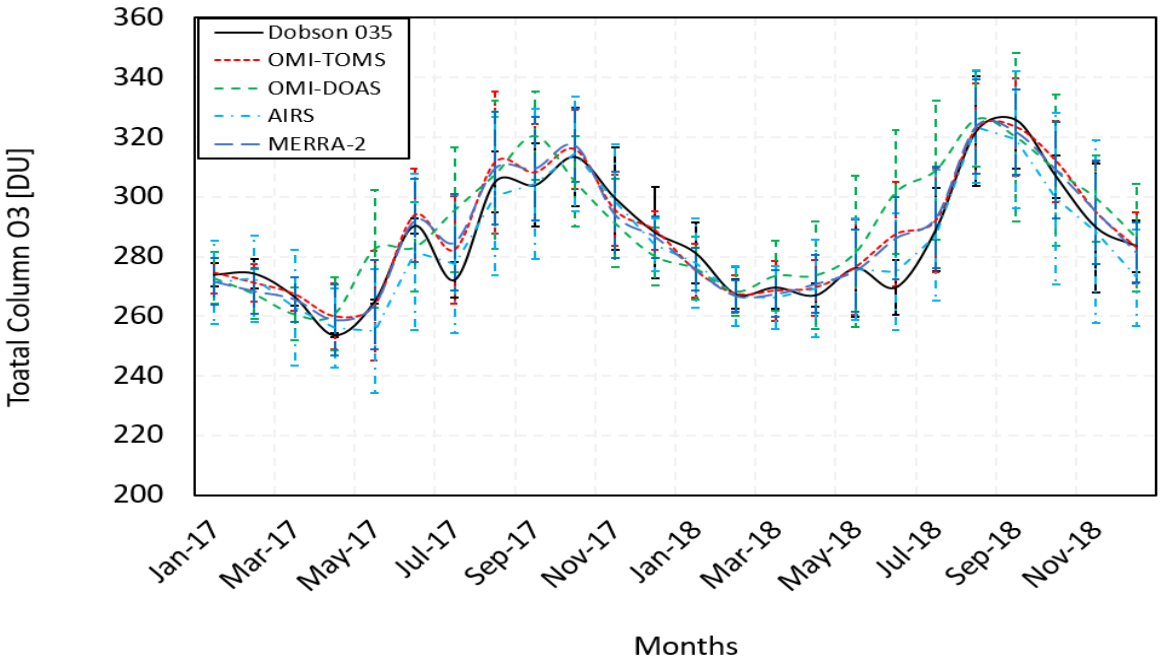

Figure 4.1: Time series of monthly average TCO obtained from Dobson spectrophotometer (solid line), OMI-TOMS (square dot), OMI-DOAS (Dash), AIRS (Dash dot) and MERRA-2 (Long dash) for Stellenbosch site from January 2017 to December 2018. The vertical bars indicate the associated standard-deviations at ±1 sigma.

Figure 4.2 shows daily percentage differences obtained between Dobson#035 and satellite TCO observations (OMI-TOMS (a), DOAS (b), AIRS (c) and MERRA-2 (d)). As indicated in Figure 4.2, daily percentage differences fluctuate between 2% and -2% with few days where the percentage difference between Dobson#035 and satellite observations was above 2% or below -2%. A similar percentage difference of 2% was reported over Seoul Korea between ground-based and satellites observations (Kim et al., 2017). Based on these results, we conclude that satellite observations and MERRA-2 assimilation show reasonable agreement with Dobson#035 TCO observations over Stellenbosch.

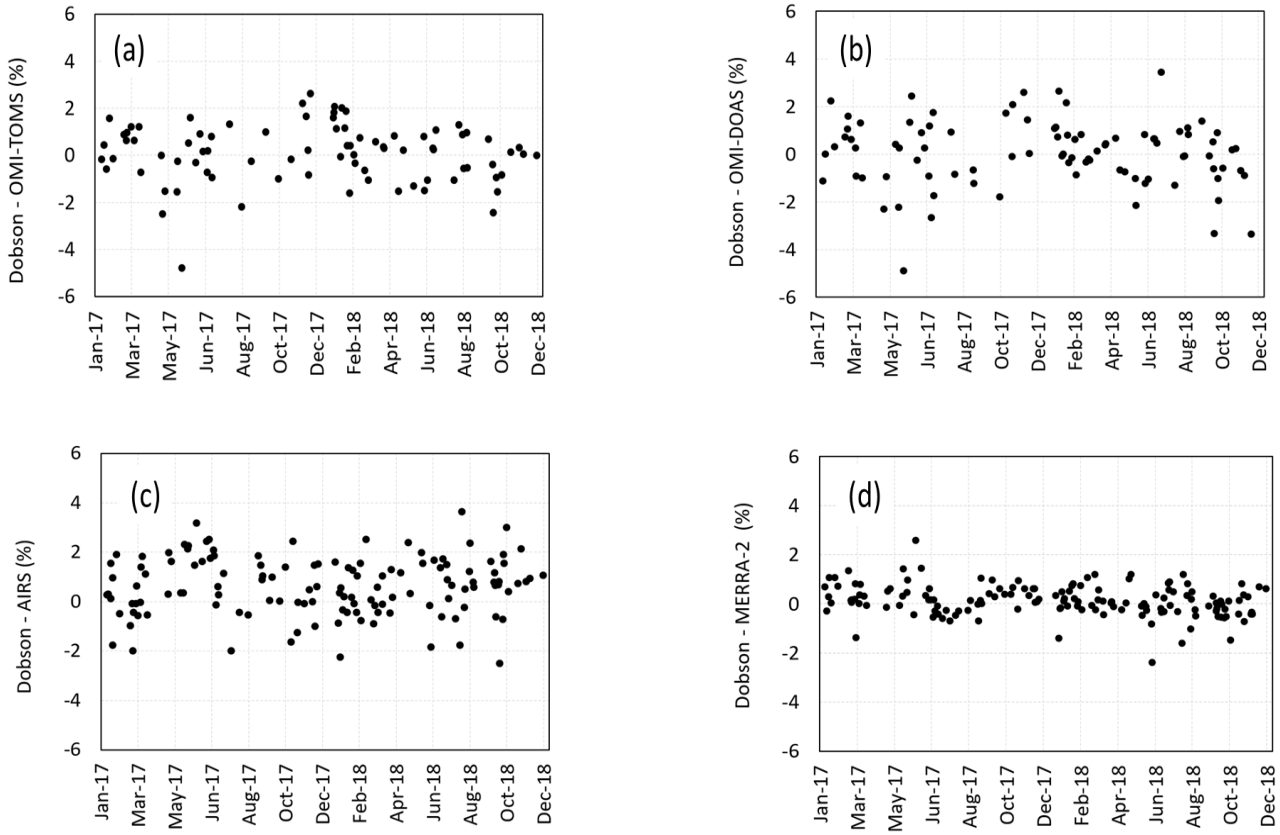

Figure 4.2: Time series of daily relative differences obtained between Dobson and OMI-TOMS (a), Dobson and OMI-DOAS (b), Dobson and AIRS (c), and Dobson and MERRA-2 (d).

Table 4.2 indicates the statistical analysis conducted between satellites and Dobson#035 TCO observations from January 2017 to December 2018. A difference of -0.60 DU and -0.24 DU was obtained from OMI-TOMS and MERRA-2, respectively. A positive difference of 2.00 DU was

obtained between Donson#035 and OMI-DOAS while a negative difference of -4.63 DU was obtained between Dobson#035 and AIRS TCO observations. A percentage error of -0.21%, 0.70%, -1.61% and -0.08% was obtained from OMI-TOMS, OMI-DOAS, AIRS and MERRA-2, respectively. In general, these observations show a good agreement between Dobson#035 and satellite TCO observations. In fact, the observed percentage difference (0.17%) between Dobson#035 and OMI-DOAS is lower than the average percentage difference of 1.65 ± 0.38% that was reported for OMI-DOAS in the Southern Hemisphere. Similarly, the observed percentage difference of -0.05% between Dobson#035 and OMI-TOMS is lower than the average percentage difference of 0.79 ± 0.36% that was reported for OMI-TOMS in the Southern Hemisphere (Balis et al., 2007). In general, Balis et al. (2007) reported that OMI products slightly overestimates Dobson observations in the mid-latitudes and overestimation increases with increasing latitude. In all three satellites used for Dobson#035 validation, OMI-TOMS shows a good agreement of -0.05 % while MERRA-2 assimilation data show an agreement of -0.02%. This good agreement could be related to the fact that OMI-TOMS use similar methodology to spectrophotometers (two wavelengths for analyses) while MERRA-2 uses OMI to assimilate TCO data and that could be the reasons for the observed good agreement for MERRA-2 and OMI-TOMS observations. OMI-DOAS principle differs from the Dobson spectrophotometers. Furthermore, OMI-DOAS and OMI-TOMS use different principles for cloud treatment. The former use spectral fitting, while OMI-TOMS use empirical correction (Millán and Manney, 2017). AIRS performance depends on the altitudes, closer to tropopause, AIRS is more sensitive to temperature (Monahan et al., 2007). Hence, O_3 mole fractions are higher in the lower atmosphere and lower in the upper atmosphere relative to Dobson observations (Monahan et al., 2007). The difference in methodology between AIRS and Dobson spectrophotometers might be the reason for the observed slightly high difference between AIRS and Dobson#035 TCO observations. It is noted that the agreement for OMI-DOAS and AIRS is also good. However, OMI-TOMS and MERRA-2 provide better agreement with Dobson#035.

Table 4.2: Composite statistical analysis of TCO as observed by Dobson and satellite instruments from January 2017 to December 2018.

Annual	**Dobson 035**	**OMI–TOMS**	**OMI–DOAS**	**AIRS**	**MERRA–2**
Average	286.86	286.26	288.87	282.24	286.63
Std. deviation	23.45	22.99	26.16	26.27	22.83

Maximum	373.30	373.40	382.70	383.00	358.50
Minimum	232.65	236.30	233.50	221.38	238.99
Delta		-0.60	2.00	-4.63	-0.24
% Difference		-0.05	0.17	-0.41	-0.02
% Error		-0.21	0.70	-1.61	-0.08

4.5.2 Monthly and seasonal TCO comparisons

Figure 4.3 shows TCO seasonal composites obtained from Dobson#035, OMI-TOMS, OMI-DOAS, AIRS and MERRA-2 based on 2-years observations. A minimum of 260.3 DU and a maximum of 314.8 DU (peak-to-peak of 54.5 DU) was observed from Dobson#035 TCO observations in autumn and spring, respectively. Satellites present similar seasonal cycles as Dobson observations. A minimum of 264.7 DU, 267.2 DU, 262.6 DU and 264.8 DU was obtained from OMI-TOMS, OMI-DOAS, AIRS and MERRA-2, respectively, while a maximum of 317.2 DU, 320.2 DU, 311.9 DU and 316.6 DU was obtained for OMI-TOMS, OMI-DOAS, AIRS and MERRA-2, respectively. Similar observations of low O_3 in autumn and high O_3 in spring were reported in previous studies over Irene and Reunion (Thompson et al., 2003; Sivakumar et al., 2007; Toihir et al., 2018). In addition, Vaz Peres et al. (2017) reported similar observations over Southern Space Observatory in Brazil. The observed seasonal cycle is driven by Brewer-Dobson stratosphere circulation that causes high O_3 concentrations in spring. The observed season cycle is inversely related to solar radiation seasonal cycle. Solar radiation increases in late spring and reach its maximum in summer while O_3 decrease is observed in summer (London, 1985). These results agree with previous results reported over Portugal, Tibet and Lauder in New Zealand (Antón et al., 2010; Zou et al., 2000; Brinksma et al., 1998).

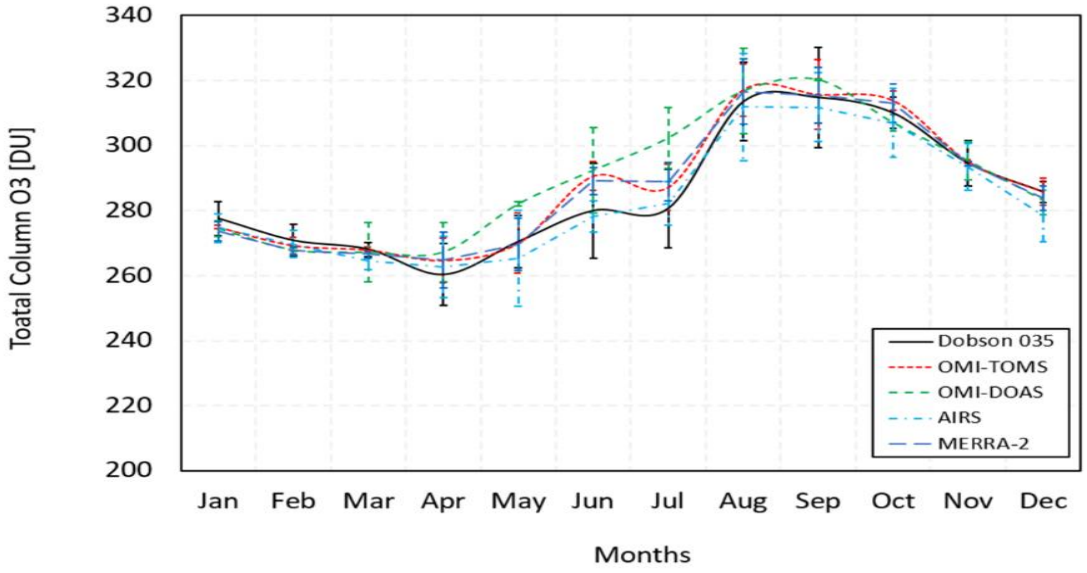

Figure 4.3: TCO monthly mean values as derived from 2-years observations by Dobson spectrophotometer (black solid line), OMI-TOMS (red square dot), OMI-DOAS (green Dash), AIRS (Dash dot) and MERRA-2 (blue long dash) over Stellenbosch. The vertical bars indicate the associated standard-deviations at ±1 sigma.

Table 4.3 presents results of seasonal analysis. It was observed that summer months show a percentage variation of -0.34% and -0.53% between satellites and Dobson#035 observations. This suggests a good agreement between Dobson and satellite observations in summer. Similarly, a good agreement was obtained in autumn and spring. While winter months (JJA) show a slightly higher percentage difference relative to other seasons. However, the percentage difference was less than 0.8% and that indicates a good agreement between Dobson#035 and satellite TCO observations. OMI-DOAS percentage difference was slightly high in winter as compared with other satellite observations. Antón et al. (2011) reported that OMI-DOAS is sensitive to clouds while OMI-TOMS observations show a stability for all cloud conditions. Winter months are cool and overcast in Cape Town (Wichmann, 2006), and that could be the reason for the slightly high OMI-DOAS percentage difference in winter. In general, slightly high percentage difference was observed in winter while low percentage difference was observed in summer

Table 4.3: Seasonal percentage difference and percentage error between satellites and Dobson.

Altitude	**DJF % dif.**	**DJF % err.**	**MAM % dif.**	**MAM % err.**	**JJA % dif.**	**JJA % err.**	**SON % dif.**	**SON % err.**
OMI–TOMS - Dobson	-0.34	-1.36	0.02	0.10	0.40	1.62	-0.05	-0.20
OMI–DOAS - Dobson	-0.43	-1.73	0.31	1.23	0.70	2.82	-0.10	-0.40

AIRS - Dobson	-0.53	-2.08	-0.29	-1.16	-0.23	-0.92	-0.27	-1.08
MERRA–2 - Dobson	-0.42	-1.66	0.03	0.13	0.43	1.73	0.13	0.53

Figure 4.4 shows a Taylor diagram that displays statistical comparison between the Stellenbosch Dobson spectrophotometer TCO data and OMI-TOMS, OMI-DOAS, AIRS and MERRA-2 data. In general, a Taylor diagram is a useful method for evaluating model performance by showing how the correlation coefficient, standard deviation and root mean square error statistics vary simultaneously. In a Taylor diagram, the three different statistics (correlation coefficient R, the standard deviation (sigma) and the (centered) root-mean-square error (RMSE)) are plotted in one 2D graph because they are related to one another and can be represented through the Law of Cosines. Further information on Taylor diagrams is provided by Taylor (Taylor, 2001).

The representation of a Taylor Diagram presented in Figure 4.4 shows a significant correlation of approximately 0.97 between OMI-TOMS and Dobson#035 TCO observations while MERRA-2 shows a correlation of approximately 0.95. A standard deviation of less than 6.0 DU was observed between Dobson#035, OMI-TOMS, and MERRA-2. These observations are in agreement with the correlation coefficient of 0.96 that was previously reported for OMI-TOMS (Kim et al., 2017). A good correlation of approximately of 0.92 was obtained between Dobson#035 and AIRS TCO observations. On the other hand, a correlation coefficient of approximately 0.85 was obtained between Dobson#035 and OMI-DOAS TCO observations. Based on these observations, we may conclude that OMI-TOMS and MERRA-2 observations are in good agreement with the Dobson observations over Stellenbosch, and hence correlates better with Dobson#035 as compared to OMI-DOAS and AIRS satellites.

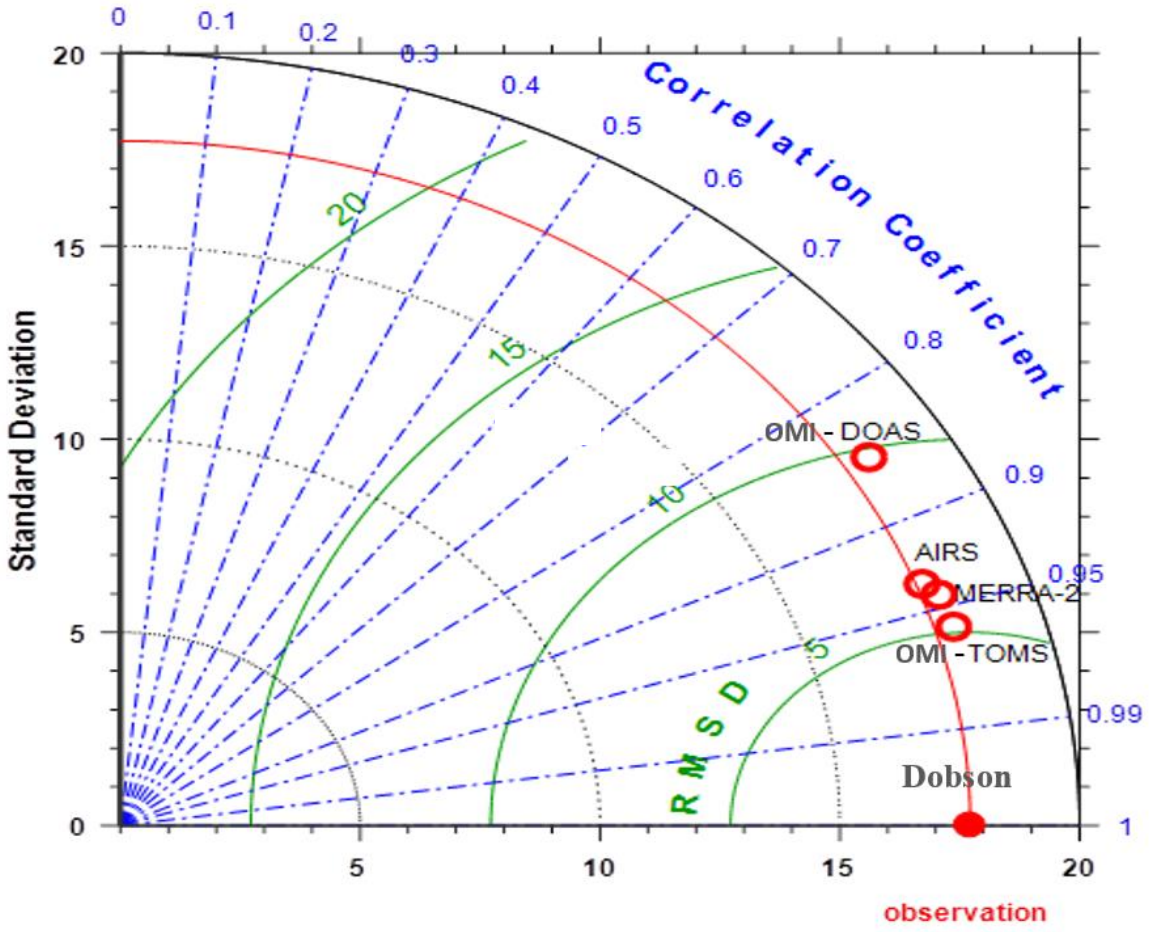

Figure 4.4: TCO correlation coefficient between Dobson observations and satellites observations over the study site, Stellenbosch.

4.6. Summary

The current study aims to validate Dobson#035 TCO with satellite TCO observations (OMI-TOMS, OMI-DOAS and AIRS) and Merra-2 assimilation. Based on the Dobson#035 operating at Stellenbosch site, a comparison of all available data from 2017 to 2018 was performed, for the first time. Daily percentage difference, percentage error, root square mean error, mean bias error, mean absolute bias error and correlation coefficient was calculated between Dobson#035 and satellites observations.

An average composite of 286.86 ± 23.45 DU, 286.26 ± 22.99 DU, 288.87 ± 26.16 DU, 282.24 ± 26.27 DU and 286.63 ± 22.83 DU was obtained from Dobson#035, OMI-TOMS, OMI-DOAS,

AIRS and MERRA-2, respectively. Based on our observations, it is found that daily percentage differences between Dobson and satellites vary within ±2%. However, in some days, the percentage difference was lower than -2% or higher than 2%.

The composite percentage difference was calculated between satellites and Dobson#035 TCO observations. An average percentage difference of -0.05%, 0.17%, -0.41% and -0.02% was calculated over two years for OMI-TOMS, OMI-DOAS, AIRS and MERRA-2, respectively. These observations indicate a good agreement between Dobson#035 and satellite TCO observations. In addition to the composite percentage differences, seasonal percentage difference was calculated between Dobson#035 and satellite observations. A percentage difference of -0.34%, -0.43%, -0.53% and -0.42% was obtained in summer from OMI-TOMS, OMI-DOAS, AIRS and MERRA-2, respectively. In general, summer months show a percentage difference variation between -0.53% and -0.34%. While in autumn, a percentage difference of 0.02%, 0.31%, -0.29% and 0.03% was obtained from OMI-TOMS, OMI-DOAS, AIRS and MERRA-2, respectively. With the exception of AIRS (- 0.23%), a positive percentage difference of 0.40%, 0.70% and 0.43% was obtained in winter from OMI-TOMS, DOAS and MERRA-2, respectively. While in spring, percentage differences of -0.05%, -0.10% and -0.27% and 0.13% was obtained from OMI-TOMS, OMI-DOAS, AIRS and MERRA-2, respectively. Among the used satellite products, OMI-TOMS was in good agreement with Dobson#035 spectrophotometer with a correlation coefficient of 0.97. The likely reason for this good agreement could be related with the retrieval algorithm adopted between OMI-TOMS and Dobson spectrophotometer. MERRA-2 assimilation are closer to OMI-TOMS with a correlation coefficient of 0.95 and it could be related to the OMI observation method that is used by MERRA-2 for O_3 assimilation. The algorithms for OMI-DOAS and AIRS are different to Dobson spectrophotometers. OMI-DOAS showed a correlation coefficient of 0.85, while AIRS showed the lowest correlation of 0.92. All satellites show mean absolute bias error (MABE) values of less than 2.0% when compared with Dobson spectrophotometer. Therefore, the results show a good agreement between Dobson spectrophotometer and satellites observations.

Despite these small differences, there is a good correlation between satellites and Dobson observations. However, OMI-TOMS and MERRA-2 observations correlate better with Dobson observations relative to OMI-DOAS and AIRS observations.

The downside of this study was that TCO diurnal cycles were not studied due to the current Dobson technique that need manual operation for measurements. Dobson manual operation lead to data gaps during the day.

Recommendations

We recommend to continue with Stellenbosch Dobson TCO observations and it may provide observations gives an idea of TCO behavior in Cape Town region. Long term data base further strengthen the climatological results.

References

1. Antón, M., López, M., Vilaplana, J. M., Kroon, M., McPeters, R., Bañón, M. and Serrano, A. Validation of OMI-TOMS and OMIDOAS total ozone column using five Brewer spectroradiometers at the Iberian Peninsula. J. *Geophys. Res.-Atmos.*, 114, D14307, doi:10.1029/2009JD012003, 2009.

2. Antón, M., Vilaplana, J. M., Kroon, M., Serrano, A., Parias, M., Cancillo, M. L. and De la Morena, B. A. The Empirically Corrected EP-TOMS Total Ozone Data Against Brewer Measurements at El Arenosillo (Southwestern Spain), IEEE T. *Geosci. Remote Sens*., 48, 7, 3039–3045, doi:10.1109/TGRS.2010.2043257, 2010b.

3. Toihir, A. M., Bencherif, H., Sivakumar, V., El Amraoui, L., Portafaix, T. and Mbatha, N.: Comparison of total column ozone obtained by the IASI-MetOp satellite with ground-based and OMI satellite observations in the southern tropics and subtropics. *Ann. Geophys*., 33, 1135–1146, doi:10.5194/angeo-33-1135-2015, 2015.

4. Antón, M. and Loyola, D. Influence of cloud properties on satellite total ozone observations. *J. Geophys. Res*., 2011, 116, D03208, doi:10.1029/2010JD014780.

5. Antón, M., Bortoli, D., Costa, M.J., Kulkarni, P.S., Domingues, A.F., Barriopedro, D., Serrano, A. and Silva, A.M. Temporal and spatial variabilities of total ozone column over Portugal, *Remote Sens. Environ.*, 2011, 115, 855–863, doi:10.1016/j.rse.2010.11.013.

6. Aumann, H.H., Chahine, M.T., Gautier, C., Goldberg, M.D., Kalnay, E., McMillin, L.M., Hank Revercomb, H., Rosenkranz, P.W., Fellow, IEEE, Smith, W.L., Staelin, D.H., Fellow, IEEE, L. Larrabee Strow, L. and Susskind. J. AIRS/AMSU/HSB on the aqua mission: design, science objectives, data products, and pro25 cessing systems., IEEE T. *Geosci. Remote*, 2003, 41, 253–264.

7. Balis, D., Kroon, M., Koukouli, M.E., Brinksma, E.J., Labow, G., Veefkind, J.P. and McPeters, R.D. Validation of Ozone Monitoring Instrument total ozone column measurements using Brewer and Dobson spectrophotometer ground-based observations, J. *Geophys. Res*. 2007, 112, D24S46.

8. Bekki, S and Lefevre, F. Stratospheric ozone. History and concepts and interactions with climate. *Eur. Phys. J. Conferences*, 2009, 1, 113–136 (2009). doi: 10.1140/epjconf/e2009-00914-y.

9. Bencherif, H., El Amraoui, L., Semane, N., Massart, S., Charyulu, D.V., Hauchecorne, A. and Peuch, V.H. Examination of the 2002 major warming in the southern hemisphere using ground-based and Odin/SMR assimilated data: stratospheric ozone distributions and tropic/mid-latitude exchange, *Can. J. Phys*., 2007, 85, 1287-1300.

10. Bencherif, H.B., Morel, A., Moorgawa, M., Michaelis, J., Leveau, J., Porteneuve, A.H. and Faduilhe D. Observation and first validation of stratospheric temperature profiles obtained by a Rayleigh-Mie LIDAR over Durban, South Africa, S. Afr. J. Sci. 2000, 96, 487-492.

11. Bertman, S.B. and Roberts, J.M. A PAN analog from isoprene photo-oxidation. *Geophys. Res. Lett*., 1991, 18, 1461-1464.

12. Bian, J., Gettelman, A., Chen, H. and Pan, L.L. Validation of satellite ozone profile retrievals using Beijing ozonesonde data. *J. Geophys. Res*., 2007, 112, D06305, doi:10.1029/2006JD007502.

13. Bosilovich, M., Akella, S., Coy, L., Cullather, R., Draper, C., Gelaro, R., Kovach, R., Liu, Q., Molod, A., Norris, P., Wargan, K., Chao, W., Reichle, R., Takacs, L., Vikhliaev, Y., Bloom, S., Collow, A., Firth, S,. Labow, G., Partyka, G., Pawson, S., Reale, O., Schubert, S.D. and Suarez, M. MERRA-2. Initial Evaluation of the Climate, Series on Global Modeling and Data Assimilation, Greenbelt, MD, USA, NASA/TM–2015-104606, Vol. 43, NASA; 2015.

14. Bosilovich, M.G., Lucchesi, R. and Suarez, M. 2016. MERRA–2: File Specification. GMAO Office Note No. 9 (Version 1.1), 73 pp, available from http://gmao.gsfc.nasa.gov/pubs/office_notes.

15. Bramstedt, K., Gleason, J., Loyola, D., Thomas, W., Bracher, A., Weber, M. and Burrows, J. P. Comparison of total ozone from the satellite instruments GOME and TOMS with measurements from the Dobson network 1996–2000, *Atmos. Chem. Phys*., 2003, 3, 1409–1419, doi:10.5194/acp-3-1409-2003.

16. Brinksma, E.J., Meijer, Y.J., Connor, B.J., Manney, G.L., Bergwerff, J.B. and Bodeker, G.E., Boyd, I.S., Liley, J.B., Hogervorst, W., Hovenier, J.W., Livesey, N.J. and Swart, D.P.J. Analysis of record-low ozone values during the 1997 winter over Lauder, New Zealand, *Geophys. Res. Lett*., 1998, 25, 2785–2788, doi:10.1029/98GL52218.

17. Cho, H.K., Kim, J., Oh, S.N., Kim, S.K., Baek, S.K. and Lee, Y.G. A climatology of stratospheric ozone over Korea, A*PJAS*., 2003; 6, 97–112.

18. Cizkova, K., Laaaska, K., Metelka, L. and Stanek. M. Intercomparion of Ground- and Satellite-Based Total Ozone Data Products at Marambio Base, Antarctic Peninsula Region. *Atmosphere*, 2019, 10, 721, doi:10.3390/atmos10110721.

19. Darrall, N.M. The effect of air pollutants on physiological processes in plants. *Plant Cell Environ*., 1989, 12, 1-30.

20. Derwent, R.G. The estimation of global warming potentials for a range of radiatively active gases. In non-CO2 Greenhouse Gases, Vann Ham, J., Janssen, L.J.H.M., Swart, R.J.(eds). 1995, 289-299. Kluwer, Dordrecht.

21. Diab, R.D., Thompson, A.M., Mari, K., Ramsay, L. and Coetzee G.J.R. Tropospheric ozone climatology over Irene, South Africa from 1990 to 1994 and 1998 to 2000. *J. Geophys. Res*. 2004, 109, JD00479.

22. Fetzer, E.J., Lambrigsten, B.H., Eldering, A., Aumann, H.H. and Chahine, M.T. Biases in total precipitable water vapor climatologies from atmospheric infrared sounder and advanced microwave scanning radiometer, *J. Geophys. Res*., 2006, 111, D09S16, doi:10.1029/2005JD006598.

23. Finkelstein, J.N. and Johnston, C.J. Enhanced sensitivity of the postnatal lung to environmental insults and oxidant stress. *Pediatrics*, 2004, 113, 1092-1096.

24. Gelaro, R., McCarty, W., Suárez, M.J., Todling, R., Molod, A. and Takacs, L., Randles, C., Darmenov, A., Bosilovich, M.G., Reichle, R., Wargan, K., Coy, L., Cullather, R., Draper, C., Akella, S., Buchard, V., Conaty, A., da Silva, A., Gu, W., Kim, G.K., Koster, R., Lucchesi, R., Merkova, D., Nielsen, J.E., Partyka, G., Pawson, S., Putman, W., Rienecker, M., Schubert, S.D., Sienkiewicz, M. and Zhao, B. The Modern-Era Retrospective analysis for Research and Applications, Version 2 (MERRA-2). *J. Clim*. 2017, 30, 14, 5419–5454. https://doi.org/10.1175/JCLI-D-16-0758.1.

25. Gimeno, B.S., Peñuelas, J., Porcuna, J.L. and Reinert RA. Biomonitoring ozone phytotoxicity in eastern Spain. *Water Air Soil Poll*., 1995, 85, 1521-1526.

26. Kim, J., Kim, J., Cho, H.K., Herman, J., Park, S.S. and Lim, H.K, Kim, J.H., Miyagawa, K. and Lee, Y.G. Intercomparison of total column ozone data from the Pandora spectrophotometer with Dobson, Brewer, and OMI measurements over Seoul, Korea. *Atmos. Meas. Tech*. 2017, 10, 3661–3676.

27. Kinney, P.L., Thurston, G.D. and Raizenne M. The effects of ambient ozone on lung function in children: A reanalysis of six summer camp studies. *Environ. Health Persp*., 1996, 104, 2, 170-174.

28. Komhyr, W.D., Grass, R.D., Leonhard, R.K. Dobson spectrophotometer 83: A standard for total ozone measurements, 1962–1987. *J. Geophys. Res*. 1989, 94, 9847–9861, doi:10.1029/JD094iD07p09847.

29. Kroon, M., Brinksma, E.J., Labow, G. and Balis, D. OMTO3 Validation Status 200604. RP-OMIE-KNMI-820, 2006, Version 1.1, 1–24.

30. Lacis, A.A., Wuebbles, D.J. and Logas, J.A. Radiative forcing of climate by changes in the vertical distribution of ozone. *J. Geophys. Res*., 1990, 95, 9971-9981.

31. London, J. Observed distribution of atmospheric ozone and its variations, in: Ozone in the free atmosphere, edited by: Whitten RC, Prasad SS, New York: Van Nostrand Reinhold, 1985, 1, 11– 80.

32. Martens, W. Health impacts of climate change and ozone depletion: an ecoepidemiologic modeling approach. *Environ. Health Persp*., 1998, 106, 241–251.

33. Millán, L.F. and Manney, G.L. An assessment of ozone mini-hole representation in reanalyses over the Northern Hemisphere. *Atmos. Chem. Phys*., 2017, 17, 9277–9289.

34. Molod, A., Takacs, L., Suarez, M. and Bacmeister, J. Development of the GEOS-atmospheric general circulation model: evolution from MERRA to MERRA2, *Geosci. Model Dev*., 2015, 8, 1339–1356, https://doi.org/10.5194/gmd-8-1339-2015.

35. Monahan, K.P., Pan, L.L., McDonald, A.J., Bodeker, G.E., Wei, J., George, S.E., Barnet, C.D. and Maddy, E. Validation of AIRS v4 ozone profiles in the UTLS using ozonesondes from Lauder, NZ and Boulder, USA. J. *Geophys. Res*., 2007, 112, D17304, doi:10.1029/2006JD008181.

36. Morgan, P.B., Mies, T.A., Bollero. G.A., Nelson, R.L. and Long, S.P. Season-long elevation of ozone concentration to projected 2050 levels under fully open-air conditions substantially decreases the growth and production of soybean. *New Phytol*., 2006, 170, 333–343.

37. National Research Council (1999). Ozone-Forming Potential of Reformulated Gasoline. National Academy Press, Washington.

38. Penuelas, J., Ribas, A., Gimeno, B.S. and Filella, I. Dependence of ozone biomonitoring on meteorological conditios of different sites in Catalonia (N.E. Spain). *Environ. Monit. Assess*., 1999, 56, 221-224.

39. Rienecker, M.M., Suarez, M.J., Gelaro ,R,. Todling, R., Bacmeister, J., Liu, E. et al. MERRA - NASA's Modern-Era Retrospective Analysis for Research and Applications. *J. Climate*. 2011, 24, 3624–3648, doi:10.1175/JCLI-D-11-00015.1.

40. Roberts, G., Wooster, M.J. and Lagoudakis, E. Annual and diurnal African biomass burning temporal dynamics. *Biogeosciences*, 2009, 6, 849–866. doi:10.5194/bg-6-849-2009.

41. Sivakumar, V., Portafaix, T., Bencherif, H., Godin-Beekmann, S. and Baldy, S. Stratospheric ozone climatology and variability over a southern subtropical site: Reunion Island (21° S; 55° E). *Ann. Geophys*., 2007, 25, 2321–2334.

42. Sivasakthivel, T. and Reddy, K.K.S.K. Ozone Layer Depletion and Its Effects: A Review. IJESD, 2011, 2, 30-32.

43. Strow, L.L., Hannon, S.E., Machado, S.D.S., Motteler, H.E and Tobin, D.C. Validation of the Atmospheric Infrared Sounder radiative transfer algorithm. *J. Geophys. Res*., 2006, 111,D9, D09S06, doi:10.1029/ 2005JD006146.

44. Susskind, J., Barnet, C.D. and Blaisdell, J.M. Retrieval of atmospheric and surface parameters from AIRS/AMSU/HSB data in the presence of clouds, IEEE Trans. *Geosci. Remote Sens*., 2003, 41, 390–409, doi:10.1109/TGRS.2002.808236.

45. Susskind, J., Barnet, C.D., Blaisdell, J.M., Iredell, L., Keita, F., Kouvaris, L., Molnar, G. and Chahine, M.T. Accuracy of geophysical parameters derived from Atmospheric Infrared Sounder/Advanced Microwave Sounding Unit as a function of fractional cloud cover. *J. Geophys. Res*., 2006, 111, D09S17, doi:10.1029/2005JD006272.

46. Takacs, L.L., Suárez, M.J. and Todling, R. Maintaining atmospheric mass and water balance in reanalyses. *Q. J. Roy. Meteor. Soc*., 2016, 142, 1565–1573.

47. Taylor, K.E. Summarizing multiple aspects of model performance in a single diagram. *J. Geophys. Res: Atmospheres.* 2001, 106, D7, 7183-7192.

48. The National Aeronautics and Space Administration. NASA; [cited 2018 Sep 13]. Available from: https://giovanni.gsfc.nasa.gov/giovanni/.

49. Thompson, A.M., Witte, J.C., McPeters, R.D., Oltmans, S.J., Schmidlin, F.J., Logan, J.A., Fujiwara, M., Kirchhoff, V.W.J.H., Posny, F., Coetzee, G.J.R., Hoegger, B., Kawakami, S., Ogawa, T., Johnson, B.J., Vomel, H. and Labow, G. Southern Hemisphere Additional Ozonesondes (SHADOZ) 1998–2000 tropical ozone climatology. *J. Geophys. Res*., 2003, 108, D2, 8238, doi:10.1029/2001JD000967.

50. Toihir, A.M., Portafaix, T., Sivakumar, V., Bencherif, H., Pazmiño, A. and Bègue, N. Variability and trend in ozone over the southern tropics and subtropics. *Ann. Geophys*., 2018, 36, 381-404, https://doi.org/10.5194/angeo-36-381-2018.

51. Treshow, M. and Stewart, D. Ozone sensitivity of plants in natural communities. *Biol*., 1973, 5, 3, 209-214.

52. Vanicek, K., Martin, S. and Martin, D. Evaluation of Dobson and Brewer total ozone observations from Hradec Kralove Czech republic, 1961-2002. Report of the project CANDIDOZ, working group WG-15th RTD framework programme, project No.: EVK2-CT-2001-00133. Czech Hydrological Institute Prague, September, 2003.

53. Vaz Peres, L., Bencherif, H., Mbatha, N., Schuch, A.P., Toihir, A.M. and Bègue, N., Portafaix, T., Anabor, V., Pinheiro, D.K., Leme, N.M.P., Bageston, J.V. and Schuch, N.J. Measurements of the total ozone column using a Brewer spectrophotometer and TOMS and OMI satellite instruments over the Southern Space Observatory in Brazil. *Ann. Geophys*., 2017, 35, 25–37.

54. Veefkind, J.P., de Haan, J.F., Brinksma, E.J., Kroon, M. and Levelt, D.F. Total ozone from the Ozone Monitoring Instrument (OMI) using the OMI DOAS technique, IEEE Trans. *Geosci. Remote Sens*., 2006, 44, 5, 1239– 1244.

55. Wichmann J. Seasonal inter-site correlation among air pollution monitoring sites in Cape Town, Pretoria, University of Pretoria, 2006.

56. World Meteorological Organization (WMO). Assessment for Decision-Makers: Scientific Assessment of Ozone Depletion: 2014, Global Ozone Research and Monitoring Project – Report No. 56, 88 pp, Geneva, Switzerland, 2014.

57. Ziemke, J.R., Strode, S.A., Douglass, A.R., Joiner, J., Vasilkov, A., Oman, L.D., Liu, J., Strahan, S.E., Bhartia, P.K. and Haffner, D.P. A cloud-ozone data product from Aura OMI and MLS satellite measurements. *Atmos. Meas. Tech*., 2017, 10, 4067–4078.

58. Zou, H., Chongping, J. and Libo, Z. QBO signal in total ozone over Tibet. *Adv. Atmos. Sci*., 2000, 17, 562–568, doi:10.1007/s00376- 000-0019-4.

CHAPTER 5: SURFACE AND TOTAL COLUMN OZONE OBSERVATIONS AT CAPE POINT GAW STATION AS OBSERVED BY GROUND BASED AND SATELLITE INSTRUMENTS

This chapter presents some of the work that was published on a manuscript: Day-time and Night-time Ozone increase at Cape Point GAW Station as observed by ground based instruments. T. Mkololo, N. Mbatha, V. Sivakumar, C. Labuschagne, W. Jourbet, E.T. Mbambalala and L. Martin. *Proc. of the 35th Annual conference of South African Society for Atmospheric Sciences (SASAS), River Sun, Vanderbijl Park, Gauteng,* ISBN : 978-0-6398442-0-6, Pg84-87, 8-9 October, 2019.

5.1 Abstract

This study presents analysis of the variability and trends of the all-day, day- and night-time surface ozone (O_3) data measured from 2000 to 2018 at Cape Point Global Atmosphere Watch (GAW) station. Annual, seasonal and weekday-weekend trends were investigated by using two approaches; such as, linear regression slope and Theil-Sen slope. All seasons show negative trends in day-time data subsets while positive trends were observed in night-time data subsets. The annual linear regression slope of 0.28 ppb/year and 0.19 ppb/year was observed for the night-time and day-time, respectively. On the other hand, Theil-Sen trend estimated an increase of 0.67%/year and 0.02%/year for night-time and day-time, respectively. Our observations indicate that the observed trends were not influenced by weekend effect because weekdays and weekends trends were similar for day-time and night-time data subsets. In addition to trend analysis, wind and radon data was used to investigate if the observed O_3 increase was related to changes in winds. Hence, radon concentration rose and percentage frequency occurrence of wind speed and radon relative to wind direction were calculated. The relationship between TCO and surface O_3 was investigated by using linear regression method. The percentage R square of 30.1%, 24.1%, 24.4% and 34.7% was obtained between OMI-TOMS vs. surface O_3, OMI-DOAS vs. surface O_3, AIRS vs. surface O_3 and MERRA-2 vs. surface O_3, respectively. Extreme maximum and minimum values of O_3 have been identified and explored a pilot study.

Keywords: Surface ozone, Day-time, Night-time, Trend analysis, Wind direction, Radon, Cape Point.

5.2 Introduction

Cape Point Global Atmosphere Watch (GAW) is one of the World Meteorological Organization (WMO) GAW stations that monitor continuously surface ozone (O_3) to study atmospheric constituents and pollutants background-level trends. Approximately 90% of the total O_3 is located in the stratosphere and only 10% is located in the troposphere. Stratospheric O_3 acts as a shield that protects the Earth from harmful radiation from the sun. On the other hand, the tropospheric O_3 is formed through photochemical reactions of nitrogen oxides (NO_x) and volatile organic compounds (VOCs) or through downward movement of O_3 from the stratosphere to the troposphere. Nitrogen oxides and VOCs are emitted from anthropogenic sources such as fossil fuel power plants, industrial activities, and transportation as well as natural sources such as lightning and soil (NO_x). In the presence of sunlight, nitrogen dioxide (NO_2) undergoes photochemical reactions to produce oxygen atom (O), which reacts with oxygen molecule (O_2) to form O_3 (Lelieveld and Dentener, 2000).

In general, O_3 mole fractions are expected to be higher during day-time as compared to night-time because of photochemical reactions that take place during the day (Seinfeld and Padis, 2006). Night-time is characterized by low O_3 mole fractions, O_3 destruction by NO titration and deposition processes (Ghosh et al., 2013). Earlier studies reported the importance of separating day and night-time O_3 analysis due to different influencing factors that take place during these times (Özbay et al., 2011). Dinitrogen pentoxide (N_2O_5) in the night-time O_3 chemistry strongly affects the depletion process (Ghosh et al., 2013). Therefore, the Cape Point O_3 data is separated into day and night-time data in order to investigate whether O_3 increase occurs in both data subsets or is related to photochemical reactions that occurs during day-time only.

5.3 Data and method

The Cape Point GAW station was established in 1978. The surface O_3 long-term monitoring program began in 1983 from 30 m air intake line above the ground. In 1996, a second instrument was installed at the 4 m above the ground. Since then, the surface O_3 mole fractions have been

monitored continuously in the atmosphere using two Thermo Electron (Teco) analyzers based on an ultraviolet (UV) detection technique. Continuous O_3 mole fraction data are averaged in 30 min averages. Daily zeroes are performed to check the long-term stability of the instruments. Furthermore, instrumental verifications are performed quarterly using the primary calibrator (TEI 49i-PS) traceable to WMO World Calibration Centre (WCC-EMPA) based in Switzerland.

In addition to the site verifications, calibrations are performed by WCC-EMPA every four years as from 1997. The latest O_3 instrument performance audit was performed in 2015.

The main aim of this study is to investigate day and night-time surface O_3 variability and trends. The second objective of the study is to identify extreme maximum and minimum surface O_3 events. The third objective of the study is to investigate the relationship between total column ozone (TCO) and surface O_3. The trends and its significance are investigated using the Mann–Kendall trend test statistic. This method is defined as a non-parametric, rank-based method which is commonly used to extract monotonic trends in the time series of climate data, environmental data or hydrological data. Mann-Kendall test statistics was computed using the formula:

$$S = \sum_{k=1}^{n-1} \sum_{j=k+1}^{n} sign(X_j - X_k) \quad (1)$$

where,

$$sign(x) = \begin{cases} +1, & \text{if } x > 1 \\ 0, & \text{if } x = 0 \\ -1, & \text{if } x < 1 \end{cases},$$

average value of S is $E[S] = 0$, and the variance σ^2 is given by the equation:

$$\sigma^2 = \left\{ n(n-1)(2n+5) - \sum_{j=1}^{p} t_j (t_j - 1)(2t_j + 5) \right\} / 18 \quad (2)$$

In respect to the above-defined Z-transformation equation, this study reflects a 5% confidence level, where the null hypothesis of no trend is rejected if |Z|>1.96.

5.4 Results and discussion

5.4.1 Long-term trends

As indicated in Figure 5.1, the average surface O_3 diurnal cycle show a minimum of 23.9 ± 6.9 ppb at 09:00 am and start to increase after the morning traffic peak hour (09:30 am). A maximum of 27.2 ±7.7 ppb was observed at 03:00 pm. Such an increase is followed by a decrease after 05:00 pm. Therefore, the current study uses local time intervals of 11:00 am to 04:00 pm and 11:00 pm to 04:00 am for day and night-time, respectively. However, the actual day and night-time vary with seasons.

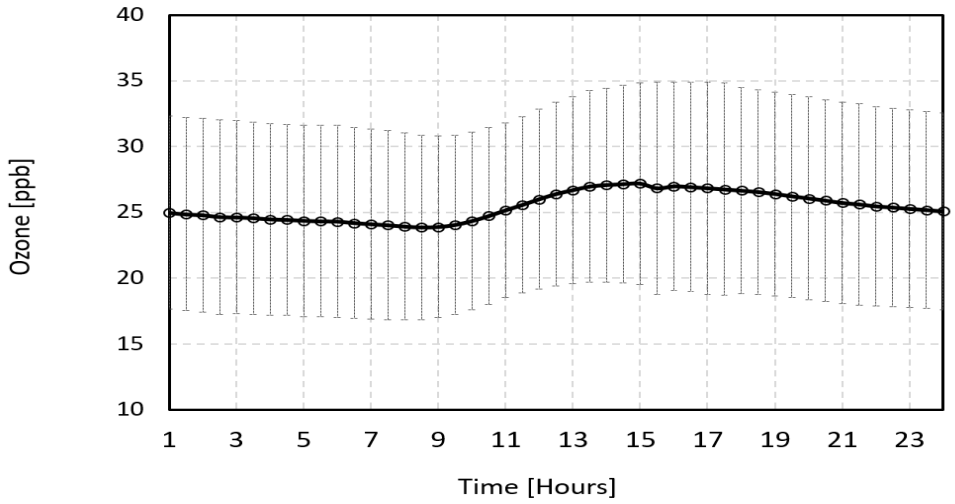

Figure 5.1: The average diurnal cycle of all year average surface O_3 mole fractions during 2000 to 2018.

An average composite of 26.6± 5.7 ppb and 24.9± 5.0 ppb was observed over a period of 18 years for day and night-time, respectively. The observed results of slightly higher surface O_3 mole fractions during the day are in agreement with previous studies that reported the occurrence of photochemical reactions in day-time (e.g. Seinfeld and Pandis, 2006; Alghamdi et al., 2014). However, due to the geographical location of the station, there is less O_3 destruction by Nitrogen Oxide (NO) during night-time (as compared to a city environment, for example). Hence, night-time O_3 mole fractions at Cape Point were not as low as in the stations located in Cape Town sub-urban and urban areas (Nzotungicimpaye et al., 2014). These observations can be related to less effect of anthropogenic activities that release NO_x in the atmosphere. Previous studies (Mkololo,

2013; Nzotungicimpaye et al., 2014) reported that O_3 diurnal cycle is inversely proportional to NO_x diurnal cycle in Cape Town urban stations and O_3 diurnal cycle is more pronounced in Cape Town urban stations showing a peak-to-peak is approximately 12 ppb.

As indicated in Table 5.1, the linear regression trends show an increase of 0.19 ppb/year, 0.14 ppb/year and 0.22 ppb/year for all-day, day and night-time, respectively, with the strongest z-score of 3.30 observed with night-time data. With the exception of day-time, time series indicates a significant increase of O_3 trends with positive z-score which are above 1.96 (95% confidence level). The Theil-Sen trend shows a similar strong increase of 0.66 %/year in the night-time data, while an increase of 0.39 %/year and 0.01 %/year was observed for the all-day and day-time data, respectively. As indicated in Figure 5.2, more increase was observed from 2017 to 2018. Hence, we excluded these years for the second calculation of trends. The 2000 to 2016 Theil-Sen trend showed an increase of 0.28 %/year and 0.03 %/year in the night-time and all-day, respectively. On the other hand, a decrease of -0.34 %/year was observed in day-time. Similar results on high night-time trends relative to day-time were reported by Xu et al (2016) at the Mt Waliguan GAW station in China.

Remarkably, Oltmans et al. (2013) conducted an earlier study on tropospheric O_3 changes using 1983 to 2010 dataset and reported O_3 increase at Cape Point and other GAW stations in the Southern Hemisphere (Cape Grim and Lauder). This shows that Cape Point O_3 increase was recorded prior to 2015. However, our statistical analysis show a stronger increase in recent years, especially in the time period from 2016 to 2018. An average of 25.5 ppb, 26.6 ppb and 24.9 ppb was recorded over the study period for all-day, day and night-time, respectively. In 2018 alone, the O_3 average exceeds the long-term average by 7.1, 7.6 and 6.8 ppb for all-day, day and night-time, respectively.

Table 5.1: The linear regression slope, z-score and the p-values of all year surface ozone mole fraction for the all-day, day-time and night-time data subsets during 2000 to 2018.

Data subset	Linear slope (ppb/year)	z-score	p-value
All-day	0.19	2.82	0.0048
day-time	0.14	1.71	0.0872
Night-time	0.22	3.30	0.0010

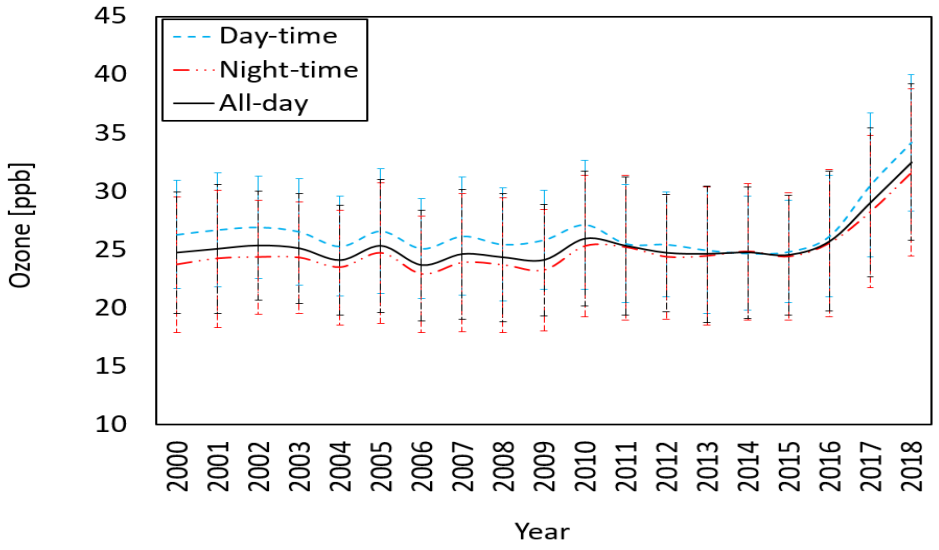

Figure 5.2: The average and the standard deviation (error bars) of all year average surface O_3 mole fractions for the all-day (diamond), day-time (circle) and night-time (tri-angle) data subsets during 2000 to 2018.

5.4.2 Seasonal and weekend effect dependence

Our observations indicate that day-time O_3 mole fractions were higher by 2.7 ±1.3 ppb, 2.1± 0.7 ppb, 0.6±0.1 ppb and 1.3±0.5 ppb in summer, autumn, winter and spring, respectively, relative to night-time O_3 mole fractions. However, day-time significant trends (p-value less than 0.05) are only observed in annual, summer and spring dataset. The p-value obtained in autumn and winter linear regression was higher than 0.05 (Table 5.1). Hence, the observed trends were non-significant at 95% confidence level. On the other hand, night-time dataset show significant trends in autumn and winter dataset. It is evident from these observations that the observed night-time annual significant trend was due to night-time autumn and winter significant trends. Figure 5.3 shows high standard deviations during the day-time and in months with strong solar radiation. On the other hand, low O_3 variation was observed at night-time and in months with weaker solar radiation. This is in line with the understanding that solar radiation is important parameter in the production and destruction of O_3.

Ozone maximum was observed in winter when temperatures are low and less O_3 photolysis took place during this season. While in summer, temperatures are high and more O_3 photolysis occurred (Figure 5.3). Figure 5.3 shows all-day, day-time and night-time seasonal cycles with

O_3 maximum in winter and spring and minimum in summer. The observed seasonal pattern was previously reported for stations in the Northern and Southern Hemisphere, e.g. Barbados (Oltmans and Levy III, 1994), Cape Grim (Ayers et al., 1997) and Cape Point (Labuschagne et.al, 2018). Cape Point is dominated by south easterly winds that brings clean air to the station. As shown in chapter 3, STE events predominantly occur in winter and spring over South Africa (Irene). Similar results of high STE occurrence in winter and spring was previously reported by Diab et al. (2004). The Cape Point O_3 seasonal cycle coincides with the maximum occurrence of STEs in the country. In addition the observed seasonal cycle could be related to O_3 photolysis (Labuschagne et al., 2018). On the other hand, urban environment seasonal cycle is predominantly driven by nitrogen oxides (NO_x) chemistry. It is noted that O_3 maximum at Cape Point occurs in winter when temperatures are low. The observed O_3 seasonality can be related to the stratosphere-troposphere exchange that predominantly occur in winter and spring months (Diab et al., 2004).

Equation: $O_3 + hv \rightarrow O_2 + O$ (Levy, 1971) (3)

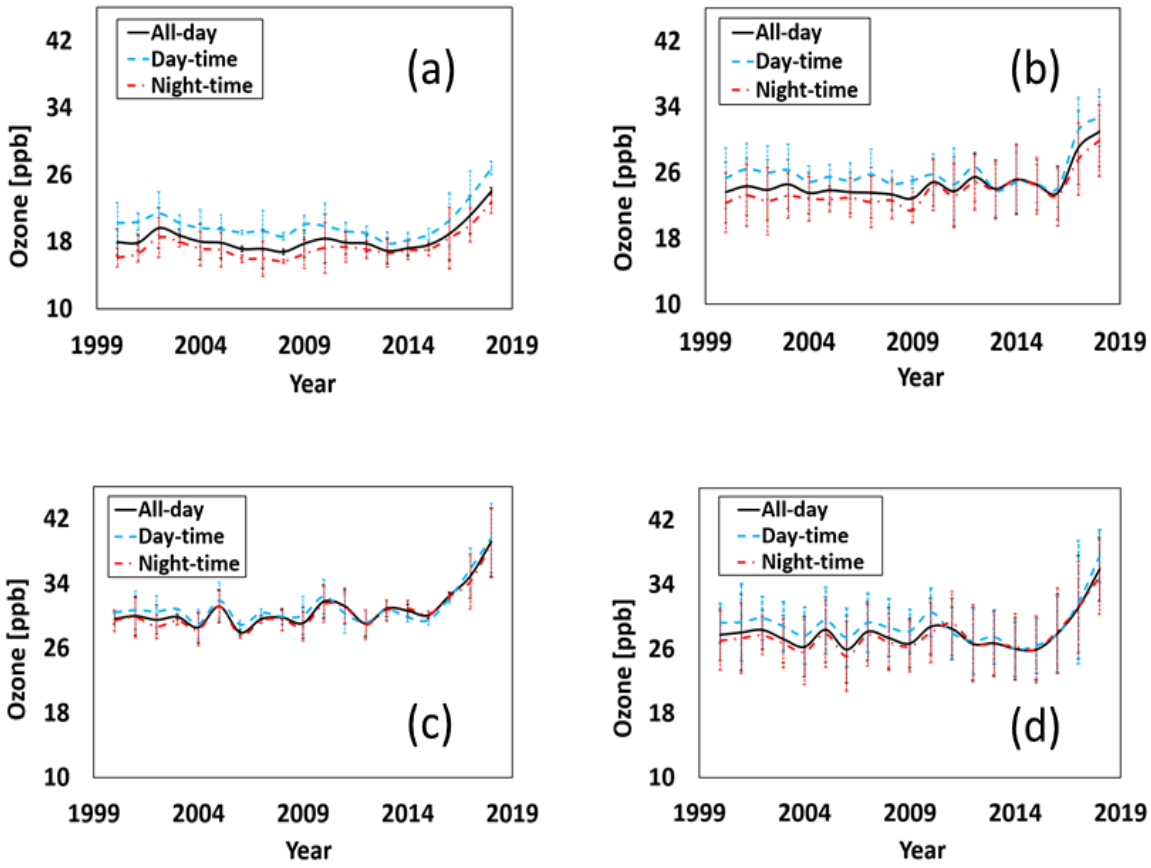

Figure 5.3: All-day (solid line), day-time (dash line) and night-time (dash dot line) surface ozone long-term trend observed in summer (a), autumn (b), winter (c) and spring (d) from 2000 to 2018.

In addition to the annual trends, seasonal day-time and night-time trends were calculated using 2000 to 2016 surface O_3 dataset (Table 5.2 (a), (b) and (c)). With the exception of winter, negative trends were observed during the day in summer, autumn and spring. While all seasons show a positive night-time trend. However, day-time trends show significant trends in summer and spring (5.2 (a)). On the other hand, night-time trends show significant trends in autumn and winter (5.2 (b)). Negative trend were observed in day-time for both weekdays and weekends while positive trends were observed in night-time (Table 5.3). This indicate that O_3 trends are not driven by the weekend effect. However, with the exception of night-time dataset, weekdays and weekends trends were non-significant at 95% confidence level showing a p-value of more than 0.05 (Table 5.3). O_3 increase at Cape Point could be related to changes in meteorological

parameters such as wind speed, wind direction, solar radiation, temperature and humidity as these factors play an important role in O_3 chemistry. Winds with low speed, high solar radiation, high temperatures and low humidity promotes O_3 increase (Tarasova and Karpetchko, 2003). The prevailing winds at Cape Point were south-easterlies that brings clean air from the ocean to the station. This is evidence from both wind speed and radon percentage frequency of occurrence observations (Figure 5.4 and 5.5). The prevailing south-easterlies were characterized by low radon concentrations while high radon concentrations were observed from west to north-east (Figure 5.6). As from 2014 to 2018, a change in the average wind direction from south-east to east was observed. In the years that seem to indicate high O_3 mole fractions at Cape Point station, the year 2016 is only year that seem to indicate a typical south-east direction while 2017 show dominant north-easterlies. It is noted that wind data availability was 61% in 2017.

The caveat here is that during this year the data is potentially seasonally biased with a lack of wind observations during summer months when south-easterlies are more dominant at the station. Therefore, the lack of summer wind data might be a reason for the observed dominant north-easterlies in 2017. The longer-term impact of changes in the wind characteristics require further investigation.

Table 5.2: Seasonal trends calculated by using linear regression and Sen's slope (brackets) from 2000 to 2016 (ppb/year).

	Slope (ppb/year)	**Multiple R**	**R square**	**Standard error**	**P-value**
		(a). All-day			
Annual	0.01 (0.01)	0.10	0.01	0.62	0.70
Summer	-0.03 (-0.03)	0.25	0.06	0.75	0.34
Autumn	0.03 (0.01)	0.26	0.07	0.69	0.32
Winter	0.11 (0.12)	0.47	0.22	1.07	0.05
Spring	-0.06 (-0.09)	0.31	0.09	0.97	0.23
		(b). Day-time			
Annual	-0.08 (-0.12)	0.51	0.26	0.68	0.04
Summer	-0.10 (-0.13)	0.54	0.29	0.81	0.02
Autumn	-0.09 (-0.13)	0.43	0.18	0.75	0.08
Winter	0.01 (-0.02)	0.00	$1.78e^{-05}$	1.08	0.99
Spring	-0.15 (-0.18)	0.59	0.35	1.10	0.01

		(c). Night-time			
Annual	0.07 (0.08)	0.49	0.24	0.68	0.04
Summer	0.03 (0.01)	0.16	0.05	0.86	0.54
Autumn	0.11 (0.09)	0.56	0.31	0.86	0.01
Winter	0.14 (0.15)	0.55	0.30	1.16	0.02
Spring	0.01 (-0.008)	0.04	0.00	1.10	0.89

Table 5.3: Weekdays and weekends linear regression and Sen's slope (brackets) from 2000 to 2016.

	Slope (ppb/year)	**Multiple R**	**R square**	**Standard error**	**P-value**
		(a). All-day			
Weekdays	0.00 (0.02)	0.00	1.48^{e-05}	0.70	0.99
Weekends	0.01 (-0.02)	0.18	0.03	0.22	0.50
		(b). Day-time			
Weekdays	-0.09 (0.02)	0.21	0.04	0.67	0.41
Weekends	-0.08 (-0.12)	0.13	0.02	0.93	0.61
		(c). Night-time			
Weekdays	0.05 (0.06)	0.61	0.38	1.07	0.01
Weekends	0.05 (0.03)	0.66	0.44	1.03	0.04

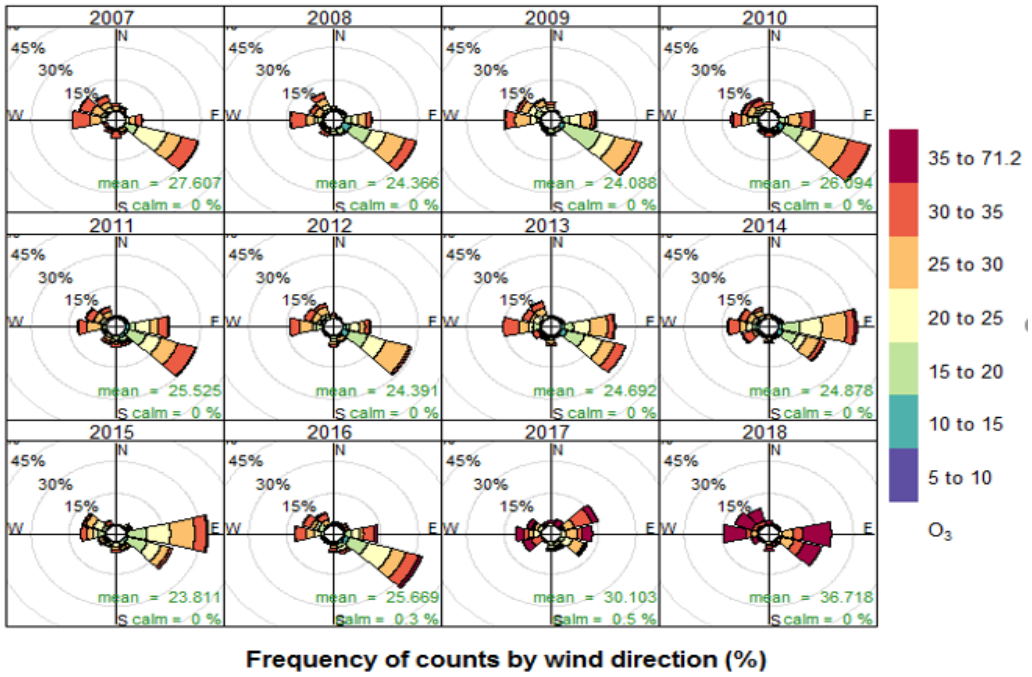

Figure 5.4: Percentage frequency occurrence of surface ozone relative to wind direction from 2007 to 2018.

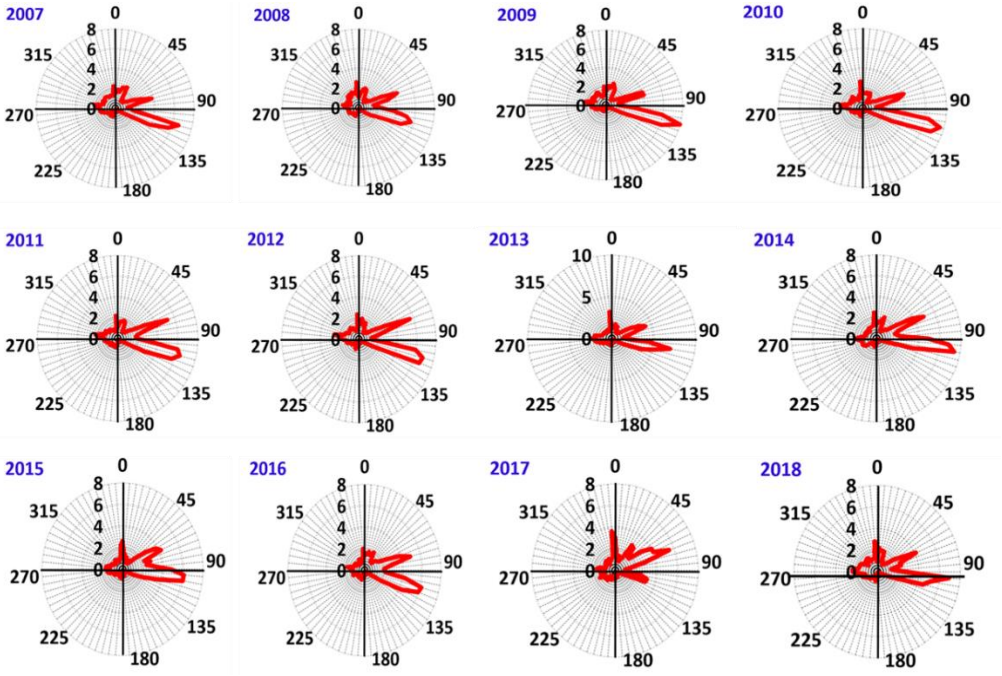

Figure 5.5: Percentage frequency occurrence of radon relative to wind direction from 2007 to 2018.

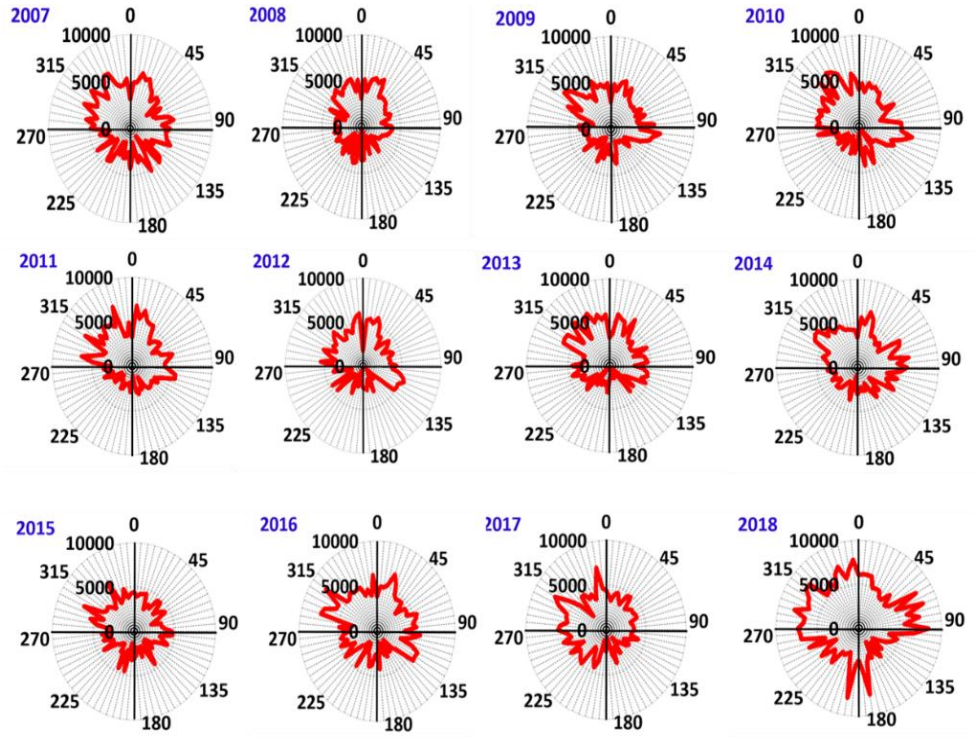

Figure 5.6: Maximum radon in air relative to wind direction from 2007 to 2018.

5.4.3 Identification of extreme maximum and minimum surface ozone events

Table 5.4 (a) indicates extreme maximum surface O_3 events that were identified at Cape Point from 2000 to 2016. These events were identified by using 2000 to 2016 average and standard deviation. The standard deviation was increased by a factor of two in order to determine the overall maximum of surface O_3. Events exceeding the overall maximum of 40.47 ppb were classified as extreme maximum surface O_3 events. One hundred and five events were identified by using this method. Most of the events were just above the limit of 40.47 ppb and below 50.00 ppb. The extreme maximum surface O_3 events predominantly occur in winter and spring, while few events were observed in autumn. Sixteen extreme maximum surface O_3 events were identified by increasing standard deviation by a factor of three (Table 5.4 (b)). In this case, an overall maximum of 48.00 ppb was used to identify extreme maximum surface O_3 events. With the exception of 04 October 2001 and 09

October 2011, all the identified events were higher than 100 ppb. As indicated by extreme maximum surface O_3 events that occurred on the 10 April 2001 and 13 September 2005, the increase in surface O_3 mole fractions coincides with the increase in CO mole fractions (Figure 5.7). These observations indicate the arrival of polluted air to Cape Point. Surface O_3 mole fraction is controlled by its sources and sinks. Tropospheric O_3 is secondary pollutant that is formed through the reactions of its precursors involving VOCs, nitrogen oxides (NO_x) and CO (Sillman et al., 1990; Sillman, 1999). Hence, increase in CO mole fractions affect surface O_3 mole fractions. The majority of the identified extreme surface O_3 events coincides with the season of dominant occurrence of STEs. In addition to this, the Cape Point surface O_3 seasonal cycle maximize in spring. A few of the extreme surface O_3 maximum events identified at Cape Point occurred on the first or second day after the occurrence of Irene STE event (e.g. 09 August 2002 and 09 July 2004). However, these events were also characterized by high CO mole fractions of more than 60 ppb. These observations suggest that these extreme maximum surface O_3 events could be related to the occurrence of STEs or pollution or be affected by both. CO is one of the parameters that is used to identify pollution and high CO mole fractions are associated with the occurrence of pollution while low CO mole fractions are associated with clean air masses (Brunke et al., 2004). It is notable that the observed extreme maximum surface O_3 events occurred during non-background conditions (high CO mole fractions). The identified events predominantly occur in winter when Cape Point is affected by polluted air masses coming from the north (Brunke and Scheel, 1998). The autumn events coincides with increase in CO mole fractions and that suggests that these events are not of stratospheric origin because stratospheric air is characterized by low CO and high O_3 mole fractions (Dessler et al., 1995). As indicated by NOAA HYSPLIT (Hybrid Single Particle Lagrangian Integrated Trajectory) backward trajectories (Figure 5.8), the extreme maximum surface O_3 events occur when air masses originate from the north of the country or have touched the land before diverting towards the ocean. The observed backward trajectories together with high CO mole fractions during

the occurrence of extreme maximum surface O_3 events suggest that these events occurred during non-background conditions (when polluted air arrived at the station).

Table 5.4 (a): Extreme maximum surface O_3 selected by using mean and 2 sigma (mean = 25.41, Stdev = 7.53, overall min = 10.35, overall max = 40.47 ppb) from 2000 to 2016.

Date	O_3 (ppb)	CO (ppb)	Date	O_3 (ppb)	CO (ppb)
19-01-00	45.70	123.54	17-10-05	46.77	190.05
20-01-00	55.46	216.49	18-10-05	41.22	114.93
7-04-00	42.61	79.82	11-05-06	41.46	118.46
6-06-00	40.74	115.57	26-08-06	50.71	110.46
22-09-00	42.66	123.21	7-09-06	45.41	105.95
12-05-01	43.60	155.24	19-10-06	41.38	62.01
13-05-01	41.98	106.14	3-04-07	55.32	122.00
15-05-01	40.91	146.27	20-04-07	42.26	98.38
26-07-01	42.70	116.86	21-06-07	40.82	103.14
30-07-01	44.26	175.48	20-10-07	41.70	85.30
8-08-01	45.42	144.38	19-03-08	44.20	#N/A
9-08-01	46.04	85.34	5-03-09	57.42	246.02
8-09-01	42.51	87.51	6-03-09	43.04	106.56
15-09-01	40.51	76.98	19-07-09	46.75	#N/A
30-09-01	43.02	73.70	27-07-09	40.57	#N/A
3-10-01	41.63	78.96	4-03-10	41.51	65.84
4-10-01	48.94	85.53	23-05-10	41.15	86.63
16-10-01	40.68	110.46	28-06-10	43.04	89.47
15-04-02	46.66	84.63	21-07-10	44.78	146.62

20-04-02	45.83	171.50	31-07-10	40.90	81.31
20-05-02	44.17	141.35	4-08-10	46.44	108.40
21-07-02	45.62	114.62	6-08-10	46.33	139.94
22-07-02	42.63	104.65	12-08-10	42.68	106.04
9-08-02	40.78	131.31	14-08-10	43.48	96.77
10-08-02	47.41	125.61	6-10-10	51.48	116.72
11-08-02	46.17	124.83	7-10-10	41.32	85.26
20-08-02	48.24	123.09	10-07-11	46.33	132.64
7-09-02	42.99	85.68	15-07-11	42.03	70.92
17-09-02	43.85	70.92	16-07-11	43.59	96.53
9-10-02	44.27	63.98	2-08-11	43.07	113.34
21-05-03	48.33	156.86	17-08-11	41.82	96.41
27-06-03	44.47	96.88	7-09-11	41.00	83.00
28-06-03	49.16	106.04	9-10-11	50.06	92.71
29-06-03	49.41	132.77	10-10-11	40.76	74.21
30-06-03	49.39	105.73	1-08-13	42.28	#N/A
16-07-03	42.22	121.87	30-09-13	45.89	102.84
30-08-03	41.62	73.26	10-04-14	41.67	91.55
1-09-03	43.86	69.71	11-04-14	51.56	107.22
12-10-03	42.77	144.49	12-04-14	43.67	75.28
21-10-03	42.47	82.84	13-04-14	42.79	105.29
9-07-04	43.15	60.90	25-06-14	40.91	79.84
17-07-04	46.28	70.90	17-08-14	42.93	109.28
18-07-04	45.08	61.11	4-09-14	48.43	110.43
19-07-04	43.93	61.55	2-08-15	46.42	122.95
3-10-04	42.96	75.33	5-09-15	45.64	98.35

19-10-04	40.69	108.75	6-09-15	42.11	98.08
5-04-05	44.80	110.73	7-06-16	45.10	91.21
9-07-05	44.47	164.78	8-06-16	44.79	105.61
10-07-05	45.57	103.32	27-06-16	43.55	54.27
11-07-05	42.18	105.99	13-07-16	42.02	101.02
16-07-05	50.02	125.34	26-08-16	42.38	65.88
17-07-05	47.27	106.80	28-08-16	41.69	83.71
13-09-05	64.25	129.93			

Table 5.4 (b): Extreme maximum surface O_3 selected by using mean and 3 sigma (mean = 25.41, Stdev = 7.53, overall min = 2.82, overall max = 48.00 ppb) from 2000 to 2016.

Date	O_3 (ppb)	CO (ppb)
20-01-00	55.46	216.49
4-10-01	48.94	85.53
20-08-02	48.24	123.09
21-05-03	48.33	156.86
28-06-03	49.16	106.04
29-06-03	49.41	132.77
30-06-03	49.39	105.73
16-07-05	50.02	125.34
13-09-05	64.25	129.93
26-08-06	50.71	110.46
3-04-07	55.32	122.00
5-03-09	57.42	246.02
6-10-10	51.48	116.72
9-10-11	50.06	92.71

11-04-14	51.56	107.22
4-09-14	48.43	110.43

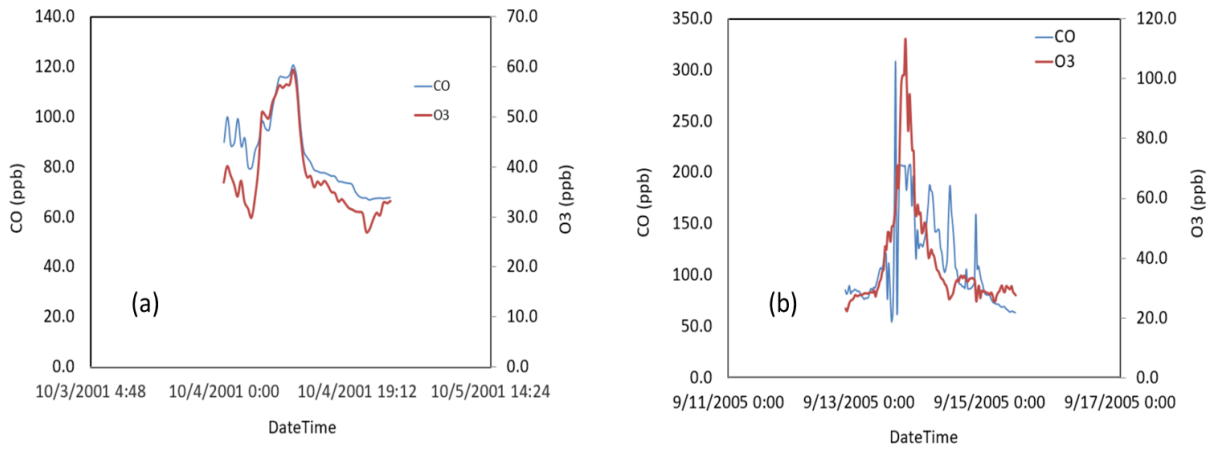

Figure 5.7: CO and O_3 mole fractions that were observed on the 10 April 2001 (a) and 13 September 2005 (b).

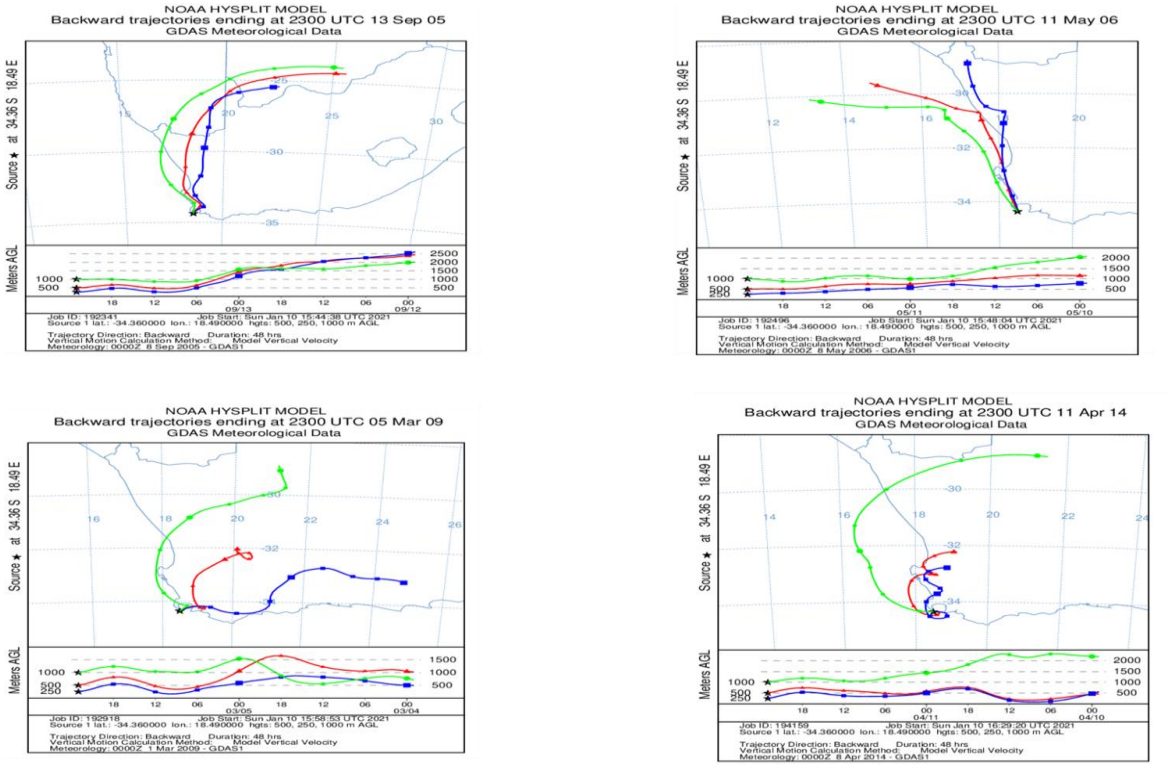

Figure 5.8: Two days HYSPLIT backward trajectories at 250, 500 and 1000 meters above ground level for the selected extreme maximum O_3 events (13 September 2005 (top right), 11 May 2006 (top left), 05 March 2009 (bottom left) and 11 April 2014 (bottom right).

Table 5.5 indicates extreme minimum surface O_3 events that were identified at Cape Point from 2000 to 2016. These events were identified by using 2000 to 2016 average and standard deviation. The standard deviation was increased by a factor of two to determine the overall minimum. Events exceeding an overall minimum of 10.35 ppb were classified as the extreme minimum surface O_3 events. Forty seven events were identified by using this method. No extreme minimum surface O_3 event was identified by increasing standard deviation by a factor of three (overall minimum decreased to 2.82 ppb). In addition to the use of overall minimum of 10.35 ppb to classify extreme minimum surface O_3 events, CO was used as a pollution indicator while NOAA HYSPLIT backward trajectories were used to trace the origin of air masses. The majority of extreme minimum surface O_3 events were observed when CO mole fractions were below 50 ppb. As indicated by some of the identified extreme minimum surface O_3 events, the CO and O_3 mole fractions are low during the occurrence of extreme minimum surface O_3 events (Figure 5.9). These observations show the absence of pollution during the occurrence extreme minimum surface O_3 events. Moreover, NOAA HYSPLIT backward trajectories show south westerly winds during the occurrence of extreme minimum surface O_3 (Figure 5.10). These events are characterized by clean air masses coming straight from the Atlantic Ocean without being affected by pollution. The majority of extreme minimum surface O_3 events occurred in summer when Cape Point is less affected by pollution and south westerly winds prevail (Brunke and Scheel, 1998). Even though Cape Point surface O_3 seasonal cycle is similar to SANAE IV surface O_3 seasonal cycle (Mkololo, 2013), the O_3 depletion events predominantly occur in spring in Antarctic stations while extreme minimum surface O_3 events predominantly occur in summer at Cape Point. In addition to this, the Cape Point surface O_3 seasonal cycle show minimum mole fractions during this period. On the other hand, Du Preez et al. (2018) reported the occurrence of low TCO events in summer and spring over Cape Point and associated such events with the breakup of polar vortex. However, this study show no event that occurred on the dates that were reported for low TCO. The current observations indicate the effect of winds in O_3 mole fractions.

Table 5.5: Extreme minimum surface O_3 selected by using mean and 2 sigma (mean = 25.41, Stdev = 7.53, overall minimum = 10.35, overall maximum = 40.47 ppb) from 2000 to 2016.

Date	O_3 (ppb)	CO (ppb)	Date	O_3 (ppb)	CO (ppb)
8-02-00	10.06	42.53	20-01-08	9.19	40.23
10-02-00	9.99	46.76	21-01-08	10.04	40.98
22-12-01	9.23	49.68	23-01-08	10.31	40.17
23-12-01	10.30	49.52	23-06-08	10.00	57.59
22-01-02	10.27	#N/A	23-01-09	9.91	36.43
23-01-02	10.28	#N/A	24-01-09	9.66	43.68
6-02-02	8.99	42.30	1-02-09	10.24	38.31
6-01-03	10.00	46.36	18-06-09	9.77	52.18
14-01-03	10.18	54.47	6-02-10	9.79	66.66
15-01-03	8.52	55.20	7-02-10	9.66	45.37
28-01-03	10.15	45.69	19-02-10	9.09	41.14
7-02-03	9.81	48.25	14-01-13	9.51	42.68
19-01-04	10.13	42.39	20-01-13	9.08	42.23
5-01-05	9.80	44.45	22-01-13	9.00	43.69
6-01-05	10.15	45.93	24-01-13	9.97	44.06
22-01-05	9.90	46.92	11-02-13	10.09	56.94
25-01-05	10.26	45.09	21-12-13	8.50	45.94
11-02-05	9.74	40.03	22-12-13	8.86	48.34
16-02-05	9.32	47.87	22-01-16	8.95	#N/A
22-02-05	10.02	42.42	23-01-16	8.77	#N/A
28-02-05	10.35	40.80	24-01-16	10.22	#N/A
18-01-06	7.52	38.91	4-04-16	9.33	45.04

4-01-08	5.28	42.07
6-01-08	8.12	61.45

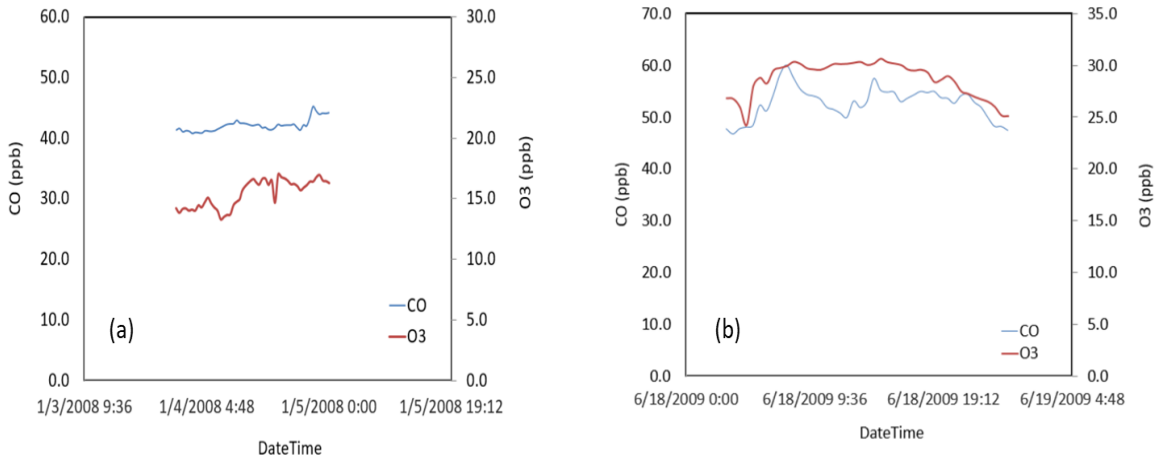

Figure 5.9: CO and O_3 mole fractions that were observed on the 04 January 2008 (a) and 18 June 2009 (b).

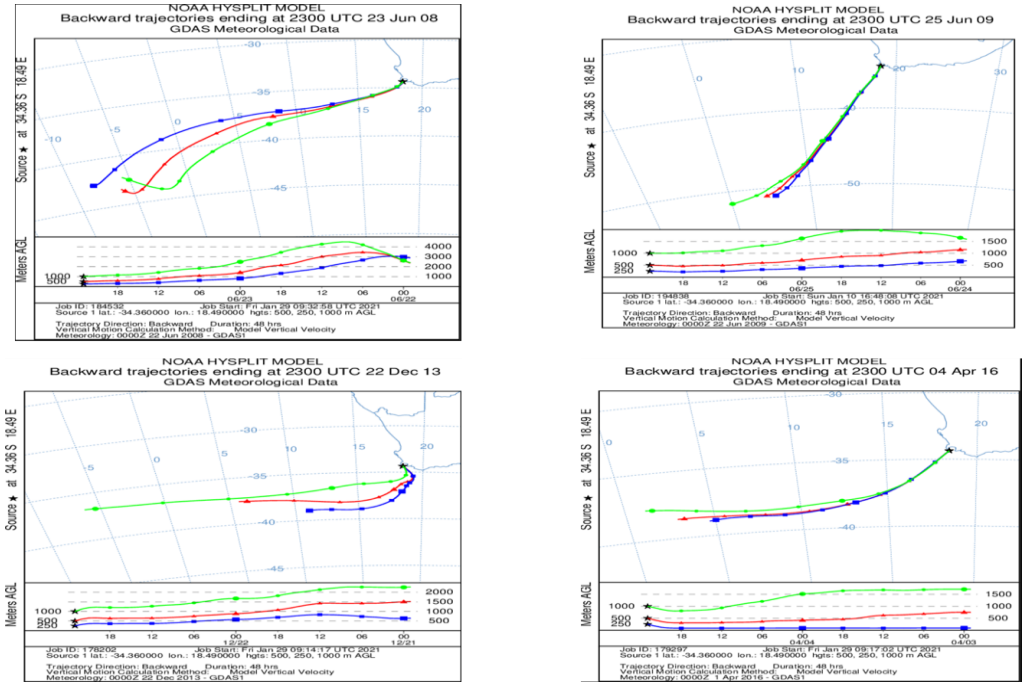

Figure 5.10: Two days HYSPLIT backward trajectories at 250, 500 and 1000 meters above ground level for the selected extreme minimum O_3 events (23 June 2008 (top right), 25 June 2009 (top left), 22 December 2013 (bottom right) and 04 April 2016 (bottom left)).

5.4.4 TCO relationship with surface O_3

The relationship between Cape Point TCO and surface O_3 was conducted by using 2005 to 2018 satellite and surface O_3 observations. This period was selected due to the availability of satellites data. The statistics between satellites and Cape Point surface O_3 was conducted by using linear regression method between TCO obtained from OMI-TOMS, OMI-DOAS, AIRS and MERRA-2 (Figure 5.11). R square, multiple r and percentage r square were determined from the linear regression of satellites TCO versus surface O_3. R square percentage was used to determine the relationship between TCO and surface O_3. Similar method was used by Combrink et al. (1995) when investigating the relationship between surface, free tropospheric and TCO in two contracting areas in South Africa. However, OMI was the only satellite used for their study. As indicated in Table 5.6, less than 35% of the variance in TCO is accounted for surface O_3 variations. The percentage r square of 31% obtained between OMI-TOMS and surface O_3 was higher than 15% that was reported by Combrink et al. (1995). A correlation coefficient of 0.56, 0.49, 0.56 and 0.62 was obtained between OMI-TOMS vs. surface O_3, OMI-DOAS vs. surface O_3, AIRS vs. surface O_3 and MERRA-2 vs. surface O_3, respectively. Correlation coefficient show weaker relationship between TCO and surface O_3 at Cape Point. However, these results are statistically significant at the 95% level. Table 5.7 shows seasonal variation of TCO obtained from satellites versus surface O_3. The percentage r square obtained between satellites TCO and surface O_3 show less than 22%, 25%, 13% and 28% variance in TCO accounted for surface O_3 in summer, autumn, winter and spring, respectively. In general, the obtained seasonal variation results are significant at 95% level with winter being exceptional showing significant relationship for MERRA-2 vs. surface O_3. The correlation coefficient show weaker relationship in all seasons between TCO and surface O_3. Amongst all the TCO observations used in this study, the MERRA-2 TCO shows better correlation with surface O_3.

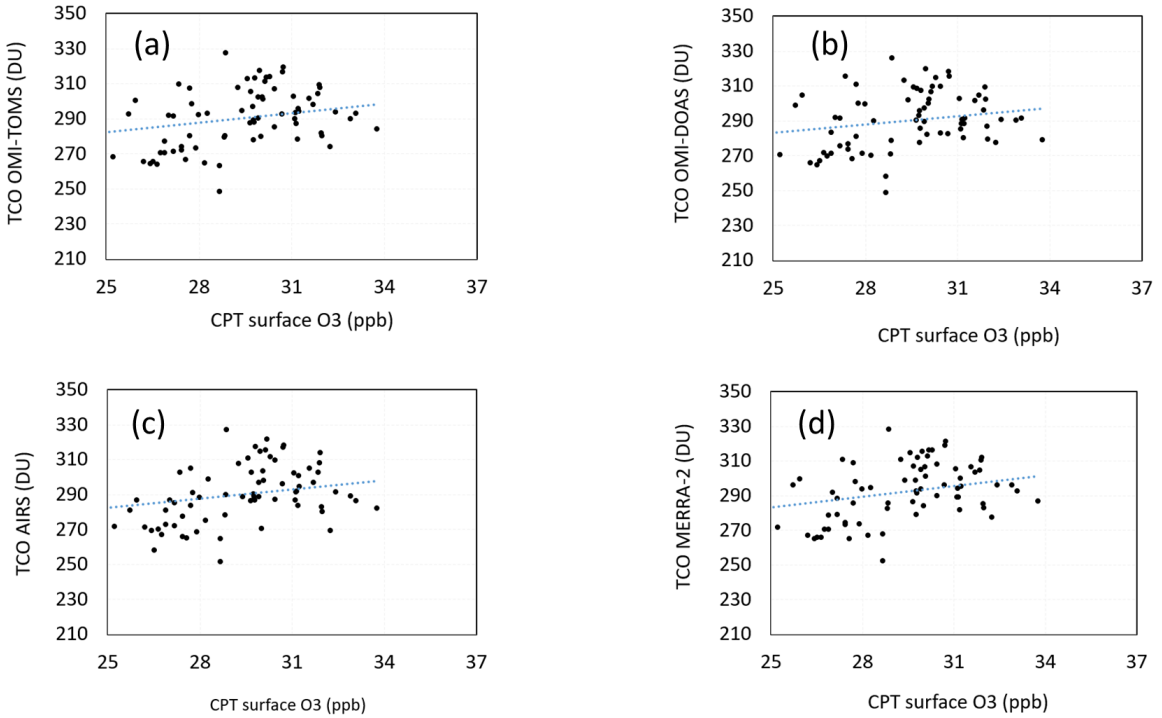

Figure 5.11: Correlation between Cape Point surface O_3 and satellite TCO observations (a), OMI-TOMS vs surface O_3 (b), OMI-DOAS vs surface O_3 (c) AIRS vs surface O_3 and MERRA-2 vs surface O_3 (d) from 2005 to 2016.

Table 5.6: Statistical analysis of TCO and surface O_3 comparison from 2005 to 2016.

	Multiple R	**R square**	**% R square**	**P-value**
TCO OMI-TOMS vs. surface O_3	0.56	0.31	31.36	$2.93e\text{-}^{13}$
TCO OMI-DOAS vs. surface O_3	0.49	0.24	24.05	$4.40e\text{-}^{10}$
TCO AIRS vs. surface O_3	0.56	0.31	31.15	$3.64e\text{-}^{13}$
TCO MERRA-2 vs. surface O_3	0.62	0.38	38.50	$1.37e\text{-}^{16}$

Significant at 95% confidence level.

Table 5.7: Seasonal statistical analysis of TCO and surface O_3 comparison from 2005 to 2016.

	Multiple R	**R square**	**% R square**	**P-value**
	(a). Summer			
TCO OMI-TOMS vs. surface O_3	0.40	0.16	16.51	0.01
TCO OMI-DOAS vs. surface O_3	0.42	0.17	17.33	0.01
TCO AIRS vs. surface O_3	0.36	0.13	13.07	0.03
TCO MERRA-2 vs. surface O_3	0.46	0.21	1.18	0.00

(b). Autumn				
TCO OMI-TOMS vs. surface O_3	0.42	0.17	17.55	0.01
TCO OMI-DOAS vs. surface O_3	0.45	0.20	20.08	0.00
TCO AIRS vs. surface O_3	0.24	0.06	5.93	0.15
TCO MERRA-2 vs. surface O_3	0.49	0.24	23.97	0.00
(c). Winter				
TCO OMI-TOMS vs. surface O_3	0.32	0.11	10.69	0.05
TCO OMI-DOAS vs. surface O_3	0.26	0.07	7.01	0.12
TCO AIRS vs. surface O_3	0.23	0.05	5.45	0.17
TCO MERRA-2 vs. surface O_3	0.34	0.12	12.06	0.04
(d). Spring				
TCO OMI-TOMS vs. surface O_3	0.46	0.21	21.51	0.00
TCO OMI-DOAS vs. surface O_3	0.36	0.11	11.26	0.04
TCO AIRS vs. surface O_3	0.51	0.27	26.55	0.00
TCO MERRA-2 vs. surface O_3	0.52	0.27	27.36	0.00

5.5 Summary

- Our observations show a negative trend in day-time while a positive trend was observed in night-time data subsets.
- Based on 2014, 2015 and 2018 observations, wind changes could potentially be the reason for the observed surface O_3 increase. However, further investigation is required from 2019 onwards because of 2017 data gap and dominant south-easterlies observed in 2016.
- It is evidenced from wind and Rn^{222} concentration roses that south-easterlies brings clean air to the station. Hence Rn^{222} roses show low concentrations in the southern sector and high concentrations observed in the northern sector.
- Solar radiation plays a critical role in O_3 formation and destruction. Hence, slightly high standard deviations were observed during the day and in months with strong solar radiation. While slightly low standard deviations were observed at night and in months with less solar radiation.
- Weekdays and weekend trends show almost similar results. Therefore, we conclude that the observed O_3 increase at Cape Point is not driven by the weekend effect.

- In general, the percentage r square obtained between satellites TCO and surface O_3 shows less than 39% variance in TCO accounted for surface O_3 at Cape Point. Although the results are significant at 95% level except in winter, the correlation is week between TCO and surface O_3.
- Moreover, further investigation is required on:
    - O_3 data from other southern hemisphere stations need to be analysed for trends in order to know if the current O_3 increase is the southern hemisphere phenomenon.
    - O_3 data from Cape Town stations such as Goodwood and Molteno need to be analysed for trends in order to know if the current O_3 increase is related to 2017 Cape Town drought.
    - Long-term changes in the wind characteristics and its impact on tropospheric O_3 concentrations.
    - NO_x trend analysis will be conducted as soon as enough NO_x data is available.
    - The effect of STE on surface O_3 remains a gap that need to be investigated in future studies.
    - The future study will investigate the impact of meteorology and dynamic factors on the identified extreme maximum and minimum surface O_3 events.

References

1. Alghamdi, M., Khoder, M., Harrison, R.M., Hyvärinen, A.-P., Hussein, T., Al-Jeelani, H. and Almehmadi, F. Temporal variations of O3 and NOx in the urban background atmosphere of the coastal city Jeddah, Saudi Arabia. *Atmos. Environ*., 2014, 94, 205- 214.

2. Ayers, G.P., Granek, H. and Boers, R. Ozone in the marine boundary layer at Cape Grim: model simulation. *J. Atmos. Chem.* 1997, 27, 179–195.

3. Brunke, E.G. and Scheel, H.E., 1998. Surface ozone measurements at Cape Point (343S, 183E). In: Bojkov, R.D., Visconti, G. (Eds.), Atmospheric Ozone. Proceedings of the XVIII Quadrennial Ozone Symposium, L'Aquila, Italy, 12-21 September 1996, 331-334.

4. Combrink, J., Diab, R.D., Sokolic, F and Brunke, E.G. Relationship between surface, free tropospheric and 'total column ozone in two contrasting areas in South Africa. *Atmos. Environ*., 1995, 29, 6, 685-691.

5. Dessler, A.E., Hintsa, E.J., Weinstock, E.M., Anderson, J.G. and Chan, K.R. Mechanisms controlling water vapor in the lower stratosphere: "A tale of two stratospheres". *J. Geophys. Res*., 1995, 100(D11), 23167–23176.

6. Du Preez, J.D., Bègue, N., Bencherif, H. and Wright, C.Y. An exploratory analysis of low-ozone events during spring and summer months over Cape Point, South Africa. 34th Annual conference of South African Society for Atmospheric Sciences (SASAS) 2018**.**

7. Ghosh, D., Lal, S. and Sarkar, U. High nocturnal ozone levels at a surface site in Kolkata, India: Trade-off between meteorology and specific nocturnal chemistry. *Urban Clim*., 2013, 5, 82-103.

8. Labuschagne, C., Kuyper, B., Brunke, E.G., Mkololo, T., van der Spuy, D., Martin, L., Mbambalala, E., Parker, B., Anwar, M., Khan, H. Michael T. Davies-Coleman, Dudley E. Shallcross & Warren Joubert. A review of four decades of atmospheric trace gas measurements at Cape Point, South Africa. Transactions of the Royal Society of South Africa, 2018, 2154-0098.

9. Lelieveld, J. and Dentener, F. What controls tropospheric ozone. *J. Geophys. Res*., 2000, 105, 3531-3551.

10. Mkololo, T. Analysis of Surface Ozone Measurements at Cape Point, SANAE and City of Cape Town. Dissertation, University of Kwa-Zulu Nata.

11. Nzotungicimpaye, C.L., Abiodun, B.J. and Steyn. D.G. Tropospheric ozone and its regional transport over Cape Town. *Atmos. Environ*., 2014, 87, 228-238.

12. Oltmans, S.J. and Levy II, H. Surface ozone measurements from the global network. *Atmos. Environ.*, 1994, 28, 9-24.

13. Oltmans, S.J., Lefohn, A.S., Shadwick, D., Harris, J.M., Scheel, H.E., Galbally, I., Tarasick, D.W., Johnson, B.J., Brunke, E.G., Claude, H., Zeng, G., Nichol, S., , Schmidlin, F., Davies, J., Cuevasm, E., Redondasm, A., Naoe, H., Nakano, T., Kawasato, T. Recent tropospheric ozone changes — A pattern dominated by slow or no growth. *Atmos. Environ*., 2013, 67,331–351.

14. Özbay, B., Keskin, G.A., Doğruparmak, Ş.Ç. and Ayberk, S. Multivariate methods for ground-level ozone modeling. *Atmos. Res*., 2011, 102, 1, 57-65.

15. Seinfeld, J.H. and Pandis, S.N. Atmospheric Chemistry and Physics: From Air Pollution to Climate Change. Hoboken, N.J., J. Wiley, 2006.

16. Sillman, S., Logan, J. A. and Wofsy, A. C. The Sensitivity of Ozone to Nitrogen Oxides and Hydrocarbons in Regional Ozone Episodes. J. *Geophys. Res*., 1990, 95, 1837-1851.

17. Sillman, S. The relation between ozone, NOx and hydrocarbons in urban and polluted rural environments. *Atmos. Environ*., 1999, 33, 1821-1845.

18. Tarasova, O.A. and Karpetchko, A.Y. Accounting for local meteorological effects in the ozone time-series of Lovozero (Kola Peninsula). *Atmos. Chem. Phys. Discus.*, 2003, 3, 655–676.

19. Xu, W., Lin, W., Xu, X., Tang, J., Huang, J., Wu, H. and Zhang. X. Long-term trends of surface ozone and its influencing factors at the Mt Waliguan GAW station, China – Part 1: Overall trends and characteristics. *Atmos. Chem. and Phys*., 2016, 16, 6191-6205.

CHAPTER 6: SUMMARY AND RECOMMENDATIONS

This chapter gives a summary on the studies conducted using Irene vertical O_3 profiles (2000 to 2015), Stellenbosch Dobson spectrophotometer TCO observations (2017 and 2018) coupled with satellites (OMI–TOMS, OMI–DOAS, AIRS and MERRA–2) TCO observations. In addition, this chapter gives a summary of annual, seasonal and weekday-weekend O_3 changes observed by using 2000 to 2018 Cape Point surface O_3 data (all-day, day-time and night-time).

6.1 Summary

Ozonesondes data was used to identify high O_3 events over Irene. Days with O_3 exceeding the monthly 90^{th} and 95^{th} percentile composites were selected and investigated if the observed O_3 increase was related to STE. In addition, PV was used to identify stratospheric air masses. Two categories were used to identify high O_3 events of stratospheric origin. The first category used the monthly 95^{th} percentile composite and 2 PVU. The second category used the monthly 90^{th} percentile composite and 2 PVU. Events exceeding these thresholds were classified as high O_3 events and were associated with stratospheric origin because high PV only exists in the stratosphere. More events were identified by using the monthly 90^{th} percentile composite and 2 PVU while less events were identified by using the monthly 95^{th} percentile composite and 2 PVU. PV charts showed that there are more high O_3 events over Irene that could be identified by using a PV threshold of less than 2 PVU. Such events are indicated in PV charts in chapter 3. These events were observed in all seasons between 7 km and 11 km. However, they were more dominant in winter and spring. In addition, O_3 changes at different altitudes were investigated by calculating annual composites for the medians, 5^{th} and 95^{th} percentiles. A positive increase of 0.07±0.22, 0.02±0.17 and 0.07±0.27 ppb/year was observed at 7-9 km for the medians, 5^{th} and 95^{th} percentiles, respectively. A negative O_3 decrease of -2.38±3.28 ppb/year was observed at 13–15 km for the 95^{th} percentiles while medians and 5^{th} percentiles O_3 decrease was observed from 16–18 km layer. More O_3 decrease was observed at 22–24 km for the medians (-16.16±21.83 ppb/year), 5^{th} (-21.19±27.39 ppb/year) and 95^{th} percentile (-14.81±21.82 ppb/year). In general, linear trend analysis showed O_3 decrease in the lower stratosphere while O_3 increase was observed in the lower troposphere in all seasons. High standard deviation was observed in altitudes closer to the tropopause.

This chapter also presents summary of Stellenbosch Dobson#035 TCO validations conducted by using OMI-TOMS, OMI-DOAS and AIRS satellite observations. In addition, MERRA-2 assimilation data was compared with Dobson#035 TCO observations. Validation between Dobson#035 TCO observation and satellite TCO observations was done by calculating percentage difference, percentage error and correlation coefficient. Daily percentage differences between Dobson#035 and satellites TCO observations varied within ±2%. However, in some days, the percentage difference was lower than -2% or higher than 2%. A correlation coefficient of 0.97 was observed between OMI–TOMS and Dobson#035 TCO observations. The likely reason for this good agreement could be related with the retrieval algorithm adopted between OMI-TOMS and Dobson spectrophotometer. MERRA-2 shows a correlation coefficient of 0.95 when compared with Dobson#035 TCO observations. The obtained good correlation between MERRA-2 and Dobson#035 could be related to the OMI observation method that is used by MERRA-2 for O_3 assimilation. OMI-DOAS showed a correlation coefficient of 0.85 while a correlation coefficient of 0.92 was observed between AIRS and Dobson#035 TCO observations.

Lastly, this chapter presents a summary of all-day, day and night-time O_3 changes conducted using 2000 to 2018 surface O_3 data measured at Cape Point. The later years, 2017 and 2018 were excluded in trend analysis due to high O_3 mole fractions observed in these years. Annual, seasonal and weekday-weekend changes were calculated by using linear trend regression and Theil-Sen trend analysis. Linear trend regression showed an increase of 0.24 ppb/year, 0.28 ppb/year and 0.19 ppb/year for all-day, night and day-time, respectively. On the other hand, Theil-Sen analysis showed an increase of 0.40%/year, 0.67%/year and 0.02%/year for all-day, night and day-time, respectively. Slightly high O_3 mole fractions were observed in day-time dataset relative to night-time. This could be related to photochemical reactions that takes place during the day. While slightly low O_3 mole fractions at night could be related to O_3 destruction by NO and deposition processes that takes place during this time. The observed extreme maximum surface O_3 events coincides with high CO mole fractions and NOAA HYSPLIT backward trajectories show continental air masses that comes up the country. On the other hand, extreme minimum surface O_3 events coincides with low CO mole fractions and NOAA HYSPLIT backward trajectories show clean air from the Atlantic Ocean. The relationship between satellites and surface O_3 was conducted by using TCO observations obtained from OMI-TOMS, OMI-DOAS, AIRS and

MERRA-2. The statistics between satellites and surface O_3 was conducted by using linear regression method. A correlation coefficient of 0.56, 0.49, 0.56 and 0.62 was obtained between OMI-TOMS vs. surface O_3, OMI-DOAS vs. surface O_3, AIRS vs. surface O_3 and MERRA-2 vs. surface O_3, respectively.

6.2 Conclusions

Based on the findings from the objectives of this study, the following can be concluded:

- High O_3 of stratospheric origin can reach down to 7 km over Irene. However, the majority of these events occurred between 9 km and 10 km and only few events reached down to 7 km region.
- The observed positive O_3 changes in the lower troposphere could be related to manmade activities.
- High standard deviation closer to the tropopause could be related to STE and other atmospheric dynamic factors occurring in tropopause region.
- O_3 decrease observed in the lower stratosphere over Irene was more dominant in winter and spring seasons.
- In general, the percentage difference between satellites and Stellenbosch Dobson TCO observations varied between ±2%.
- Despite the small differences between Dobson and satellites TCO observations, there is a good correlation coefficient between satellites (MERRA–2, OMI–TOMS, AIRS and OMI–DOAS) and Stellenbosch Dobson TCO observations.
- O_3 increase at Cape Point was observed in all data (all-day, day and night-time data) subsets. However, the main reason for the observed increase is not yet clear.
- O_3 increase at Cape Point could be influenced by:
    - Changes in winds and other meteorological parameters.
    - Changes in regional or hemisphere O_3 souces and sinks.
- In general, the observed extreme maximum surface O_3 events at Cape Point could be related to the arrival of polluted air to the station that is influenced by anthropogenic activities. While extreme minimum surface O_3 events occurred under clean air masses that originate from the Atlantic Ocean.

- TCO observations obtained from MERRA-2 correlates better with surface O_3 measurements as compared with the correlation of OMI-TOMS vs. surface O_3, OMI-DOAS vs. surface O_3, AIRS vs. surface O_3.

6.3 Limitations of the Study

- The current Dobson technique requires manual operation and result to non-continuity of TCO observations during the day. This limits the understanding of diurnal TCO behavior in South Africa.
- Some of the high O_3 events were not identified over Irene due to data gaps in ozonesondes launches.
- NO_x and other O_3 precursor measurements are important to understand surface O_3 changes (seasonal fluctuations and long term trends). The absence of NO_x measurents at Cape Point during the study period limits the conclusions that can be drawn from the observed O_3 changes.

6.4 Recommendations

- It is recommended to continue with ozonesondes launches and conduct more studies on STE statistical analysis.
- Depending on the availability of funds, it is recommended to have a Brewer instrument in South Africa in inorder to conduct continous TCO observations that will enable to study TCO behaviour throughout the day.
- It is recommended to use other Southern Hemisphere GAW surface O_3 data to investigate the annual, seasonal and weekday-weekend changes in all-day, day and night-time data subsets.
- Furthermore, long-term trend analysis from closer stations such as Molteno and Goodwood is required to investigate if the observed O_3 increase at Cape Point is caused by regional changes or related to 2016 to 2017 drought.
- In addition to surface O_3 data, NO_x and meteorological parameters (wind, solar radiation and temperature) can add more value on the study.
- It is recommended to investigate the effect of meteorology and PV on the observed Cape Point extreme maximum and minimum surface O_3 events.